Design of novel nano-carriers for multi-enzyme co-localization

by

Feng Jia

A dissertation submitted to the graduate committee
In partial fulfillment of requirements for the degree of
DOCTOR OF PHILOSOPHY

Major: Chemical Engineering

Program of Study Committee
Balaji Narasimhan Major Professor
Surya K Mallapragada Major Professor
Ian C Schneider
Reuben J Peters
Malika Jeffries-EL

Iowa State University
Ames, Iowa
2013

DEDICATION

I would like to take this opportunity to express my sincere grateful appreciatation to all the people who have inspired and helped me throughout my PhD study. Without their impacts and supports, I could not write this righ now.

First of all, I would like to thank my wife Xunpei Liu, who is also graduating in two months with a PhD degree in the same major. She has accompanyed me for college, master and PhD study for the past ten years as a classmate and best friend. Her insightful profesional discussion and suggestions have always been very invalable for me. She has also experienced my happyness, frustrations and always been standing behing me to give me the power to get through my PhD study. I am so lucky to have her aside.

Next, I would like to thank my parents, my father, Mr. Jinwei Jia and my mother, Mrs. Yi Sun. They have been always supportive thourghout my life. My parents did their best to provide me the best education they can offer. They taught me how to be a person I am like today. My father has shown me from his real practice on how to be a responsible man in the society and his own family. My mother always encouraged me to follow my heart to pursure my dream. No word can describe my appreciation for what they have been doing for me.

I also dedicate my dissertation to my two co-advisors Profs. Balaji Narasimhan and Surya Mallapragada. They have been more than good mentors to me. They are also good friends who respected me, trusted me and supported me so much . Their guidance and supports in my PhD study were extremely important to me. Their success in both academy and life have really set a good

model for me to follow not only in my PhD study but also thourghout my life. Without them I could not complete my PhD study.

My project is a multi-discipline collobrateive project, from which I learned how to effectively collorobrate with researchers in different discipline. I really appreacte our collolaborator, Prof. Reuben Peters, the prestigious professor and scientst in plant biology's guidance on my project. He has provided many unique opinions and suggestions from biological perspetive for my research, which has inspired me to explore more on our project. I also would like to thank Dr. William Colonna, who I worked with closely in the colloborative effort on this project. I have learned much from him. Emily Dovenport, Molly Tienan and Kevin Port, the three graduate students from Porf. Peters' group who also work on this project. I really appreciate their helps and hard work on this project, as well.

I would like to thank my other POS committee professors, Profs. Ian Schneider and Malika Jeffries-EL. They have provided me many helpful comments and suggustions on my PhD study and inspired me to think more on my research.

No one can work alone to finsh their jobs nowadays, including graduate students. I also thank my group members from two research groups. They have been really helpful and I have spent most of my time in the lab with them. Group memebers from Prof Narasimhan's group: Dr. Yanjie Zhang, Dr. Kathleen Ross, Julia Vela Ramirez, Shannon Haughney, Dr. Tim Brenza, Jonathan Goodman, Dr. Latrisha K. Petersen, Dr. Bret Ulery, and Dr. Brenda Carrillo-Conde and Dr. Rebecca Cademartiri. Group members from Prof. Mallagragada's group: Xunpei

Liu, Dr. William Colonna Justin Adams, Dr. Bingqi Zhang, Dr. Tanya Prozorov, Dr. Robert J Lipert, , Dr. Mustafa Marti, Anup Dutt Sharma, Metin UZ and Dr. Natia Ochkhikidze and Dr. Vikash Malik.

I also would like to thank the undergraduate students I mentered in the REU programs and my PhD study. Their points of view were also important for me . I would llke to thank researchers and scientists I met and talked in my PhD study. Iowa State University has an exellent research environment that nurtures so many brilliant researchers and scientits in the community. I really appreaciate their helps and time on my work as well as the facility and instrument that I can reach out at the university.

I also would like to thank the faculty and stuff members as well as the friends in the chemial and biological engineering department, because they have made me feel like to be part of the whole family. I really enjoyed the peaceful life in Ames.

At last but not least, I would like to thank our finincial support, National Science Fundation, who has provided us the finantial supports on our project.

Table of Contents

List of Figures

List of Tables

Chapter 1 Introduction and objectives

Enzymes, Nature's highly specific catalysts, have played a significant role in metabolism of living organisms, where they are involved in several essential processes such as protein synthesis, DNA replication and transcription, signal transduction, cell regulation and energy generation.[1–6] Multiple enzymes, which work cooperatively to catalyze cascaded reactions, are sometimes associated and organize compactly to form multi-enzyme complexes (MECs) containing multiple catalytic centers with highly proximate active sites.[7–11] MECs promote the reaction efficiency in enabling rapid transport of the reactive intermediates among the active sites to avoid major losses caused by diffusion and maintain high local concentration of intermediates. [12–16]

Although enzymes possess tremendous powerful functionalities *in vivo*, they have limitations for application in the *in vitro* environment due to their vulnerable delicate structures and short bioactive lifetimes. The enzyme proteins are relatively unstable to changes of local environment (e. g., pH or temperature) due to the induced unfavorable structural changes, which are critical for enzyme specific functionalities. In addition, if enzymes are in solution, it makes separation of enzymes from the reaction products and reusability difficult. To overcome these drawbacks, enzyme immobilization techniques have been developed, where enzymes are attached or entrapped physically or chemically to a support material to stabilize the enzymes and prevent free movement through the reaction medium. Through immobilization, enzymes can acquire characteristics such as enhanced catalytic performance and stability under optimal harsh process reactions environments (extreme pH, temperature and organic solvent), facile separation from the reaction medium, and efficient recovery of enzymes for economic multiple uses. [17–19] Immobilized enzymes biocatalysts have been widely used in in food

processing, pharmaceuticals, chemical transformation, detergent applications, bioremediation, biosensors, and biofuel cells.

The success in single enzyme immobilization and the highly efficient catalytic mechanism of MECs have inspired researchers to devote efforts to bring naturally existing MECs *in vitro* with delicate engineering design. [20–22] Since multiple enzyme co-localization is derived from single enzyme immobilization, the challenges faced in multi-enzyme co-localization are much more daunting than immobilization of single enzymes. For instance, appropriate attachment techniques need to be adopted; otherwise, strong non-specific interactions between amphiphilic proteins and hydrophobic surfaces could induce unwanted structural change to jeopardize the enzymatic activity. The advances in materials science provide more options for platforms, from which the researchers can compare and provide the most appropriate carriers to maximize the performance in terms of optimizing loading quantity stabilizing the enzymes and enzymatic activity. The involvement of multiple enzymes makes the design of co-localization strategies including selection of attachment techniques, platforms more complicated. The different properties of the various enzymes require researchers to take each component into consideration to optimize the co-localization process. In addition, unlike single enzyme immobilization, the unique challenge in co-localization is how to effectively control the relative positions of multiple enzymes on the platform. In the native MECs, the enzyme subunit components are associated tightly to enable of highly cooperative catalytic mechanism. Therefore, to mimic the functionality of MECs, maximizing the proximity of the active sites on different enzymes in co-localization is very critical.

In Nature, such multi-enzyme co-localization concepts are used to control biosynthetic pathways and enhance the desired reaction efficiency. In the natural biosynthesis of sclareol, which is a fragrant chemical product existing in the plant *Salvia*

sclarea, two types of enzymes catalyzing class II and class I reactions, are critical in mediating the sequential pathway as illustrated in figure 1.1.[23] A biosynthetic approach co-localizing the two enzymes on nanocarriers to mimic naturally occurring MEC can potentially improve the product yield significantly and lead to industrial applications. The broad goal of this work is to design bioinspired MECs in vitro using materials-based approaches to co-localize enzymes on nanocarriers.

1.1 Objectives

The main objective of this project is to design novel nano-structured carriers and strategies to co-localize multiple enzymes to mimic the functionalities of MECs. In order to achieve this goal, distinct approaches for enzyme co-localization were developed and evaluated. Specifically, we investigated different polymeric nano-carriers, both flexible and rigid, as platforms for co-localization, as well as distinct enzyme attachment techniques using model enzyme systems using glucose oxidase and horseradish peroxidase to control the spatial arrangement of the multiple enzymes on the nanocarriers. This platform technology can be potentially used to co-localize various enzyme systems and its broad applicability will be tested using the sclareol biosynthesis process to control the formation of products through the formation of MECs with multiple enzymes NgCPS and sSsSS to regulate the pathway of reactive intermediate to enhance the final product conversion rate.

1.2 Dissertation organization

The thesis is organized to six chapters. Specifically, Chapter 2 is modified from a comprehensive literature review paper that summarizes recent progress and strategies in enzyme immobilization and carrier based co-localization using materials-based approaches. Chapter 3 is modified from a paper published in *AIChE Journal Letters*,

which illustrates a sequential co-localization approach to controllably co-localize multiple enzymes on multi-functionalized rigid polymeric nanoparticles. Chapter 4 is modified from a paper published in the journal *Langmuir*, which demonstrates a strategy of constructing block copolymer-QD platforms for multiple enzyme co-localization and characterization of single or multiple enzyme attachment onto polymeric micelles by Föster resonance energy transfer (FRET). Chapter 5 is modified from a paper to be submitted to ACS Nano, which describes the impact of spatial co-localization on product formation by using DNA hybridization to direct multi-enzyme localization. Chapter 6 summarizes the individual approaches in terms of discoveries, findings and conclusions. Chapter 7 covers ongoing efforts in applying multi-enzyme co-localization concepts to investigate natural production biosynthesis and future potential directions.

References

(1) Costas, M.; Mehn, M. P.; Jensen, M. P.; Que, L. Dioxygen Activation at Mononuclear Nonheme Iron Active Sites: Enzymes, Models, and Intermediates. *Chem. Rev.* **2004**, *104*, 939–986.

(2) Falkenberg, M.; Larsson, N.-G.; Gustafsson, C. M. DNA replication and transcription in mammalian mitochondria. In *Annual Review of Biochemistry*; Annual Reviews: Palo Alto, 2007; Vol. 76, pp. 679–699.

(3) Hille, R. Molybdenum and tungsten in biology. *Trends Biochem. Sci.* **2002**, *27*, 360–367.

(4) Kuhn, H.; Borchert, A. Regulation of enzymatic lipid peroxidation: The interplay of peroxidizing and peroxide reducing enzymes. *Free Radic. Biol. Med.* **2002**, *33*, 154–172.

(5) Kurz, T.; Terman, A.; Gustafsson, B.; Brunk, U. T. Lysosomes in iron metabolism, ageing and apoptosis. *Histochem. Cell Biol.* **2008**, *129*, 389–406.

(6) Santoro, S. W.; Joyce, G. F.; Sakthivel, K.; Gramatikova, S.; Barbas, C. F. RNA cleavage by a DNA enzyme with extended chemical functionality. *J. Am. Chem. Soc.* **2000**, *122*, 2433–2439.

(7) Schoffelen, S.; van Hest, J. C. M. Multi-enzyme systems: bringing enzymes together in vitro. *Soft Matter* **2012**, *8*, 1736–1746.

(8) Lopez-Gallego, F.; Schmidt-Dannert, C. Multi-enzymatic synthesis. *Curr. Opin. Chem. Biol.* **2010**, *14*, 174–183.

(9) Fernandez-Lafuente, R. Stabilization of multimeric enzymes: Strategies to prevent subunit dissociation. *Enzyme Microb. Technol.* **2009**, *45*, 405–418.

(10) Ricca, E.; Brucher, B.; Schrittwieser, J. H. Multi-Enzymatic Cascade Reactions: Overview and Perspectives. *Adv. Synth. Catal.* **2011**, *353*, 2239–2262.

(11) Xue, R.; Woodley, J. M. Process technology for multi-enzymatic reaction systems. *Bioresour. Technol.* **2012**, *115*, 183–195.

(12) Jones, S. M.; van Dyk, J. S.; Pletschke, B. I. Bacillus Subtilis Sj01 Produces Hemicellulose Degrading Multi-Enzyme Complexes. *BioResources* **2012**, *7*, 1294–1309.

(13) Wang, Y.; Margoliash, E. Enzymatic-Activities of Covalent 1/1 Complexes of Cytochrome-C and Cytochrome-C Peroxidase. *Biochemistry (Mosc.)* **1995**, *34*, 1948–1958.

(14) Najdi, T. S.; Hatfield, G. W.; Mjolsness, E. D. A “random steady-state” model for the pyruvate dehydrogenase and alpha-ketoglutarate dehydrogenase enzyme complexes. *Phys. Biol.* **2010**, *7*.

(15) Kim, C.; Kim, D. Extracellular Cellulolytic Enzymes of Bacillus-Circulans Are Present as 2 Multiple-Protein Complexes. *Appl. Biochem. Biotechnol.* **1993**, *42*, 83–94.

(16) Cohn, M. A.; Kee, Y.; Haas, W.; Gygi, S. P.; D’Andrea, A. D. UAF1 Is a Subunit of Multiple Deubiquitinating Enzyme Complexes. *J. Biol. Chem.* **2009**, *284*, 5343–5351.

(17) Iyer, P. V.; Ananthanarayan, L. Enzyme stability and stabilization - Aqueous and non-aqueous environment. *Process Biochem.* **2008**, *43*, 1019–1032.

(18) Heredia, K. L.; Bontempo, D.; Ly, T.; Byers, J. T.; Halstenberg, S.; Maynard, H. D. In situ preparation of protein - “Smart” polymer conjugates with retention of bioactivity. *J. Am. Chem. Soc.* **2005**, *127*, 16955–16960.

(19) Hanefeld, U.; Gardossi, L.; Magner, E. Understanding enzyme immobilisation. *Chem. Soc. Rev.* **2009**, *38*, 453.

(20) Vinu, A.; Murugesan, V.; Hartmann, M. Adsorption of lysozyme over mesoporous molecular sieves MCM-41 and SBA-15: Influence of pH and aluminum incorporation. *J. Phys. Chem. B* **2004**, *108*, 7323–7330.
(21) Watanabe, J.; Ishihara, K. Sequential Enzymatic Reactions and Stability of Biomolecules Immobilized onto Phospholipid Polymer Nanoparticles. *Biomacromolecules* **2005**, *7*, 171–175.
(22) Dalal, S.; Kapoor, M.; Gupta, M. N. Preparation and characterization of combi-CLEAs catalyzing multiple non-cascade reactions. *J. Mol. Catal. B-Enzym.* **2007**, *44*, 128–132.
(23) Caniard, A.; Zerbe, P.; Legrand, S.; Cohade, A.; Valot, N.; Magnard, J.-L.; Bohlmann, J.; Legendre, L. Discovery and functional characterization of two diterpene synthases for sclareol biosynthesis in Salvia sclarea (L.) and their relevance for perfume manufacture. *Bmc Plant Biol.* **2012**, *12*.
(24) Bhatia, S. P.; McGinty, D.; Letizia, C. S.; Api, A. M. Fragrance material review on sclareol. *Food Chem. Toxicol.* **2008**, *46*, S270–S274.

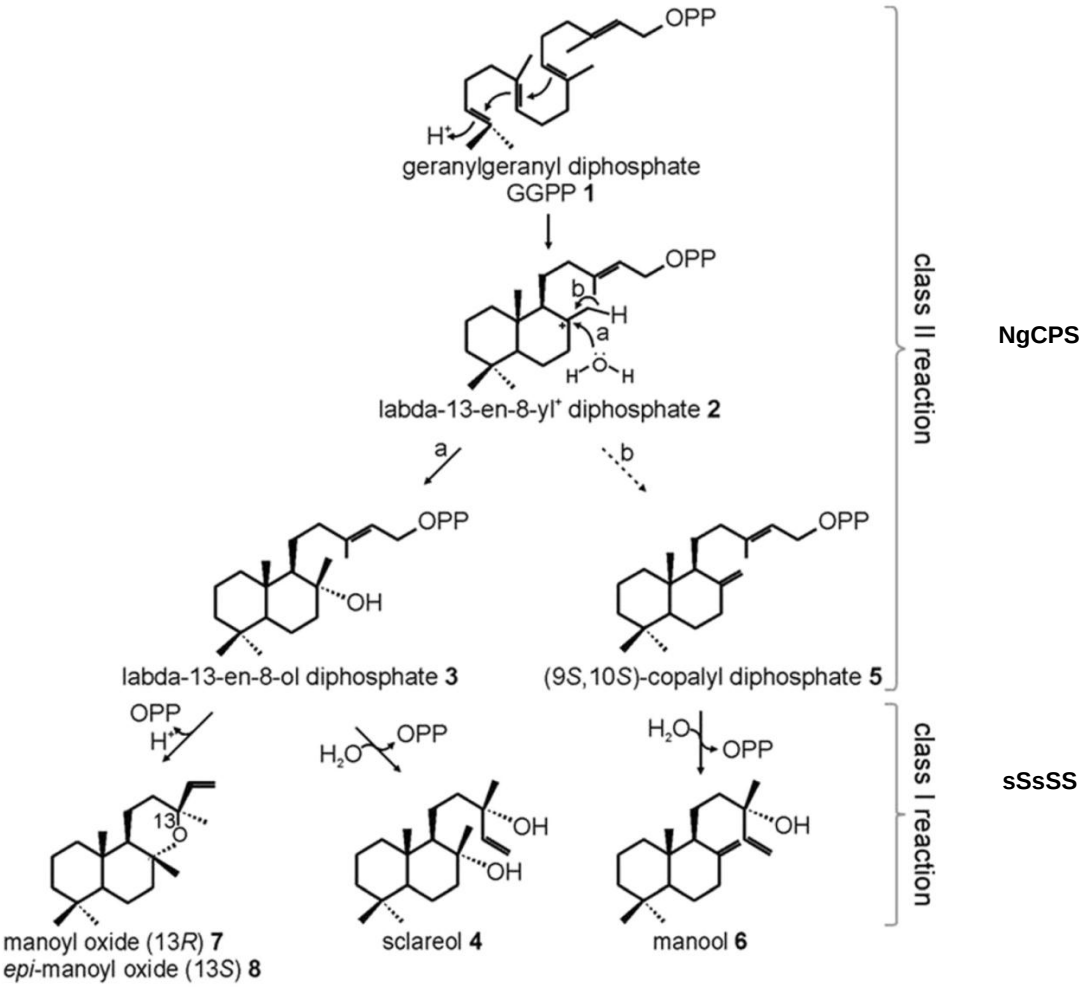

Figure 1.1 Biosynthesis pathway of sclareol with involvement of NgCPS and sSsSS enzymes. [23]

Chapter 2 Strategies for multi-enzyme immobilization and co-localization: a review

Feng Jia, Balaji Narasimhan and Surya Mallapragada*

Department of Chemical and Biological Engineering

Iowa State University, Ames, IA 50011-2230

Ph: 515-294-7407

Email: suryakm@iastate.edu

Abstract

Immobilized enzymes as biocatalysts have great potential both scientifically and industrially because of their technological and economic importance. Their highly efficient catalytic mechanisms and reusability have made them excellent candidates for green and sustainable applications. Previous studies have primarily focused on single enzyme immobilization. However, there are many situations where a single enzyme cannot completely catalyze reactions and multiple enzymes working together in a cascade are needed. It is very challenging to efficiently drive the multi-step reaction toward the desired direction, which is especially true when reactive intermediates are present. Nature overcomes this limitation through the use of multi-enzyme complexes (MECs) to promote the overall catalytic efficiency, which has inspired researchers to synthesize artificial MECs to mimic the special functionalities of the natural MECs *in vitro*. The most common approach to synthesize artificial MECs is to co-localize multiple enzymes on carriers, which builds on techniques developed for single enzyme immobilization. The attachment techniques used in single enzyme immobilization are also effective in multiple enzyme co-localization, which has a direct impact on the overall enzyme orientation and activity. For carrier-based strategies, the platforms developed for

single enzyme immobilization are also appropriate for attaching and co-localizing multiple enzymes. However, the involvement of multiple components in co-localization brings many challenges. The properties of different enzymes makes co-localization complicated when selecting attachment techniques and platforms to preserve enzymatic activity, because the structure and function of each component enzyme needs to be taken into consideration to preserve the overall enzyme activity. In addition, the relative position of the multiple enzymes in a confined space plays a significant role in the interactions between different enzymes, which makes spatial control important for co-localization. This review focuses on the potential of multiple enzyme co-localization for the design of sustainable multi-enzyme biocatalysts. A critical analysis of the attachment techniques and carriers platforms that have been used in enzyme immobilization and multi-enzyme co-localization *in vitro* is provided.

2.1 Introduction

Biocatalysts have great potential in both scientific and industrial settings due to their energy efficient catalytic mechanisms, unique selectivity for substrates, and enhanced stability under harsh reaction environments (Ansari and Husain, 2012; Ge et al., 2009; Schoffelen and van Hest, 2012; Tran and Balkus, 2011; Wang et al., 2004; Zhang et al., 2002). Developing such green and efficient catalysts has already attracted a lot of research interest.

In Nature, many cascaded reactions are catalyzed by multi-enzyme complexes (MECs) that are constituted of highly ordered assemblies of enzymes. The MECs can accomplish catalysis in a highly efficient way, where the intermediates are transported between the different active sites on enzyme subunits without leaving the MECs (Cohn et al., 2009; Jones et al., 2012; Kim and Kim, 1993; Najdi et al., 2010; Wang and Margoliash, 1995). The advantages of such a mechanism include maintaining high local concentration of the intermediates and reducing diffusion losses during transportation in order to promote overall catalytic efficiencies toward desired pathways, which is especially critical in the presence of highly reactive intermediates (Conrado et al., 2008; Schoffelen and van Hest, 2012). Many examples of such MECs can be found in Nature. In the citric acid cycle, which regulates many other metabolic biosynthetic pathways via control of the intermediates formed, five out of eight enzymes were purified as multi-enzyme clusters (Barnes and Weitzman, 1986). In tryptophan synthesis, subunits α and β which catalyze the last two steps were discovered to combine as a stable multi-enzyme complex ($\alpha_2\beta_2$) to catalyze the coupled reaction. The reactive intermediate indole is transferred from α subunit to the subunit β through a physical tunnel that is only 25 Å long (Rhee et al., 1997). The pyruvate dehydrogenase complex also exhibits cooperatively efficient catalytic principles (Smolle and Lindsay, 2006).

Drawing inspiration from these efficient MECs in Nature, researchers have devoted efforts to reconstitute MECs *in vitro* with precise engineering design (Dalal et al., 2007; Vinu et al., 2004; Watanabe and Ishihara, 2005). Applying single enzyme immobilization techniques in constructing artificial MECs is a common strategy. Numerous single enzymes have been successfully immobilized on various carriers using distinct attachment techniques to achieve reusability. Many immobilized enzymes have even been applied in industrial production (Brady and Jordaan, 2009). Compared to free enzymes in solution, immobilized enzymes exhibit superior performance under harsh environments such as high temperature and extreme pH and can be regenerated and used multiple times (Hanefeld et al., 2009; Heredia et al., 2005; Iyer and Ananthanarayan, 2008). To combinatorially exploit the highly efficiently cooperative catalytic mechanism of MECs and harness the benefits of enzyme immobilization, it is rational to develop appropriate techniques to co-localize multiple enzymes on carriers.

Methods for co-localizing multiple enzymes are based on techniques that have been developed for single enzyme immobilization. Hence, the challenges faced in single enzyme immobilization still need to be addressed to realize efficient multi-enzyme co-localization. Attachment techniques need to be engineered to maintain enzyme activity, since the delicate functionality and fragile structures of enzymes make them sensitive to environmental conditions (Hanefeld et al., 2009; Hua-Jun et al., 2008; Sheldon, 2007). Improper linkage of the amino acids to the carriers could cause unfavorable conformational changes, leading to blockage of access of the substrates to the active sites, and thus loss of enzymatic activity (Hermanson, 2008). In multi-enzyme co-localization, due to the variability of individual enzymes' tolerance for a specific attachment method, the structure and function of each enzyme component needs to be taken into consideration for selecting appropriate attachment techniques. The design of

enzyme-compatible carriers with high loading capacity is another aspect to consider. For example, strong non-specific interactions between proteins and hydrophobic platforms could induce undesirable folding of proteins and jeopardize enzymatic activity. Meanwhile, porous materials provide large surface areas that are able to accommodate large quantities of enzyme molecules. But the inherent internal diffusion resistances involved may present complications when co-localizing multiple enzymes of different sizes inside the pores. A unique challenge in co-localization is to effectively control the relative positions of multiple enzymes on the platform. In MECs, the enzyme subunit components are associated tightly to enable a highly cooperative catalytic mechanism. Therefore, to mimic the functionality of MECs, enabling proximity of the active sites on different enzymes in co-localization is critical. The shared structural characteristics of different enzymes make it difficult to differentiate one enzyme from another during immobilization. Selectively immobilizing enzymes on the platform is not straightforward. In addition, unlike small molecules, the typical large size of enzymes (>10 kDa) results in large steric effects that prevent immobilization in a compact way, which impacts the ability to co-localize multiple enzymes in close proximity to one another.

This review discusses and analyzes the various approaches used in multiple enzyme co-localization by focusing on the: (1) different attachment techniques used in enzyme immobilization and multiple co-localization and their impact on the overall enzyme activity; and (2) various platforms and spatial control strategies developed that play a significant role in co-localization of multiple enzymes. Table 2.1 presents a summary of recent representative work on multi-enzyme co-localization, wherein aspects such as different attachment techniques, platforms, enzyme models, and improvements in kinetics are listed and compared for each work.

2.2 Attachment techniques

The attachment techniques used to immobilize enzymes result in creating interactions between the enzymes and the carriers, which directly impacts enzymatic activity. Thus, appropriate attachment techniques need to be engineered to maintain the enzyme activity, since the delicate functionality along with fragile structures make enzymes sensitive to the environment. In many cases, attachment of enzymes to the carriers could cause unfavorable conformational changes of the enzymes, leading to loss of enzymatic activity. In multi-enzyme co-localization, the structure and function of each enzyme component needs to be taken into consideration in selecting appropriate attachment techniques. In this section, attachment techniques such as multi-point covalent binding, physical entrapment, physical adsorption, site-specific affinity interaction, and DNA directed self-assembly are discussed. A representative scheme of each technique is shown in Fig. 2.1.

2.2.1 Multi-point covalent binding

Multi-point covalent binding is one of the strongest chemical bonds used to immobilize enzymes. The primary abundant free functional groups on the amino acids, mainly located on the outer surface of the protein structure, serve as attachment points for the enzymes. The most common covalent attachments are amide linkages, where the amine groups on amino acids such as lysine react with the carboxyl groups on the carriers. Facilitated by reaction activators such as carbodiimide, carboxylic groups can be functionalized into active esters using *n*-hydroxysuccinimide (NHS), which can promote reaction rates to form stable amide bonds (Edlund et al., 2011; Hua-Jun et al., 2008; Park et al., 2010; Raghava et al., 2006; Saxena et al., 2011; Zhang et al., 2010). In addition, epoxy and aldehyde are often reacted with amine groups on the enzymes for immobilization (Betancor et al., 2006; Choi et al., 2005; Jonkheijm et al., 2008).

Conversely, the available carboxyl groups on amino acids (such as aspartic acid and glutamic acid) can also react with the amine groups on the carriers to immobilize enzymes (Jonkheijm et al., 2008). The thiol groups on cysteine, which create internal disulfide bonds in enzymes, can also be used to react with maleimide and disulfide, but cysteine is not usually as abundant as lysine in many enzymes. In previous work, it was shown that covalently immobilized glucose oxidase (GOX) on magnetite nanoparticles exhibited better enzymatic activity compared to free GOX in solution (Fig. 2.2) due to favorable conformational change of the enzyme (Rossi et al., 2004). Ju *et al*. covalently immobilized alpha-chymotrypsin onto magnetic Fe_3O_4-chitosan nanoparticles. Optimal immobilization conditions were identified, under which the product yield catalyzed by immobilized enzyme was comparable to that of free enzyme and over 60% of the enzymatic activity was retained after using the system twelve times (Ju et al., 2012). Covalent binding has also been used to conjugate small molecules such as fluorescent probes, as well as proteins, to the enzymes (Lin and Wang, 2008). In multi-covalent binding, the attachment points on the enzymes are relatively randomized, which implies lack of control on the position of enzyme structures. In some cases, covalent binding could induce unfavorable conformational changes in the protein structure, which could reduce enzymatic activity significantly (Jordao et al., 1996; Murtinho et al., 1998; Scotti and Hutchinson, 1995).

2.2.2 Physical entrapment

Typically, physical entrapment is a process where the biomolecules or enzymes are confined within the carrier materials during gelation or cross-linking processes (Gupta and Chaudhury, 2007). During physical gelation, at low temperature or with addition of certain polymers, salts or due to a phase inversion process, solvents are removed. In the cross-linking process, initiated by either chemical or photo irradiation-

based initiators, monomer or co-monomers can be polymerized and cross-linked (Kudaibergenov et al., 2012). Geometrically, the carriers can be made into thin films, beads, or fibers (Tischer and Wedekind, 1999). Since the physical entrapment does not involve the attachment or modification of the enzymes, it is suitable for those enzymes that are significantly deactivated by covalent binding. However, due to embedment within the carriers, there is significant diffusion resistance for the substrates and intermediates traveling inside the carrier network during catalytic processes. If there is incompatibility with the monomer or precursor of the materials, the enzymes can lose activity, but this issue can be addressed by using biocompatible materials. Recent research has investigated co-immobilizing multiple enzymes by physical entrapment to enhance catalytic efficiency for cascaded reactions (Aranaz et al., 2003). The well-known GOX/horseradish peroxidase (HRP) system has been investigated extensively as a model system for multi-enzyme co-localization. Rupcich and Brennan co-immobilized two coupled enzyme systems, GOX/HRP and urease/fluorescein dextran, by pin-printing in sol-gel biomaterials (Rupcich and Brennan, 2003).The change in intensity from the assay was found to be time-dependent and consistent with the enzyme catalyzed reaction. However, the overall enzymatic kinetic activity in both cases was not significantly increased compared to that of the free enzymes in solution. Another example is that of Nakane and co-workers who co-immobilized malic and alanine dehydrogenase on gel fibers as shown in Fig. 2.3A (Nakane et al., 2010). It was demonstrated that although the cascaded enzyme activity was only approximately one fifth of the activity of the free enzymes, the productivity after multiple uses was still very high (Fig. 2.3B).

2.2.3 Physical adsorption

In passive physical adsorption, enzymes can be immobilized on carriers through intermolecular polar, hydrophobic interactions and ionic bonds, which are unstable compared to covalent binding (Daly et al., 2005; Pai et al., 2010; Pai et al., 2012; Rusmini et al., 2007). The adsorbed enzymes form separate heterogeneous layers on the carrier surface and the capacity of the enzymes is typically limited by steric hindrance. The orientation of the adsorbed enzymes is randomized because of the interactions between the enzymes and the carriers. Pescador and co-workers (Pescador et al., 2008) used polyelectrolyte layers to assemble the GOX and HRP together on the surface of microparticles, where the net negatively charged GOX and HRP interact with the polyelectrolyte layers via electrostatic forces (Fig. 2.4A). As shown in Fig. 2.4B, it was found that the enzymes adsorbed in the same layer showed higher overall enzymatic activity compared to the enzymes in separated layers and free enzyme control. Kreft and co-workers (Kreft et al., 2007) prepared micro-sized shell-in-shell polyelectrolyte particles to co-immobilize GOX and HRP into different compartments, where the H_2O_2 produced in the outer surrounding GOX region diffused into the inner HRP compartment (SEM images of the structure are shown in Fig. 2.5), and the final product (resorufin) accumulated inside the HRP compartment (Fig. 2.5). However, similar to multi-point covalent binding, the interactions that occur in adsorption processes are generally less controllable with respect to the position of amino acid residues that are attached to the carriers. Without proper attachment strategies, the resulting conformation of enzymes after immobilization could be affected, which may be detrimental to the original structural configuration for distinct functionality (Esawy et al., 2008; Hanefeld et al., 2009; Toogood et al., 2002).

2.2.4 Site-specific affinity attachment

2.2.4.1 Histidine-Nickel binding

To protect the original orientation of the enzyme organization against unfavorable changes by non-specific interactions such as covalent binding or physical adsorption with the carrier surface, polyhistidine linkers can be genetically tagged on the recombinant enzymes to accurately capture the specific binding functional groups, typically nitrilotriacetic acid (NTA), on the carriers. In his-NTA binding, two imidazole groups on the his-tagged enzymes indirectly interact with the functional groups on the carrier via one nickel ion molecule to form an octahedral coordination structure. Previously these strategies were developed in protein purification with column chromatography (Turkova, 1999). The targeting protein molecules can be removed by addition of ethylenediaminetetraacetate (EDTA) or imidazole. This methodology has also been used for directing the attachment of proteins on carriers. Wegner and co-workers (Wegner et al., 2003) delivered multiple his-tagged proteins in NTA–functionalized self-assembled monolayers using parallel microchannels in microfluidic devices. Therefore, the interactions of antibody/antigen binding and subsequent interactions of double-stranded DNA with TATA box were monitored and it was demonstrated that the fusion protein activity was retained. Shimada and co-workers (Shimada et al., 2012) prepared DNA-enzyme conjugates using his-tag chemistry that can protect enzymes from denaturation on surfaces. In their study, the DNA was functionalized with NTA, attaching to the his-tag alkaline phosphatase in the presence of Ni^{2+} ion. The resulting DNA-enzyme conjugates were used for detection of thrombin.

2.2.4.2 Avidin-biotin binding

Avidin-biotin linkage is another popular bioaffinity attachment technique. Avidin or streptavidin proteins comprised of four identical subunits can bind up to four biotin

molecules and form a strong bond ($K = 10^{13} – 10^{15}$ M^{-1}) (Weber et al., 1989). Originally such techniques were widely used in affinity chromatography for protein purification. Compared to other affinity attachment strategies, avidin-biotin bonds form rapidly and stably under wide ranges of temperature and pH conditions. Using an enzyme linked immunosorbent assay, streptavidin-tagged HRP can bind biotinylated antibody to amplify the assay signals. For even better signal amplification, more complicated avidin-biotin complexes can be built to attach more enzymes to carry out the reaction that can be used to further boost amplified signals. In the enzyme immobilization arena, similar to the his-tag attachment strategy, streptavidin-biotin linkages can protect the enzyme from directly contacting the carrier surface, which causes denaturation of the enzyme in most cases. Yu and co-workers (Yu et al., 2012) fabricated streptavidin functionalized magnetic nanoparticles to immobilize C-terminus biotin labeled sialytransferase from *Neisseria gonorrheae* and demonstrated immobilization under mild experimental conditions (Fig. 2.6A). The enzymatic activity also showed better performance under harsh conditions (i.e., high temperature and pH). Almost 50% enzymatic activity was retained after being used ten times (Fig. 2.6B). Seong and Crooks (Seong and Crooks, 2002) designed a novel microfluidic system, where the biotin labeled GOX and HRP immobilized on streptavidin tagged PS beads were retained in well-defined micro-reactor zones. The final product was obtained by enabling the flow of the reactants through one or two sequential reactor zones. As shown in Fig. 2.7, the beads played a significant role in facilitating better mixing and served as catalyst supports.

2.2.5 DNA hybridization directed self-assembly

In multiple enzyme co-localization the spatial orientation and organization of each enzyme component is critical since it directly determines whether the multiple enzymes are close enough to synergistically catalyze the reactions. Recently, researchers have

utilized DNA to direct the immobilization and co-localization of multiple enzymes in order to spatially control their relative positions. The unique Watson-Crick base paring mechanism of DNA provides a powerful tool to arrange the relative positions of multiple enzymes in space, which is otherwise not readily achievable by other attachment techniques. The stability issues associated with most biomolecules can be alleviated with the use of DNA hybridization, which requires relatively mild conditions such as moderate pH and temperature. The controllable sequence length and base pairs of DNA provides a high degree of flexibility in regulating the positions of the multiple enzymes.

Niemeyer *et al*. (Niemeyer et al., 2002) first reported co-localization of nicotinamide adenine dinucleotide (NADH): flavin mononucleotide (FMN) oxidoreductase and luciferase (Luc) that catalyze cascaded reactions via DNA hybridization, which resulted in significant improvement in the overall enzymatic activity (Fig. 2.8). In later work, the same group designed two distinct oligonucleotides and respectively attached them onto GOX and HRP via covalent binding (Müller and Niemeyer, 2008). Complementary DNA sequences bound to the microtiter plate were used to capture the enzyme-DNA conjugates. Through gel electrophoresis, it was shown that positional and steric factors played significant roles in both DNA-enzyme conjugates. Further kinetics experiments also showed the superiority of co-localizing both enzymes on the same strand as compared to separated immobilized enzyme-DNA mixtures. Wang and co-workers (Wang et al., 2009), designed nanowires by generating circular DNA components hybridized by short nucleic acids in the presence of cocaine to co-localize GOX and HRP. The two enzymes were attached to the circular DNA to exhibit ~6-fold overall activity enhancement when compared to that of a homogeneous mixture of enzymes in solution. Moreover, Wilner and co-workers (Wilner et al., 2009) designed programmed DNA scaffolds, specifically two-hexagon and four-hexagon nanostructures,

to self-assemble either two enzymes or cofactor-enzyme pairs. It was shown that the enzyme cascades or cofactor-mediated catalysis proceeded effectively, in comparison to mixtures of the equivalent components (Fig. 2.9). Freeman and coworkers (Freeman et al., 2009) studied supramolecular cocaine-aptamer complexes for cascaded enzymatic catalyzed reactions, which were shown to control biocatalytic transformations that do not proceed in free random enzyme systems.

2.3 Platforms for enzyme immobilization and co-localization

In addition to the attachment techniques, the specific platforms onto which enzymes are loaded play a significant role in enzyme immobilization and co-localization. The properties of the platform materials determine the interactions between the enzyme and the carrier platforms. Less compatible materials tend to involve more non-specific interactions that cause unfavorable structural change of enzymes, resulting in loss of activity. In this section, porous materials, non-porous nanoparticles, and cross linked enzyme aggregates (CLEAs) and their corresponding applications in enzyme immobilization and co-localization are discussed.

2.3.1 Porous materials

2.3.1.1 Polymer monoliths

The use of porous monoliths as enzyme immobilization supports emerged two decades ago (Abou-Rebyeh et al., 1991). Monoliths provide unique advantages for immobilizing proteins because of their large surface area, easily accessible functional groups on the surface, and flexibility in fabrication into various geometries (Mallik and Hage, 2006). Compared to silica monoliths, organic polymer monoliths have greater flexibility in terms of chemistry and better biocompatibility with biomolecules (Barton et al., 1999; Samanidou and Karageorgou, 2011; Zhu and Row, 2012). In general, polymer

monoliths are stable in most solvents, at extreme pH levels, and need lower operational pressures. The enzymes can be attached on the surface of the pores by adsorption, covalent binding, entrapment, or the other specific linkages discussed earlier (Krenkova and Svec, 2009). Polymer monoliths have been used to immobilize multiple enzymes into segregated compartments or regions in channel-reactor platforms. By pumping the substrate solution through the segregated enzyme-localized region, each reaction step occurs along with the flow of the substrate, and the intermediates produced in the previous step are used as substrate in the next reaction step. The reaction is then controlled by flow direction and flow rate. Logan and co-workers (Logan et al., 2007) separately photo-patterned multiple enzymes in the polymer monolith to investigate a sequential multi-step cascade reaction (Fig. 2.10). GOX and HRP were covalently immobilized in segregate regions of a porous polymer monolith and a substrate solution containing dextrose and Amplex Red was pumped through the column. Significant product formation occurred only when the substrate was introduced in the GOX-to-peroxidase direction. Then, a third enzyme was added and a three-enzyme sequential reaction was performed using immobilized invertase, GOX, and HRP and a mixture of saccharose and Amplex Red as substrates. All six possible arrangements of the three enzymes were tested, and significant product formation was only observed when the enzymes were in the correct sequential order (Logan et al., 2007).

2.3.1.2 Mesoporous silica nanoparticles

Mesoporous silica nanoparticles (MSNs), whose pore sizes typically range from 2 to 50 nm, are some of the most commonly used porous platforms to immobilize enzymes (Popat et al., 2011). Physical adsorption is the main attractive force to retain the enzymes inside the MSNs. The development of MCM-41 has attracted a lot of attention due to its large loading capacity for enzymes originating from an oriented-ordered pore

structure with high surface area and pore volume (Trewyn et al., 2007; Wada et al., 2009). The MCM-41 type materials are most suitable for small enzymes (< 4 nm) (Diaz and Balkus, 1996), because the pore size inherently limits the accessibility of larger enzymes to internal pores. SBA-15, which has a larger pore size (5-13 nm) has allowed the use of MSNs to immobilize larger enzymes (Sun et al., 2006). Many examples have demonstrated the capability of MSNs as supporting platforms for enzyme immobilization. Lysozymes can be adsorbed in pore-enlarged conventional SBA-15, which has great promise for enzyme separations (Sun et al., 2006). It was shown that by entrapping organophosphorus hydrolase in functionalized MSNs with 30 nm open pore size, the enzymatic activity was enhanced by 2-fold and the stability of the enzyme was also preserved (Lei et al., 2002). Hollow silica spheres with ordered hexagonal mesopores arranged in the shell showed extremely rapid (<5 min to reach equilibrium) lysozyme immobilization rate with high adsorption capacity (>500 mg g^{-1}) (Liu et al., 2007). The pore size of the mesoporous materials has a significant effect on enzyme loading efficiency and immobilized enzyme activity (Fadnavis et al., 2003; Fan et al., 2003b). Large enzyme molecules cannot enter the small pores in mesoporous materials. On the other hand, pores that are too large may lead to leaching out of the enzyme. Thus, size matching of the pores and enzymes is important to stabilize the enzymes, but this makes the use of MSNs challenging for multi-enzyme co-localization, especially when different sized enzymes are involved. Additionally, modifying the internal pore surface is sometimes necessary to strengthen the bonding between the enzymes and the supports (Diaz and Balkus, 1996; Fan et al., 2003a; Takahashi et al., 2001; Vinu et al., 2004).

2.3.2 Non-porous nanoparticles

Nanoparticles have a distinct advantage for enzyme immobilization and co-localization, because of their inherently large surface area per unit volume, providing a

large capacity for accommodating biomolecules. It has been reported that up to 10 wt.% effective enzyme loading can be achieved on nanoparticles (Chen and Su, 2001). Attachment of enzymes on nanoparticle surfaces also significantly avoids the internal diffusion resistances observed with porous materials. Numerous experimental and theoretical studies have shown that the unique mobility behavior of dispersed nanoparticles in solution impacted the retention of the intrinsic activity of particle-attached enzymes (Jia et al., 2003; Sassolas et al., 2012; Zheng et al., 2011). For multiple enzyme co-localization the use of nanoparticles has been investigated as a novel approach to spatially locate the multiple enzymes in close proximity to each another on the same nanoparticle. Many researchers have reported the significance of co-localizing multiple enzymes in the same layers on the particle surface (Keighron and Keating, 2010; Nakane et al., 2010; Pescador et al., 2008). In these studies, multiple enzymes were co-localized on the nanoparticles by adsorption on non-porous nanoparticles in distinct ways to form egg-like architectures. The rigid support materials serve as cores surrounded by coronas of randomly distributed multiple enzymatic layers. The larger the nanoparticles, the higher the probability that different types of enzymes can be loaded on the same nanoparticles.

2.3.2.1 Gold nanoparticles

The excellent biocompatibility of gold has led researchers to use gold nanoparticles as supporting materials for attaching enzymes. Chirra *et al*. (Chirra et al., 2011) investigated immobilized catalase on gold nanoparticles by covalent binding and biotin-streptavidin coupling. They found that even though carbodiimide chemistry-activated coupling caused a decrease in enzyme activity compared to the biotin-streptavidin coupled approach, it showed more active catalase per gold nanoparticle compared with that of biotinylated gold nanoparticles. Li *et al*. showed that covalently

immobilized GOX on gold nanoparticles exhibited enhanced thermal stability and comparable pH-dependent behavior compared with free enzymes (Li et al., 2007). For multiple enzyme co-localization, Keating and Keighron co-immobilized malate dehydrogenase and citrate synthase on gold nanoparticles in three different ways, as shown in Fig. 2.11 (Keighron and Keating, 2010). It was found that the sequential order of enzymes adsorbed on gold nanoparticles affected the overall product conversion rate. In addition to attaching enzymes on the bare gold nanoparticles, gold nanoparticles have also been also hybridized with other materials such as carbon nanotubes, sol-gels, and polymers to prevent agglomeration (Pingarron et al., 2008). The capability of facilitating electron transfer between the immobilized enzyme and electrode has also made gold nanoparticles suitable for biosensor fabrication. Compared with other carbon composite electrodes, gold nanoparticles provide a mediator-less glucose biosensor with a remarkably higher sensitivity compared to other GOX–carbon nanotube (CNT) bioelectrodes (Manso et al., 2007). The gold nanoparticles can also be mixed with polymers to design nanocomposite bioelectrodes. Xian *et al*. designed a glucose biosensor using gold nanoparticles and conductive polyaniline to immobilize GOX and Nafion on the surface of nanocomposites, which showed excellent reproducibility and operational stability (Xian et al., 2006). An example of the application of sol-gels with gold nanoparticles is to entrap acetylcholinesterase (AChE) with gold nanoparticles within sol-gel based silica materials. In this configuration, the AChE can catalyze the growth of the gold nanoparticles that can be correlated to the amount of substrate or inhibitor detected in the test solution (Luckham and Brennan, 2010).

2.3.2.2 Polymeric nanoparticles

Like gold nanoparticles, amphiphilic core-shell polymeric particles have attracted much attention due to their versatile surface chemistry and structure as well as

biocompatibility. Enzymes can be attached onto polymeric nanoparticles via physical adsorption, covalent bonding, cross-linking or a combination thereof (Akgol et al., 2009; Daubresse et al., 1994; Matsuno and Ishihara, 2009; Palocci et al., 2007; Watanabe and Ishihara, 2004). Various polymeric materials and immobilization strategies have been designed for attaching enzymes. Caruso *et al*. used polyelectrolytes to confine charged proteins or enzymes and deposited them on polystyrene surfaces through electrostatic interaction to form uniform “core-shell” 600 nm particles (Caruso and Möhwald, 1999). In Kang’s work, amphiphilic particles fabricated using poly((methyl methacrylate-co-ethyl acrylate)-co-acrylic acid) were used to covalently immobilize trypsin and it was shown that the thermal and chemical stabilities were greatly improved for the immobilized enzymes compared to their free counterparts (Kang et al., 2005). Even after reuse ten times, over 63% of the initial activity was still maintained. Karagoz and co-workers synthesized “hair-like” poly(styrene-b-glycidylmethacrylate) brushes via atom transfer radical polymerization on bromoacetylated poly(styrene-divinylbenzene) and covalently immobilized lipase on microspheres (Karagoz et al., 2010). The immobilization was found to be effective in enhancing both thermal and storage stability. In addition, the large specific surface area led to high loading efficiency of the enzymes on the polymeric nanoparticles. Haupt *et al*. showed that when glucoamylase and β-glucosidase were individually immobilized on polyelectrolyte brushes of poly (acrylic acid) or poly(styrene sulfonic acid)-polystyrene based core–shell nanoparticles, the enzymes were able to maintain activity and loading efficiencies as high as 600 mg/g were attained (Haupt et al., 2005). Miletic and co-workers immobilized *Candida Antarctica* lipase on polystyrene nanoparticles by adsorption (Miletić et al., 2010). A high loading efficiency of 240 mg/g was reported, independent of pH. The product performance was superior to that of the crude enzyme powder and commercial novozyme 435. For multi-enzyme co-localization, in Watanabe’s work, ACHE, choline oxidase, and HRP were co-localized on

phospholipid/polystyrene core-shell nanoparticles by adsorption (Watanabe and Ishihara, 2005). The sequential enzymatic reactions catalyzed by this product were significantly higher than that of the free enzyme mixture. Jia et al. (Jia et al., 2012) designed quantum dot-incorporated block copolymer micelles as a platform to co-localize GOX and HRP by adsorption (Fig. 2.12A). The adsorption of individual enzymes and co-localization of both types of enzymes were characterized by Förster resonance energy transfer (FRET) studies. The overall conversion rate was improved by about 100% compared to equivalent concentrations of free enzymes in solution (Fig. 2.12 B). In a related study, the same enzymes were sequentially co-localized on biotin and carboxyl functionalized polystyrene nanoparticles (Fig. 2.13A) (Jia et al., 2013). The catalytic performance of the co-localized GOX and SHRP system was about 2-fold higher than that of equivalent amounts of the free enzymes in solution and a mixture of nanoparticles with immobilized GOX and SHRP alone (Fig. 2.13B).

In addition, aluminum, silica and magnetic nanoparticles have been used for enzyme immobilization and co-localization. Crestini and coworkers co-localized laccase and HRP using cross linking and Layer-by-Layer coating with polyelectrolyte (Crestini et al., 2011) and the synergistic effect of the co-localized enzymes was demonstrated. Garcia and co-workers investigated the co-localization of GOX and HRP on magnetic nanoparticles by forming multiple layers (Garcia et al., 2011). The overall enzymatic activity increased linearly with the number of HRP layers. The HRP magnetic nanoparticle system was also suitable for reuse upon application of an external magnetic field. The co-localized bi-enzyme system was used for rapid detection of glucose at micromolar concentration levels (Garcia et al., 2011).

2.3.2.3 Cross-linked enzyme aggregates (CLEAS)

Platform-less methods have also been designed in constructing artificial MECs. Unlike conventional enzyme immobilization, where the enzymes are attached onto supporting materials by physical entrapment, chemical binding or physical interactions, cross-linking of enzyme aggregates (CLEAs) does not require platform carriers. Instead, multiple enzyme components are cross-linked in a precipitation process by addition of organic solvents, salts or ionic polymers, or bi-functional linkers. Similar to conventional immobilization, the CLEAs render the enzymes more stable under harsh conditions including a broader range of pH and temperature. The CLEAs can also be reused several times. Dalal *et al*. reported that a combi-CLEA composed of cross-linked multiple enzymes retained up to 100% activity compared to that of free enzymes and could be reused twice (Dalal et al., 2007). A drawback of using CLEAs is that the activity of the enzymes could be lost during the harsh cross-linking process (Sheldon et al., 2005). The aggregates typically tend to be water insoluble, which could potentially involve a large diffusion resistance for colorimetric reactions catalyzed by the enzymes (Soares et al., 2011).

2.4 Conclusions and future perspectives

Biocatalysts have been widely studied in both scientific and industrial settings due to their energy efficient catalytic mechanisms, unique selectivity for substrates, and enhanced stability under harsh reaction environments. The widely existing MECs in Nature have inspired researchers to design synthetic analogs to co-localize multiple enzymes in order to mimic the MECs' unique functionalities in promoting the overall catalytic efficiency *in vitro*. Over the past couple of decades, numerous multiple enzyme co-localization approaches have been developed, which have shown great potential in enhancing the overall enzymatic performance.

Multiple enzyme co-localization shares many common features with single enzyme immobilization. The various attachment techniques used in single enzyme immobilization studies have been applied to multiple enzyme co-localization and they have a direct impact on the overall enzyme orientation and activity. Multi-point covalent binding is relatively strong and robust as opposed to non-specific adsorption. New site specific attachments such as biotin-streptavidin affinity linkages which can tolerate a wide range of operating conditions provide more options in selecting appropriate attachment techniques. In controlling the relative positions of different enzymes in a confined space, biomolecular scaffolds based on DNA hybridization can be particularly valuable for multi-enzyme co-localization. For carrier-based strategies, the various types of platforms developed for single enzyme immobilization again provide starting points for attaching and co-localizing multiple enzymes. Porous carriers have large surface areas to accommodate enzymes inside the carriers, but they inevitably involve internal diffusion resistance in enzyme immobilization and reaction process when enzymes, substrates, and products are transported. Non-porous nanoparticle platforms provide advantageous characteristics for enzyme immobilization and co-localization due to their inherently large surface area for attaching enzymes and their solution properties in catalytic processes.

In addition to the above-mentioned materials-based approaches, biological approaches have also been explored for multi-enzyme co-localization. Specific protein scaffolds can be biologically designed to bring the active sites on the enzymes in proximity to each other by using specific binding between the protein domains on the scaffolds and that of the targeted enzymes. In a recent study, Chen and co-workers (Liu et al., 2013) designed a protein scaffold and functionally expressed it in *Escherichia coli* to direct co-localization of the dehydrogenase-based multi-enzyme cascade on yeast

surfaces. The three different types of dehydrogenases self-assembled along the scaffold via high affinity interactions between three orthogonal-dockering pairs. The co-localized enzymes exhibited significantly higher NADH generation rates in comparison to equivalent free enzyme mixtures in solution (Liu et al., 2013). In contrast to the materials-based approaches, the use of biological approaches provides a more biomolecule-compatible strategy to direct multi-enzyme co-localization. Protein scaffolds can also be used to precisely define the relative positions of multiple enzymes by appropriate design, which is similar to DNA-directed co-localization. Hybrid methods that combine biological and materials-based approaches that will provide compatible and sustainable platforms to co-localize multiple enzymes will be an area of active research in the future.

In multi-enzyme co-localization, the involvement of multiple components and co-localization also brings unique challenges. The various properties of the different enzymes (e.g., size, conformational stability) makes the co-localization process more complicated and a careful and rational selection of appropriate attachment techniques and platforms is necessary to retain enzymatic activity and improve performance. In addition, the relative positions of the multiple enzymes in a confined space plays a significant role in affecting the interaction between different enzymes, making spatial control an important feature in co-localization. Current multi-enzyme co-localization has demonstrated the kinetic benefits in terms of promoting overall turnover number for multiple enzymes. Future studies will need to focus on the stability of the co-localized enzymes for sustainable activity with multiple uses.

In summary, in order to achieve optimized multi-enzyme co-localization, it is important to consider the following perspectives: (1) The structure and function of each enzyme component needs to be carefully considered for multi-enzyme co-localization; (2)

Appropriate attachment techniques and carrier platforms need to be rationally selected for all the enzymes; (3) Insights gained from single enzyme immobilization studies need to be used to optimize the reaction conditions for retaining the activity of the attached enzymes during co-localization; and (4) Using the above considerations, novel strategies need to be developed for single enzyme immobilization and co-localization. Overall, current research has amply demonstrated the superior potential of co-localized multiple enzymes in terms of kinetically-driven benefits. Looking forward, the design of sustainable and re-usable multi-enzyme biocatalysts would lead to both scientifically exciting research as well as economically viable designs for next generation catalysts and biosensors.

Acknowledgments

The authors are grateful to the National Science Foundation (CBET 0932517) for financial support. B.N. acknowledges the Vlasta Klima Balloun Professorship in Chemical and Biological Engineering and SKM acknowledges the Stanley Chair in Interdisciplinary Engineering.

References

Abou-Rebyeh H, Körber F, Schubert-Rehberg K, Reusch J, Josić D. 1991. Carrier membrane as a stationary phase for affinity chromatography and kinetic studies of membrane-bound enzymes. *Journal of Chromatography B: Biomedical Sciences and Applications* **566**:341–350.

Akgol S, Ozturk N, Denizli A. 2009. New Generation Polymeric Nanospheres for Catalase Immobilization. *J. Appl. Polym. Sci.* **114**:962–970.

Ansari SA, Husain Q. 2012. Potential applications of enzymes immobilized on/in nano materials: A review. *Biotechnology Advances* **30**:512–523.

Aranaz I, Ramos V, Escalera SDL, Heras A. 2003. Co-immobilization of D-hydantoinase and D-carboamylase on Chitin: Application to the Synthesis of p-hydroxyphenylglycine. *Biocatal. Biotransform* **21**:349–356.

Barnes S, Weitzman P. 1986. Organization of Citric-Acid Cycle Enzymes into a Multienzyme Cluster. *FEBS Lett.* **201**:267–270.

Barton TJ, Bull LM, Klemperer WG, Loy DA, McEnaney B, Misono M, Monson PA, Pez G, Scherer GW, Vartuli JC, Yaghi OM. 1999. Tailored porous materials. *Chem. Mat.* **11**:2633–2656.

Betancor L, Lopez-Gallego F, Hidalgo A, Alonso-Morales N, Dellamora-Ortiz Cesar Mateo G, Fernandez-Lafuente R, Guisan JM. 2006. Different mechanisms of protein immobilization on glutaraldehyde activated supports: Effect of support activation and immobilization conditions. *Enzyme Microb. Technol.* **39**:877–882.

Brady D, Jordaan J. 2009. Advances in enzyme immobilisation. *Biotechnol. Lett.* **31**:1639–1650.

Caruso F, Möhwald H. 1999. Protein Multilayer Formation on Colloids through a Stepwise Self-Assembly Technique. *J. Am. Chem. Soc.* **121**:6039–6046.

Chen JP, Su DR. 2001. Latex particles with thermo-flocculation and magnetic properties for immobilization of alpha-chymotrypsin. *Biotechnol. Prog.* **17**:369–375.

Chirra HD, Sexton T, Biswal D, Hersh LB, Hilt JZ. 2011. Catalase-coupled gold nanoparticles: Comparison between the carbodiimide and biotin-streptavidin methods. *Acta Biomater.* **7**:2865–2872.

Choi HJ, Kim NH, Chung BH, Seong GH. 2005. Micropatterning of biomolecules on glass surfaces modified with various functional groups using photoactivatable biotin. *Anal. Biochem.* **347**:60–66.

Cohn MA, Kee Y, Haas W, Gygi SP, D'Andrea AD. 2009. UAF1 Is a Subunit of Multiple Deubiquitinating Enzyme Complexes. *J. Biol. Chem.* **284**:5343–5351.

Conrado RJ, Varner JD, DeLisa MP. 2008. Engineering the spatial organization of metabolic enzymes: mimicking nature's synergy. *Current Opinion in Biotechnology* **19**:492–499.

Crestini C, Melone F, Saladino R. 2011. Novel multienzyme oxidative biocatalyst for lignin bioprocessing. *Bioorg. Med. Chem.* **19**:5071–5078.

Dalal S, Kapoor M, Gupta MN. 2007. Preparation and characterization of combi-CLEAs catalyzing multiple non-cascade reactions. *J. Mol. Catal. B-Enzym.* **44**:128–132.

Daly SM, Przybycien TM, Tilton RD. 2005. Adsorption of poly(ethylene glycol)-modified ribonuclease A to a poly(lactide-co-glycolide) surface. *Biotechnology and Bioengineering* **90**:856–868.

Daubresse C, Grandfils C, Jerome R, Teyssie P. 1994. Enzyme Immobilization in Nanoparticles Produced by Inverse Microemulsion Polymerization. *J. Colloid Interface Sci.* **168**:222–229.

Diaz JF, Balkus KJ. 1996. Enzyme immobilization in MCM-41 molecular sieve. *J. Mol. Catal. B-Enzym.* **2**:115–126.

Edlund U, Sauter T, Albertsson A-C. 2011. Covalent VEGF protein immobilization on resorbable polymeric surfaces. *Polym. Adv. Technol.* **22**:166–171.

Esawy MA, Mahmoud D a. R, Fattah AFA. 2008. Immobilisation of Bacillus subtilis NRC33a levansucrase and some studies on its properties. *Braz. J. Chem. Eng.* **25**:237–246.

Fadnavis NW, Bhaskar V, Kantam ML, Choudary BM. 2003. Highly efficient "tight fit" immobilization of alpha-chymotrypsin in mesoporous MCM-41: A novel approach using precursor immobilization and activation. *Biotechnol. Prog.* **19**:346–351.

Fan J, Lei J, Wang LM, Yu CZ, Tu B, Zhao DY. 2003a. Rapid and high-capacity immobilization of enzymes based on mesoporous silicas with controlled morphologies. *Chem. Commun.*2140–2141.

Fan J, Yu CZ, Gao T, Lei J, Tian BZ, Wang LM, Luo Q, Tu B, Zhou WZ, Zhao DY. 2003b. Cubic mesoporous silica with large controllable entrance sizes and advanced adsorption properties. *Angew. Chem.-Int. Edit.* **42**:3146–3150.

Freeman R, Sharon E, Tel-Vered R, Willner I. 2009. Supramolecular Cocaine−Aptamer Complexes Activate Biocatalytic Cascades. *J. Am. Chem. Soc.* **131**:5028–5029.

Garcia J, Zhang Y, Taylor H, Cespedes O, Webb ME, Zhou D. 2011. Multilayer enzyme-coupled magnetic nanoparticles as efficient, reusable biocatalysts and biosensors. *Nanoscale* **3**:3721–3730.

Ge J, Lu D, Liu Z, Liu Z. 2009. Recent advances in nanostructured biocatalysts. *Biochem. Eng. J.* **44**:53–59.

Gupta R, Chaudhury NK. 2007. Entrapment of biomolecules in sol–gel matrix for applications in biosensors: Problems and future prospects. *Biosensors and Bioelectronics* **22**:2387–2399.

Hanefeld U, Gardossi L, Magner E. 2009. Understanding enzyme immobilisation. *Chemical Society Reviews* **38**:453.

Haupt B, Neumann T, Wittemann A, Ballauff M. 2005. Activity of Enzymes Immobilized in Colloidal Spherical Polyelectrolyte Brushes. *Biomacromolecules* **6**:948–955.

Heredia KL, Bontempo D, Ly T, Byers JT, Halstenberg S, Maynard HD. 2005. In situ preparation of protein - "Smart" polymer conjugates with retention of bioactivity. *J. Am. Chem. Soc.* **127**:16955–16960.

Hermanson GT. 2008. Bioconjugate Techniques. Academic Press 1234 p.

Hua-Jun Q, Cai-Xia X, Guang-Lei J, Xi-Rong H, Shu-Hua H, Yi D, Yin-Bu Q. 2008. Immobilization of Laccase on Nanoporous Gold and Its Enzymatic Properties. *Acta Chim. Sin.* **66**:2075–2080.

Iyer PV, Ananthanarayan L. 2008. Enzyme stability and stabilization - Aqueous and non-aqueous environment. *Process Biochem.* **43**:1019–1032.

Jia F, Mallapragada S, Narasimhan B. 2013. Biomimetic multi-enzyme complexes based on nanoscale platforms. *AIChE J.* **59**:355–360.

Jia F, Zhang Y, Narasimhan B, Mallapragada SK. 2012. Block Copolymer-Quantum Dot Micelles for Multienzyme Colocalization. *Langmuir* **28**:17389–17395.

Jia H, Zhu G, Wang P. 2003. Catalytic behaviors of enzymes attached to nanoparticles: the effect of particle mobility. *Biotechnology and Bioengineering* **84**:406–414.

Jones SM, van Dyk JS, Pletschke BI. 2012. Bacillus Subtilis Sj01 Produces Hemicellulose Degrading Multi-Enzyme Complexes. *BioResources* **7**:1294–1309.

Jonkheijm P, Weinrich D, Schroeder H, Niemeyer CM, Waldmann H. 2008. Chemical Strategies for Generating Protein Biochips. *Angew. Chem.-Int. Edit.* **47**:9618–9647.

Jordao RCC, daSilva NH, Carvalho LB. 1996. Glyptal as a support for enzyme immobilisation. *Biotechnol. Tech.* **10**:59–62.

Ju H-Y, Kuo C-H, Too J-R, Huang H-Y, Twu Y-K, Chang C-MJ, Liu Y-C, Shieh C-J. 2012. Optimal covalent immobilization of alpha-chymotrypsin on Fe3O4-chitosan nanoparticles. *J. Mol. Catal. B-Enzym.* **78**:9–15.

Kang K, Kan C, Yeung A, Liu D. 2005. The Properties of Covalently Immobilized Trypsin on Soap-Free P(MMA-EA-AA) Latex Particles. *Macromolecular Bioscience* **5**:344–351.

Karagoz B, Bayramoglu G, Altintas B, Bicak N, Arica MY. 2010. Poly(glycidyl methacrylate)-Polystyrene Diblocks Copolymer Grafted Nanocomposite Microspheres from Surface-Initiated Atom Transfer Radical Polymerization for Lipase Immobilization: Application in Flavor Ester Synthesis. *Ind. Eng. Chem. Res.* **49**:9655–9665.

Keighron JD, Keating CD. 2010. Enzyme:Nanoparticle Bioconjugates with Two Sequential Enzymes: Stoichiometry and Activity of Malate Dehydrogenase and Citrate Synthase on Au Nanoparticles. *Langmuir* **26**:18992–19000.

Kim C, Kim D. 1993. Extracellular Cellulolytic Enzymes of Bacillus-Circulans Are Present as 2 Multiple-Protein Complexes. *Appl. Biochem. Biotechnol.* **42**:83–94.

Kreft O, Prevot M, Möhwald H, Sukhorukov GB. 2007. Shell-in-Shell Microcapsules: A Novel Tool for Integrated, Spatially Confined Enzymatic Reactions. *Angewandte Chemie International Edition* **46**:5605–5608.

Krenkova J, Svec F. 2009. Less common applications of monoliths: IV. Recent developments in immobilized enzyme reactors for proteomics and biotechnology. *J. Sep. Sci.* **32**:706–718.

Kudaibergenov SE, Nuraje N, Khutoryanskiy VV. 2012. Amphoteric nano-, micro-, and macrogels, membranes, and thin films. *Soft Matter*. http://pubs.rsc.org.proxy.lib.iastate.edu:2048/En/content/articlehtml/2012/sm/c2sm25766a.

Lei CH, Shin YS, Liu J, Ackerman EJ. 2002. Entrapping enzyme in a functionalized nanoporous support. *J. Am. Chem. Soc.* **124**:11242–11243.

Li D, He Q, Cui Y, Duan L, Li J. 2007. Immobilization of glucose oxidase onto gold nanoparticles with enhanced thermostability. *Biochem. Biophys. Res. Commun.* **355**:488–493.

Lin MZ, Wang L. 2008. Selective labeling of proteins with chemical probes in living cells. *Physiology* **23**:131–141.

Liu F, Banta S, Chen W. 2013. Functional assembly of a multi-enzyme methanol oxidation cascade on a surface-displayed trifunctional scaffold for enhanced NADH production. *Chem. Commun.* **49**:3766–3768.

Liu J, Li C, Yang Q, Yang J, Li C. 2007. Morphological and Structural Evolution of Mesoporous Silicas in a Mild Buffer Solution and Lysozyme Adsorption. *Langmuir* **23**:7255–7262.

Logan TC, Clark DS, Stachowiak TB, Svec F, Fréchet JMJ. 2007. Photopatterning Enzymes on Polymer Monoliths in Microfluidic Devices for Steady-State Kinetic Analysis and Spatially Separated Multi-Enzyme Reactions. *Anal. Chem.* **79**:6592–6598.

Luckham RE, Brennan JD. 2010. Bioactive paper dipstick sensors for acetylcholinesterase inhibitors based on sol-gel/enzyme/gold nanoparticle composites. *Analyst* **135**:2028–2035.

Mallik R, Hage DS. 2006. Affinity monolith chromatography. *Journal of Separation Science* **29**:1686–1704.

Manso J, Mena ML, Yanez-Sedeno P, Pingarron J. 2007. Electrochemical biosensors based on colloidal gold-carbon nanotubes composite electrodes. *J. Electroanal. Chem.* **603**:1–7.

Matsuno R, Ishihara K. 2009. Molecular-Integrated Phospholipid Polymer Nanoparticles with Highly Biofunctionality. *Macromol. Symp.* **279**:125–131.

Miletić N, Abetz V, Ebert K, Loos K. 2010. Immobilization of Candida antarctica lipase B on Polystyrene Nanoparticles. *Macromol Rapid Commun* **31**:71–74.

Müller J, Niemeyer CM. 2008. DNA-directed assembly of artificial multienzyme complexes. *Biochemical and Biophysical Research Communications* **377**:62–67.

Murtinho D, Lagoa AR, Garcia F a. P, Gil MH. 1998. Cellulose derivatives membranes as supports for immobilisation of enzymes. *Cellulose* **5**:299–308.

Najdi TS, Hatfield GW, Mjolsness ED. 2010. A “random steady-state” model for the pyruvate dehydrogenase and alpha-ketoglutarate dehydrogenase enzyme complexes. *Phys. Biol.* **7**.

Nakane K, Suye S, Ueno T, Ohno Y, Ishikawa T, Ogihara T, Ogata N. 2010. Coimmobilization of malic enzyme and alanine dehydrogenase on organic–inorganic hybrid gel fibers and the production of L-alanine from malic acid using the fibers with coenzyme regeneration. *Journal of Applied Polymer Science* **116**:2901–2905.

Niemeyer CM, Koehler J, Wuerdemann C. 2002. DNA-Directed Assembly of Bienzymic Complexes from In Vivo Biotinylated NAD(P)H:FMN Oxidoreductase and Luciferase. *ChemBioChem* **3**:242–245.

Pai SS, Heinrich F, Canady AL, Przybycien TM, Tilton RD. 2012. Coverage-dependent morphology of PEGylated lysozyme layers adsorbed on silica. *J. Colloid Interface Sci.* **370**:170–175.

Pai SS, Przybycien TM, Tilton RD. 2010. Protein PEGylation Attenuates Adsorption and Aggregation on a Negatively Charged and Moderately Hydrophobic Polymer Surface. *Langmuir* **26**:18231–18238.

Palocci C, Chronopoulou L, Venditti I, Cernia E, Diociaiuti M, Fratoddi I, Russo MV. 2007. Lipolytic enzymes with improved activity and selectivity upon adsorption on polymeric nanoparticles. *Biomacromolecules* **8**:3047–3053.

Park S, Pai J, Han E-H, Jun C-H, Shin I. 2010. One-Step, Acid-Mediated Method for Modification of Glass Surfaces with N-Hydroxysuccinimide Esters and Its Application to the Construction of Microarrays for Studies of Biomolecular Interactions. *Bioconjugate Chem.* **21**:1246–1253.

Pescador P, Katakis I, Toca-Herrera JL, Donath E. 2008. Efficiency of a Bienzyme Sequential Reaction System Immobilized on Polyelectrolyte Multilayer-Coated Colloids. *Langmuir* **24**:14108–14114.

Pingarron JM, Yanez-Sedeno P, Gonzalez-Cortes A. 2008. Gold nanoparticle-based electrochemical biosensors. *Electrochim. Acta* **53**:5848–5866.

Popat A, Hartono SB, Stahr F, Liu J, Qiao SZ, Lu GQ (Max). 2011. Mesoporous silica nanoparticles for bioadsorption, enzyme immobilisation, and delivery carriers. *Nanoscale* **3**:2801–2818.

Raghava S, Mondal K, Gupta MN, Pareek P, Kuckling D. 2006. Preparation and properties of thermoresponsive bioconjugates of trypsin. *Artif. Cells Blood Substit. Biotechnol.* **34**:323–336.

Rhee S, Parris KD, Hyde CC, Ahmed SA, Miles EW, Davies DR. 1997. Crystal structures of a mutant (beta K87T) tryptophan synthase alpha(2)beta(2) complex with ligands bound to the active sites of the alpha- and beta-subunits reveal ligand-induced conformational changes. *Biochemistry* **36**:7664–7680.

Rossi LM, Quach AD, Rosenzweig Z. 2004. Glucose oxidase-magnetite nanoparticle bioconjugate for glucose sensing. *Anal. Bioanal. Chem.* **380**:606–613.

Rupcich N., Brennan J.D. 2003. Coupled enzyme reaction microarrays based on pin-printing of sol-gel derived biomaterials. *Analytica Chimica Acta* **500**:3–12.

Rusmini F, Zhong Z, Feijen J. 2007. Protein immobilization strategies for protein biochips. *Biomacromolecules* **8**:1775–1789.

Samanidou VF, Karageorgou EG. 2011. An overview of the use of monoliths in sample preparation and analysis of milk. *J. Sep. Sci.* **34**:2013–2025.

Sassolas A, Blum LJ, Leca-Bouvier BD. 2012. Immobilization strategies to develop enzymatic biosensors. *Biotechnol. Adv.* **30**:489–511.

Saxena U, Chakraborty M, Goswami P. 2011. Covalent immobilization of cholesterol oxidase on self-assembled gold nanoparticles for highly sensitive amperometric detection of cholesterol in real samples. *Biosens. Bioelectron.* **26**:3037–3043.

Schoffelen S, van Hest JCM. 2012. Multi-enzyme systems: bringing enzymes together in vitro. *Soft Matter* **8**:1736–1746.

Scotti C, Hutchinson C. 1995. Immobilization and Properties of Carminomycin 4-O-Methyltranferase, the Enzyme Which Catalyzes the Final Step in the Biosynthesis of Daunorubicin in Streptomyces-Peucetius. *Biotechnol. Bioeng.* **48**:133–140.

Seong GH, Crooks RM. 2002. Efficient Mixing and Reactions within Microfluidic Channels Using Microbead-Supported Catalysts. *J. Am. Chem. Soc.* **124**:13360–13361.

Sheldon RA, Schoevaart R, Van Langen LM. 2005. Cross-linked enzyme aggregates (CLEAs): A novel and versatile method for enzyme immobilization (a review). *Biocatal. Biotransform.* **23**:141–147.

Sheldon RA. 2007. Enzyme Immobilization: The Quest for Optimum Performance. *Advanced Synthesis & Catalysis* **349**:1289–1307.

Shimada J, Maruyama T, Kitaoka M, Kamiya N, Goto M. 2012. Microplate assay for aptamer-based thrombin detection using a DNA–enzyme conjugate based on histidine-tag chemistry. *Anal. Biochem.* **421**:541–546.

Smolle M, Lindsay JG. 2006. Molecular architecture of the pyruvate dehydrogenase complex: bridging the gap. *Biochemical Society Transactions* **34**:815.

Soares JC, Moreira PR, Queiroga AC, Morgado J, Malcata FX, Pintado ME. 2011. Application of immobilized enzyme technologies for the textile industry: a review. *Biocatal. Biotransform.* **29**:223–237.

Sun JM, Zhang H, Tian RJ, Ma D, Bao XH, Su DS, Zou HF. 2006. Ultrafast enzyme immobilization over large-pore nanoscale mesoporous silica particles. *Chem. Commun.*1322–1324.

Takahashi H, Li B, Sasaki T, Miyazaki C, Kajino T, Inagaki S. 2001. Immobilized enzymes in ordered mesoporous silica materials and improvement of their stability and catalytic activity in an organic solvent. *Microporous Mesoporous Mat.* **44**:755–762.

Tischer W, Wedekind F. 1999. Immobilized enzymes: Methods and applications. *Biocatalysis - from Discovery to Application* **200**:95–126.

Toogood HS, Taylor IN, Brown RC, Taylor SJC, McCague R, Littlechild JA. 2002. Immobilisation of the thermostable L-aminoacylase from Thermococcus litoralis to generate a reusable industrial biocatalyst. *Biocatal. Biotransform.* **20**:241–249.

Tran DN, Balkus KJ. 2011. Perspective of Recent Progress in Immobilization of Enzymes. *ACS Catal.* **1**:956–968.

Trewyn BG, Giri S, Slowing II, Lin VS-Y. 2007. Mesoporous silica nanoparticle based controlled release, drug delivery, and biosensor systems. *Chemical Communications*:3236.

Turkova J. 1999. Oriented immobilization of biologically active proteins as a tool for revealing protein interactions and function. *J. Chromatogr. B* **722**:11–31.

Vinu A, Murugesan V, Hartmann M. 2004. Adsorption of lysozyme over mesoporous molecular sieves MCM-41 and SBA-15: Influence of pH and aluminum incorporation. *J. Phys. Chem. B* **108**:7323–7330.

Wada A, Tamaru S, Ikeda M, Hamachi I. 2009. MCM-Enzyme-Supramolecular Hydrogel Hybrid as a Fluorescence Sensing Material for Polyanions of Biological Significance. *J. Am. Chem. Soc.* **131**:5321–5330.

Wang P, Oberley LW, Howe D, Jarvis DL, Chauhan G, Murhammer DW. 2004. Effect of expression of manganese superoxide dismutase in baculovirus-infected insect cells. *Appl. Biochem. Biotechnol.* **119**:181–193.

Wang Y, Margoliash E. 1995. Enzymatic-Activities of Covalent 1/1 Complexes of Cytochrome-C and Cytochrome-C Peroxidase. *Biochemistry* **34**:1948–1958.

Wang Z-G, Wilner OI, Willner I. 2009. Self-Assembly of Aptamer−Circular DNA Nanostructures for Controlled Biocatalysis. *Nano Lett.* **9**:4098–4102.

Watanabe J, Ishihara K. 2004. Highly efficient sequential enzymatic reaction on bio-conjugate phospholipid polymer nanoparticles. *Kobunshi Ronbunshu* **61**:547–554.

Watanabe J, Ishihara K. 2005. Sequential Enzymatic Reactions and Stability of Biomolecules Immobilized onto Phospholipid Polymer Nanoparticles. *Biomacromolecules* **7**:171–175.

Weber P, Ohlendorf D, Wendoloski J, Salemme F. 1989. Structural origins of high-affinity biotin binding to streptavidin. *Science* **243**:85 –88.

Wegner GJ, Lee HJ, Marriott G, Corn RM. 2003. Fabrication of Histidine-Tagged Fusion Protein Arrays for Surface Plasmon Resonance Imaging Studies of Protein−Protein and Protein−DNA Interactions. *Anal. Chem.* **75**:4740–4746.

Wilner OI, Weizmann Y, Gill R, Lioubashevski O, Freeman R, Willner I. 2009. Enzyme cascades activated on topologically programmed DNA scaffolds. *Nature Nanotechnology* **4**:249–254.

Xian Y, Hu Y, Liu F, Xian Y, Wang H, Jin L. 2006. Glucose biosensor based on Au nanoparticles–conductive polyaniline nanocomposite. *Biosensors and Bioelectronics* **21**:1996–2000.

Yu C-C, Kuo Y-Y, Liang C-F, Chien W-T, Wu H-T, Chang T-C, Jan F-D, Lin C-C. 2012. Site-Specific Immobilization of Enzymes on Magnetic Nanoparticles and Their Use in Organic Synthesis. *Bioconjugate Chem.* **23**:714–724.

Zhang FM, Murhammer DW, Linhardt RJ. 2002. Enzyme kinetics and glycan structural characterization of secreted alkaline phosphatase prepared using the baculovirus expression vector system. *Appl. Biochem. Biotechnol.* **101**:197–210.

Zhang Y, Xu J-L, Li D, Yuan Z-H. 2010. Preparation and properties of an immobilized cellulase on the reversibly soluble matrix Eudragit L-100. *Biocatal. Biotransform.* **28**:313–319.

Zheng M, Zhang S, Ma G, Wang P. 2011. Effect of molecular mobility on coupled enzymatic reactions involving cofactor regeneration using nanoparticle-attached enzymes. *J. Biotechnol.* **154**:274–280.

Zhu T, Row KH. 2012. Preparation and applications of hybrid organic-inorganic monoliths: A review. *J. Sep. Sci.* **35**:1294–1302.

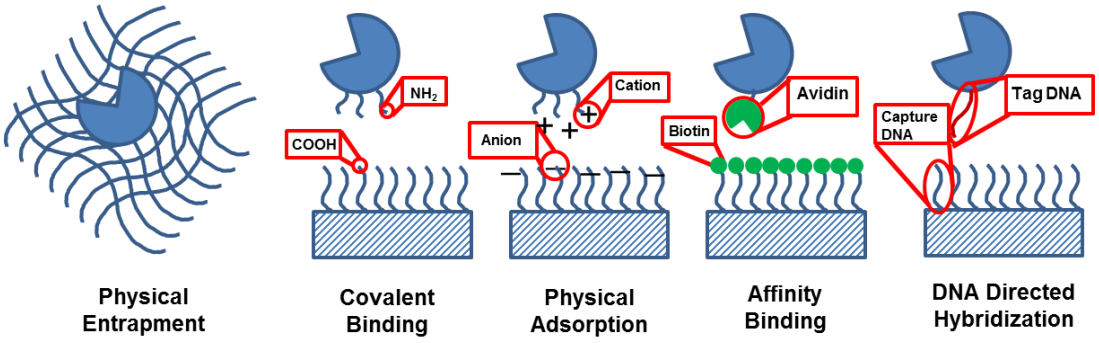

Figure 2.1 Illustration of representative examples of physical entrapment, covalent binding (amide bond formed by carboxyl and amine groups), physical adsorption (ionic interaction), affinity binding (biotin-streptavidin interaction), and DNA hybridization directed self-assembly of enzymes on carriers

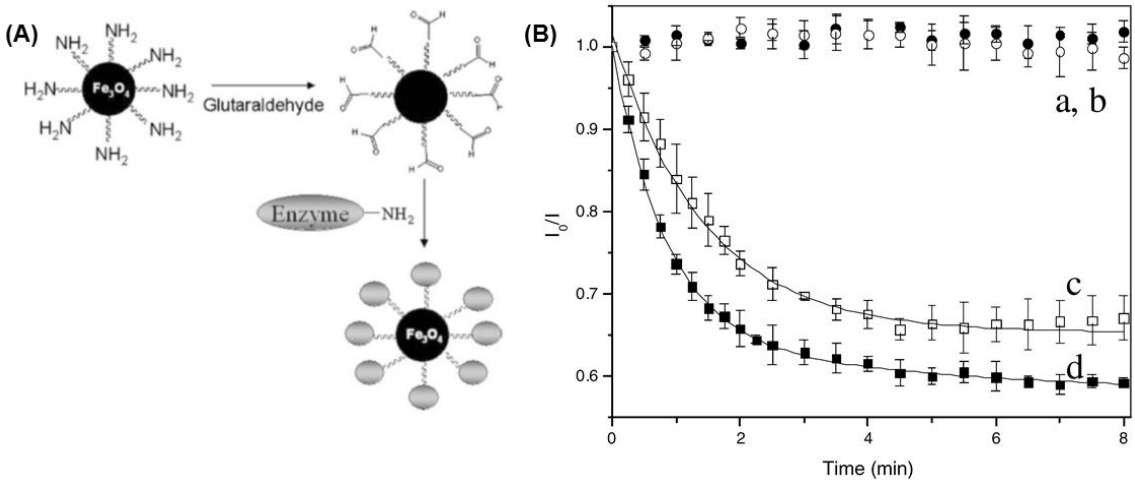

Figure 2.2 (A) Scheme of GOX covalently immobilized on Fe_3O_4 nanoparticles. (B) Temporal dependence of oxygen consumption during oxidation of glucose by GOX: monitoring I_0/I of $Ru(phen)_3$ solutions (I_0 is the initial fluorescence intensity; I is the fluorescence intensity at a given time interval). a**. blank control experiment with no enzymes during the enzymatic reaction. Glucose oxidase–magnetite nanoparticles prepared by** b. **physical adsorption** c. **covalent coupling. and** d **Free enzyme. Figure reprinted from Rossi et al. (2004) with permission from Springer.**

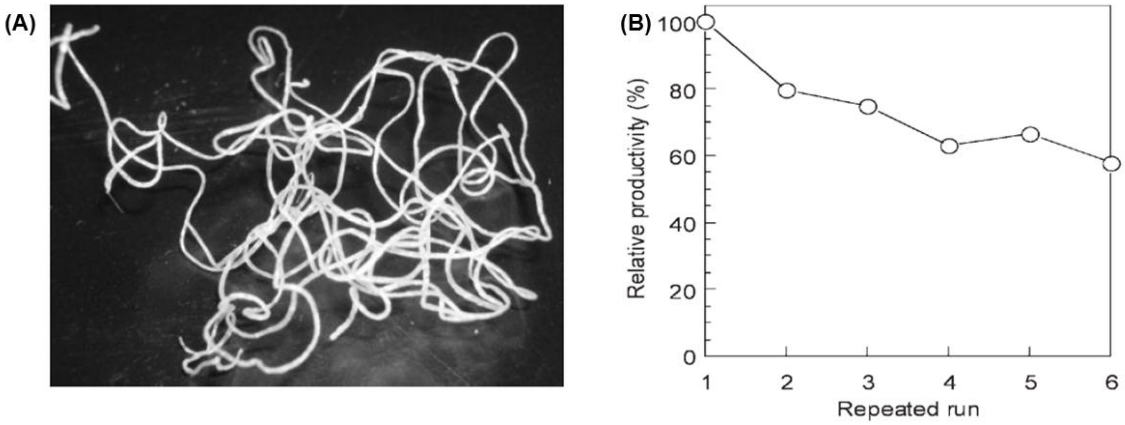

Figure 2.3 (A) Photograph of the CA–Zr gel fiber-immobilized malic enzyme and alanine dehydrogenase. (B) Productivity maintained after multiple uses. Figure reprinted from Nakane et al. (2010) with permission from Wiley.

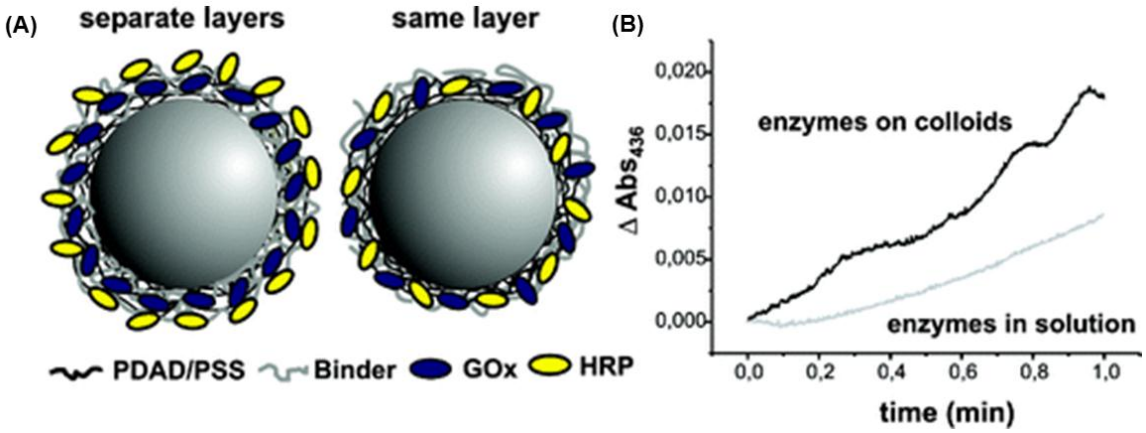

Figure 2.4Scheme of GOX and HRP co-localization on silica microparticles via polyelectrolyte layers. (b) Kinetic enhancement by co-localizing multiple enzymes compared to mixture of homogeneous enzymes Reprinted from Pescador et al. (2008) with permission from ACS.

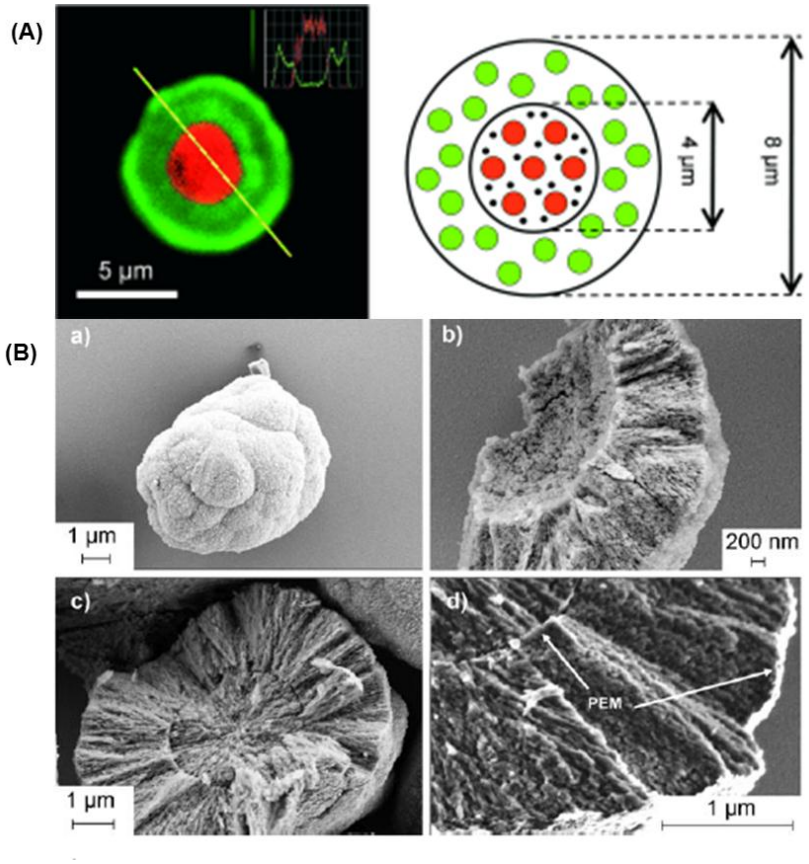

Figure 2.5 (A) Confocal laser scanning microscopic image of ball-in-ball particles with distinct dyes in two compartments and dimension of shell-in-shell microcapsule and schematic illustration of the particle structure. (B) SEM images of ball-in-ball particles (type II). Intact (a) and outer compartment (b) particles after mechanical particle rupture. c) Cross section of ball-in-ball particle. d) Cross section showing intersecting and enclosing PEMs (indicated by arrows). Reprinted from Kreft et al. (2007) with permission from Wiley.

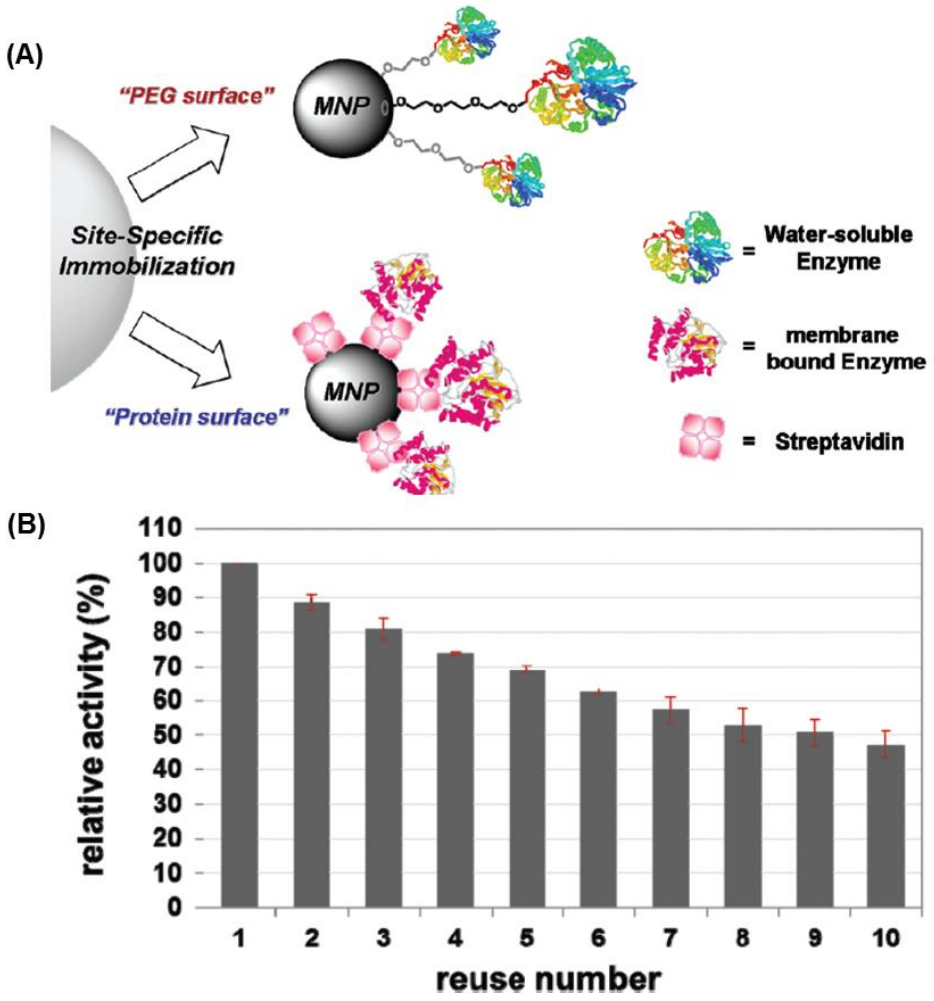

Figure 2.6 (A) Two strategies for site-specific enzyme immobilization: poly(ethylene glycol) surface-functionalized magnetic nanoparticles were used for water-soluble enzyme immobilization and protein surface-functionalized magnetic nanoparticles were suitable for membrane-bound enzyme immobilization. (B) Separated immobilized enzyme mixture retained about 50% activity after using ten times. Reprinted from Yu et al. (2012) with permission from ACS.

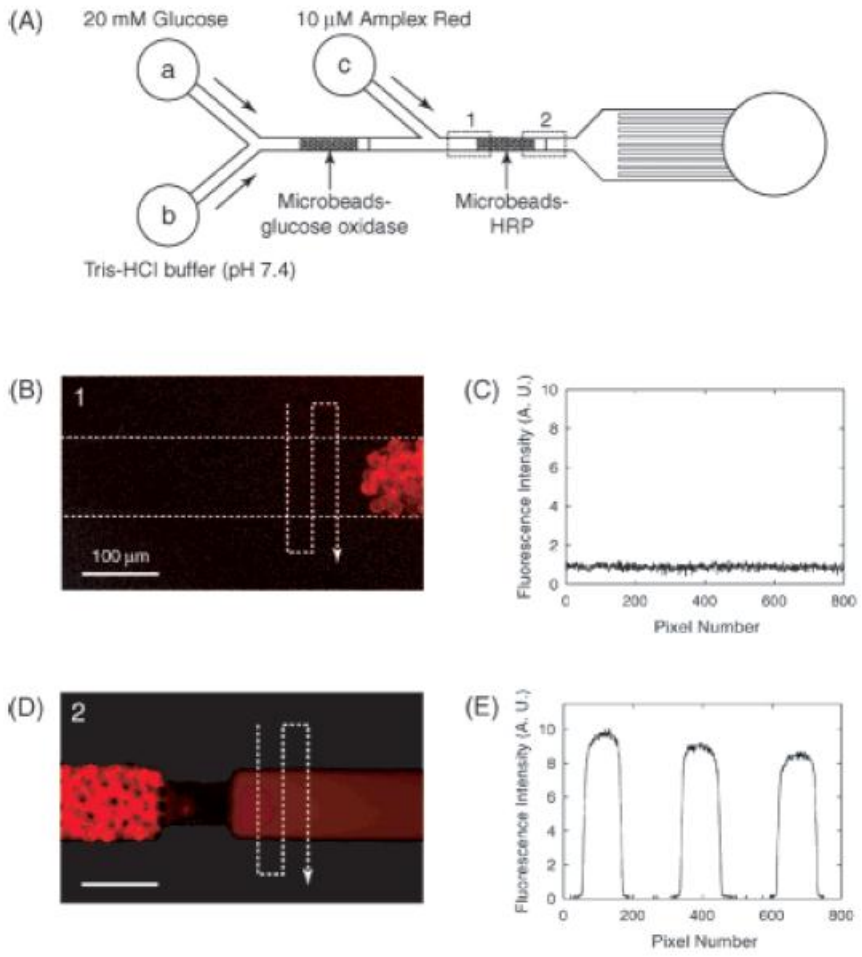

Figure 2.7 (A) Schematic illustration of microdevice used to demonstrate multiple, sequential reactions. (B) FM of the inlet stream just before it enters the HRP microreactor (region 1 in (A)). (C) Fluorescence intensity line scans at the locations indicated by the dashed line in (B). (D) FM of the outlet stream just after exiting the HRP microreactor (region 2 in (A)). (E) Fluorescence intensity line scans at the locations indicated by the dashed line in (D). Excitation wavelength: 563 nm; maximum emission wavelength: 587 nm. The flow rate was 0.5 μL/min in all cases. Reprinted from Seong and Crooks, (2002) with permission from ACS.

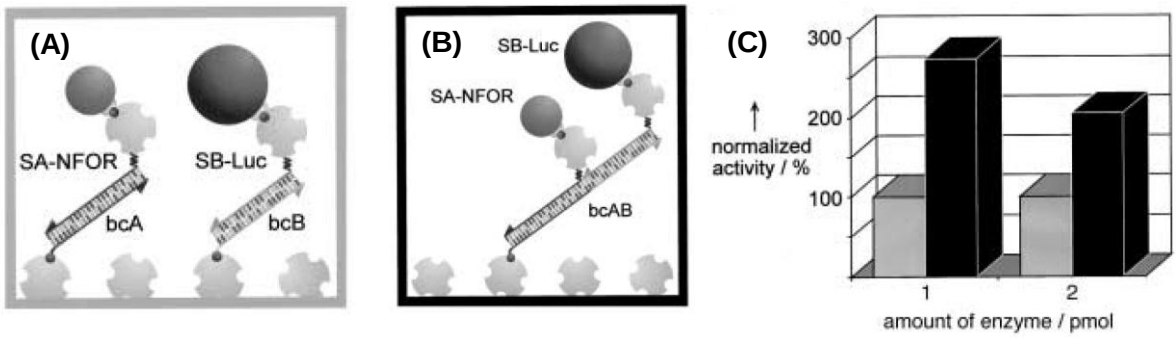

Figure 2.8 Graphical representation of the effect of spatial proximity on the activity of bi-enzymatic constructs. The heights of the histograms (C) correspond to the overall enzymatic activities obtained from conjugates (A) immobilized through random hybridization (grey bars) or (B) from assembly in direct proximity at a DNA carrier strand (dark bars). Reprinted from Niemeyer et al. (2002) with permission from Wiley.

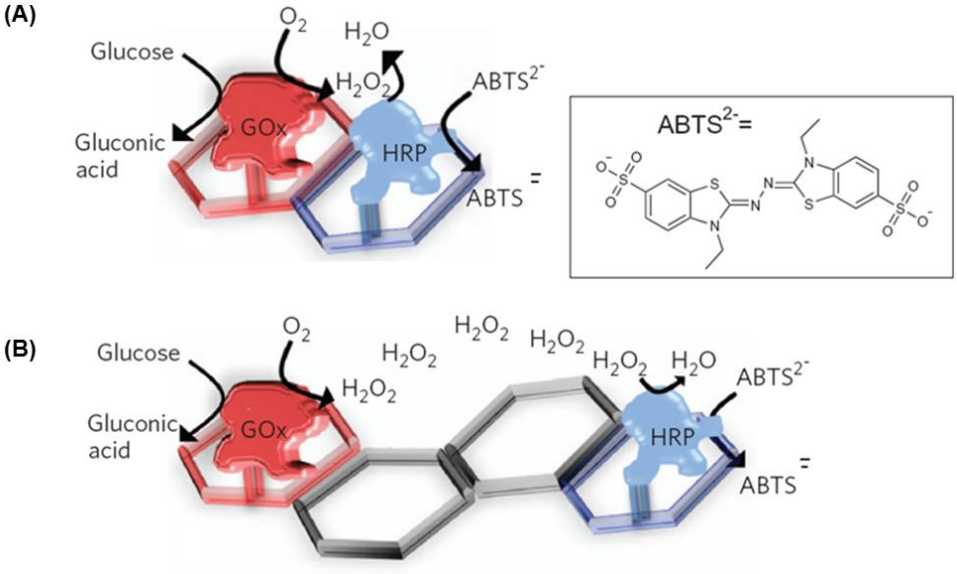

Figure 2.9 Assembly of enzyme cascades or cofactor–enzyme cascades on hexagon-like DNA scaffolds, their imaging and their functional characterization. Assembly of the GOx and HRP enzymes on two-hexagon (A) and four-hexagon (B) strips. Reprinted from Wilner et al. (2009) with permission from Nature Publishing Group.

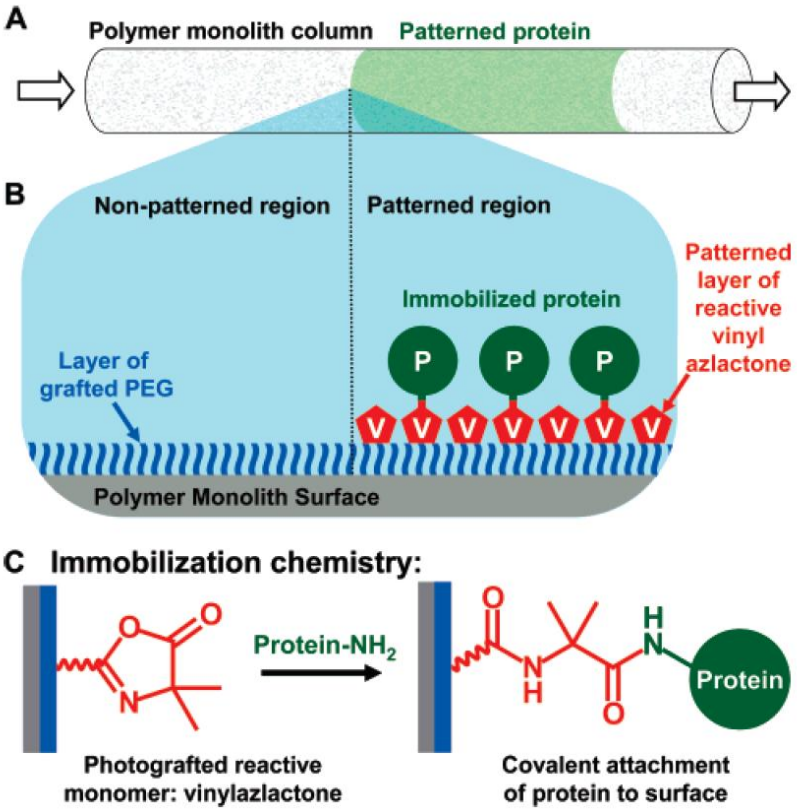

Figure 2.10 Schematic of the photopatterning process. (A) Protein is immobilized to the surface of a polymer monolith in patterned regions within a microfluidic channel. (B) PEG is grafted to the surface of the polymer monolith to prevent non-specific protein adsorption. Vinyl azlactone is photopatterned onto the PEG surface and activates the surface for protein immobilization. (C) Azlactone functionality reacts with amines of proteins to form a covalent amide bond between the protein and the polymer monolith surface. Reprinted from Logan et al. (2007) with permission from ACS.

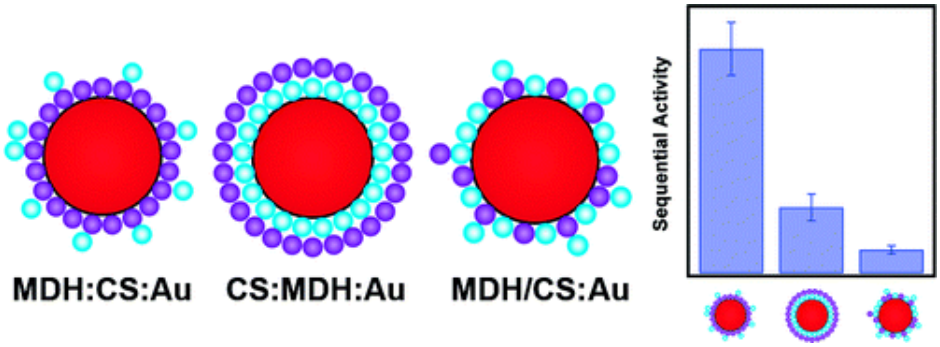

Figure 2.11Schemes of co-localizing MDH and CS on gold nanoparticles in three configurations and the comparison of corresponding sequential enzymatic activity. Reprinted from Keighron and Keating, (2010) with permission from ACS.

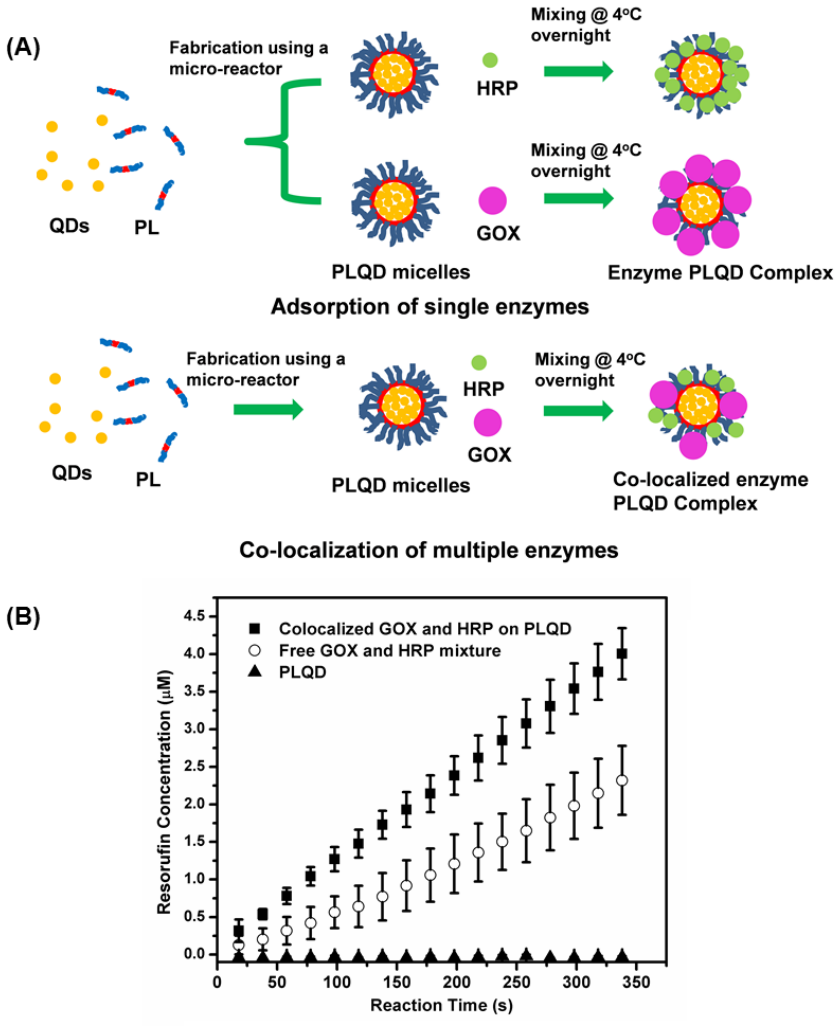

Figure 2.12 Enzyme immobilization and co-localization on PLQD micelles. (A) The representative strategies used including sequential adsorption of single enzymes and co-localization of multiple enzymes. (B) Overall product conversion rate comparison of co-localized enzymes and equivalent free enzyme mixture Reprinted from Jia et al. (2012) with permission from ACS.

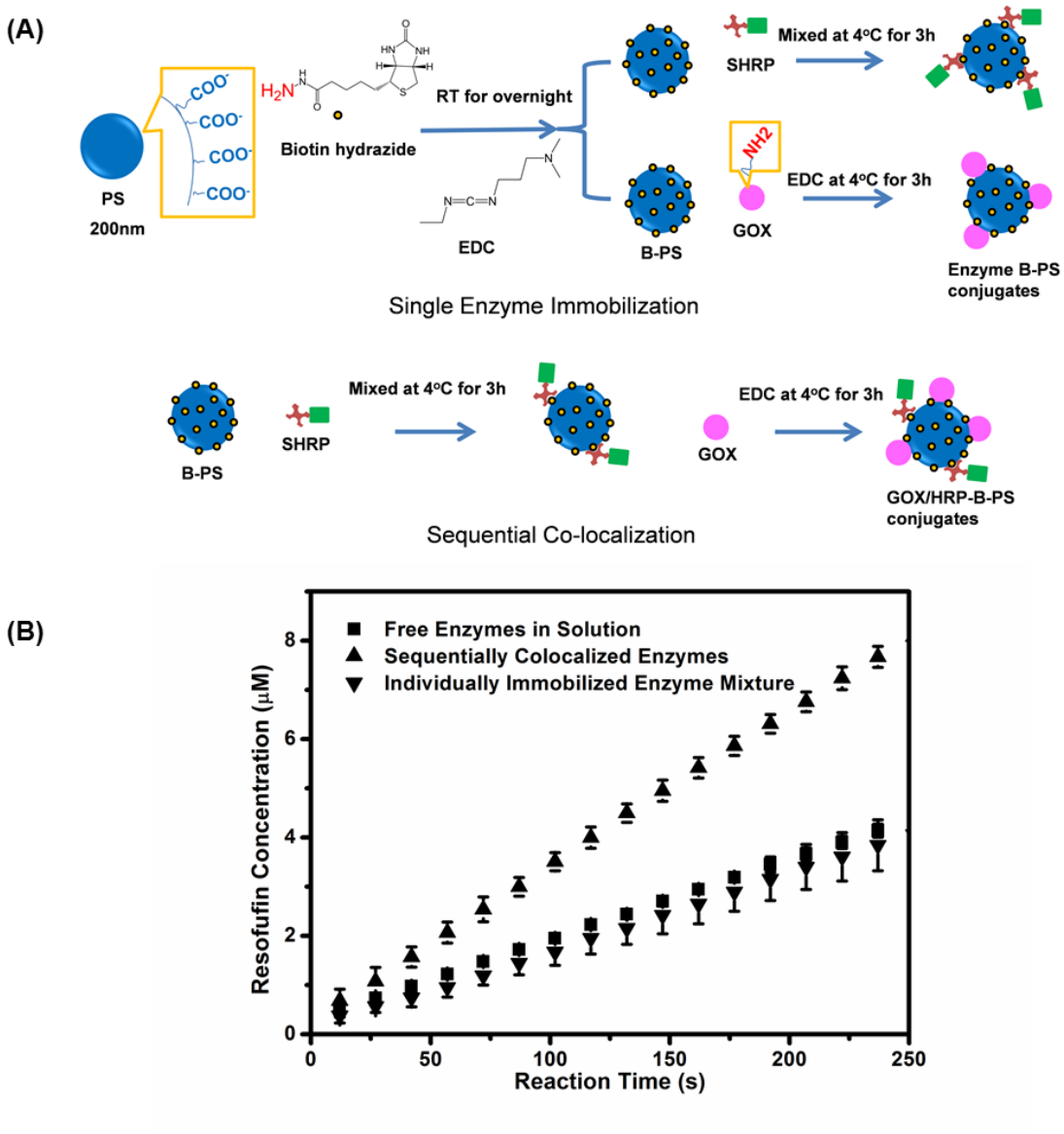

Figure 2.13 (A) Schemes of single enzyme immobilization and multi-enzyme co-localization on bi-functional PS nanoparticles. (B) The kinetics of the overall product yield was improved by 2-fold in comparison to a free enzyme combination and individually immobilized enzyme mixture. Reprinted from Jia et al., (2013) with permission from Wiley.

Table 2-1 Summary of recent multiple enzyme co-localization studies

Platform	Attachment techniques	Enzymes	Conversion enhancement vs. free enzymes	Reference
Sol-gel biomaterials sodium silicate solution	physical entrapment	GOX, HRP/ Urease, fluorescein dextran	decrease	(Rupcich and Brennan, 2003)
Gel-fiber	physical entrapment	malic and alanine dehydrogenase	0.2	(Nakane et al., 2010)
Chitin	Physical adsorption/covalent binding	D-hydantoinase and D-carboamylase	N/A	(Aranaz et al., 2003)
PLQD micelles	Physical adsorption	GOX, HRP	Up to 2 fold	(Jia et al., 2012)
Shell in shell polyelectrolyte particles	Physical entrapment	GOX, HRP	N/A	(Kreft et al., 2007)
Polymer monolith	covalent binding in different region	GOX, HRP	N/A	(Logan et al., 2007)
Polystyrene beads in microreactor	Biotin-streptavidin separate compartments	GOX, HRP	N/A	(Seong and Crooks, 2002)
Bi-functionalized PS nanoparticles	Biotin-streptavidin/covalent binding	GOX, HRP	Up to 2 fold	(Jia et al., 2013)
Magnetic nanoparticles	Biotin-strepatavin/covalent binding	GOX, HRP	N/A	(Garcia et al., 2011)
Silica microparticles	L-b-L polyelectrolyte	GOX, HRP	up to 2.5 fold	(Pescador et al., 2008)
Alumina pellets	L-b-L polyelectrolyte	Laccase, HRP	N/A	(Crestini et al., 2011)
Gold nanoparticles	L-b-L polyelectrolyte	Malate dehydrogenase, citrate synthase	N/A	(Keighron and Keating, 2010)
Polystyrene microplate surface	DNA directed self-assembly	GOX, HRP	up to 2 fold	(Müller and Niemeyer, 2008)
Polystyrene microplate surface	DNA directed self-assembly	NFOR, LUC	up to 3 fold	(Niemeyer et al., 2002)
Programmed DNA scaffolds	DNA directed self-assembly	GOX, HRP/GDH NAD+	Significantly higher	(Wilner et al., 2009)
Aptamer Circular DNA nanostructures	DNA directed self-assembly	GOX, HRP	up to 6 fold	(Wang et al., 2009)
Cocaine-Aptamer complexes	Supramolecular aptamer-substrate complexes	GOX, HRP/AlcDH, amino-NAD+	N/A	(Abou-Rebyeh et al., 1991)

Chapter 3 Novel sequential co-localization of multiple enzymes on multifunctional nanoparticles

(Modified from a paper submitted to AIChE Letters)

Feng Jia, Balaji Narasimhan, and Surya K. Mallapragada

Department of Chemical and Biological Engineering, Iowa State University, Ames, IA 50011

Abstract

Inspired by the widely present multi-enzyme complexes in Nature, we designed novel dual-functionalized nanoparticles for co-localizing multiple enzymes. To demonstrate this concept, glucose oxidase (GOX) and horseradish peroxidase (HRP) were used as model enzymes and co-localized on biotinylated carboxylic acid-functionalized polystyrene nanoparticles. Covalent binding and streptavidin-biotin coupling were evaluated and optimized by immobilizing GOX and Streptavidin tagged HRP (SHRP) on biotinylated carboxylic acid-functionalized polystyrene nanoparticles. The results showed that both GOX and SHRP activity was retained after immobilization. The optimized sequential co-localization of GOX and SHRP was found to improve the overall conversion rate by approximately 100% compared to the equivalent amount of free enzymes in solution and a physical mixture of individual immobilized enzymes on nanoparticles. This study demonstrates the design of a simple and effective platform for multi-enzyme co-localization to mimic the multi-enzyme complex structure and function observed in Nature.

3.1 Introduction

The design and fabrication of biomolecule-nanoparticle conjugates have attracted much attention for applications in biosensors, biocatalysis, and biomedicine.(Albertsson and Varma, 2003; Berron et al., 2011; Carrillo-Conde et al., 2010; Christie et al., 2011; Determan et al., 2006; Hrapovic et al., 2003; Jia et al., 2002; Lim et al., 2005; Liu et al., 2009; Narang et al., 1994; Torres et al., 2007; West and Halas, 2003; Xiao et al., 1999; Yi et al., 2000) In particular, the development of nanoscale platforms for spatial control of multiple active enzymes has been an area of interest.(Keighron and Keating, 2010; Liu et al., 2009; Pescador et al., 2008; Watanabe and Ishihara, 2005) It is known that multi-enzyme complexes enable highly cooperative catalytic mechanisms in Nature, where the reactive intermediates can be transported rapidly from one active site to the next to avoid diffusion losses.(Keighron and Keating, 2010) By spatially co-localizing multiple enzymes on nano-carriers, the intermediates, especially the reactive and short-lived ones, can rapidly find the next active site to accelerate the reaction efficiency and to direct the overall reaction towards the desired products, particularly in comparison with free enzymes in solution. Previous work has shown that multiple enzymes adsorbed on chitin exhibited higher overall catalytic performance and stability.(Aranaz et al., 2003) Recent work has focused on co-localizing multiple enzymes by adsorption on non-porous nanoparticles using various strategies to form egg-like architectures, where rigid support materials serve as cores with coronas of multiple enzymatic layers.(Keighron and Keating, 2010; Lundqvist et al., 2008; Pescador et al., 2008; Watanabe and Ishihara, 2005) Another recent study reported adsorption of single enzymes and cofactors on different silica nanoparticles, in which the multi-step reaction was facilitated by Brownian collisions of the nanoparticles.(Liu et al., 2009)

Keighron and Keating found that the sequential order of enzymes adsorbed on gold nanoparticles affected the overall product conversion rate.(Keighron and Keating, 2010)

In multi-step sequential reactions, the rapid transport of the intermediate between active sites plays a significant role. Compared to adsorption, multi-point covalent binding is more durable, stable under harsh micro-environments (i.e., extreme pH and temperature), and potentially provides higher loading efficiency.(Jeffrey J, 2004; Johnson et al., 2007; Williams and Blanch, 1994) In some cases, it can also enhance the enzymatic activity.(Matharu et al., 2007; Pandey et al., 2007) For example, it was found that glucose oxidase (GOX) covalently immobilized on thiolated gold nanoparticles showed higher activity than free GOX in solution.(Pandey et al., 2007) In this context, the highly specific biotin-streptavidin linkage, which has a dissociation factor of 10^{-15}, has been widely used to link biomolecules with nanoparticles for biomedicine and biosensor applications.(Cui et al., 2001; Katz and Willner, 2004; Niemeyer, 2001; Weber et al., 1989) The streptavidin label can anchor a tagged enzyme on the carrier as well as protect the enzyme from hydrophobic carrier surfaces, which could induce unwanted conformational changes.(Matsumoto et al., 2011)

In this study, we present a facile and simple approach based on sequential co-localization of multi-enzymes conjugated to nanoparticles, which is inspired by multi-enzyme complexes (Figure 3.1). The GOX and horseradish peroxidase (HRP) sequential reaction cascade was chosen as the model system, since it is a well-studied reaction, where the hydrogen peroxide formed in the first reaction catalyzed by GOX is consumed by HRP in the second reaction in the presence of N-acetyl-3,7-dihydroxyphenoxazine (Amplex Red) to yield a specific fluorescent product, resorufin.(Logan et al., 2007; Rupcich N. and Brennan J.D., 2003) Previously, GOX and HRP were adsorbed layer by layer on microparticles to form multiple enzyme

films.(Pescador et al., 2008) However, the selection of the polymer was critical for compatibility with the adsorbed enzymes, and the use of polyelectrolytes provided additional diffusion resistance. Previous work has also shown that simultaneous adsorption required an extra dye-labeling step to quantify the amount of each enzyme co-immobilized on the particle surface and that non-specific adsorption resulted in loss of enzymatic activity due to conformational changes.(Keighron and Keating, 2010)

A nano-carrier platform based on carboxylic acid-functionalized polystyrene (C-PS) nanoparticles was used to controllably attach biomolecules. Compared to porous support materials, the non-porous nanoparticles will not involve large substrate diffusion resistance and requirement of enough internal space to accommodate the large enzyme molecules.(Garcia-Galan et al., 2011) The rigid polymeric platform in aqueous solution can serve as a supporting material for immobilizing enzymes in biocatalysis.(Caruso and Schüler, 2000; Fazlollahi et al., 2011; Lvov and Caruso, 2001; Miletić et al., 2010; Watanabe and Ishihara, 2005) GOX and streptavidin-tagged horseradish peroxidase (SHRP) were sequentially co-localized on biotinylated C-PS (B/C-PS) nanoparticles via covalent coupling and streptavidin-biotin linkage, respectively. The attachment and separation processes were initially optimized to maximize the enzymatic activity by immobilizing single enzymes onto the B/C-PS nanoparticles. The corresponding kinetic parameters K_m and k_{cat} for each enzyme were determined from the initial reaction rates at various substrate concentrations. Next, the optimized immobilization technique was used to co-localize both enzymes on B/C-PS nanoparticles and resulted in a higher overall conversion rate in comparison to an equivalent mixture of single enzymes immobilized on nanoparticles, as well as a combination of free enzymes.

3.2 Materials and Methods

3.2.1 Chemicals

200 nm 4% (w/v) C-PS nanoparticles and Amplex® Red were purchased from Invitrogen (Carlsbad, CA). GOX (~200 U/mg, from *Aspergillus niger*), horseradish peroxidase (HRP) (~250 U/mg, from horseradish), resorufin, biotin hydrazide, 2-(*N*-morpholino) ethanesulfonic acid (MES) were purchased from Sigma-Aldridge (St. Louis, MO). Streptavidin-hydrogen peroxidase was purchased from BioLegend (San Diego, CA). Dimethyl sulfate (DMSO), 1-ethyl-3-(3-dimethylaminopropyl) carbodiimide (EDC), 3% hydrogen peroxide, Coomassie protein assay reagent, Pierce® biotin quantitation kit, sodium chloride, and trisodium phosphate were purchased from Fisher Scientific (Hampton, NH). All the aqueous solutions were prepared using purified water from Thermo Scientific's Barnstead Nanopure Ultrapure Water System.

3.2.2 Partial biotinylation of C-PS nanoparticles

C-PS nanoparticles were covalently modified using biotin hydrazide. Briefly, 500 µL of 4% PS nanoparticle stock solution was micro-centrifuged and re-suspended in 450 µL of 0.025 M MES buffer (pH 5.9) and then 50 µL of the 50 M biotin hydrazide (freshly prepared in DMSO) and 500 µL of 20 mg/mL EDC in MES buffer were added into the solution. The reaction solution was incubated overnight at room temperature with constant rotation. The unattached biotin hydrazide and the modified particles were separated by micro-centrifugation at 20,000 g for 30 min. The supernatants were removed and the modified particles were re-suspended in fresh MES buffer. This procedure was repeated until biotin hydrazide was not detectable in the collected supernatant using a biotin quantification kit. The biotin in each supernatant was quantified in order to determine the loading efficiency. The quantity of the biotin attached was determined by subtracting the amount in the washout from the initial amount. The

surface charge of the nanoparticles was measured using dynamic light scattering (DLS) (Zetasizer Nano, Malvern Instruments Ltd., Worcester, UK). The biotin-modified C-PS nanoparticles were stored at 4 ^{o}C for use.

3.2.3 Biotin quantification

The biotin hydrazide in each collected supernatant was assayed using a biotin quantification kit. Due to the higher affinity between avidin and biotin, 4´-hydroxyazobenzene-2-carboxylic acid (HABA), a dye that pre-binds to the avidin, is replaced by the biotin, which causes proportional fading of the color of the solution. Thus, the biotin can be quantified by the monitoring the color change. In this assay, a 20 µL of premixed dye-avidin conjugate solution was mixed with 160 µL PBS buffer in 96-well plates and the initial absorbance at 500 nm was recorded. Then, a 20 µL sample was added and the final absorbance at 500 nm was measured. The amount of biotin was quantified based on the difference in the absorbance at 500 nm before and after adding the biotin, according to a standard curve previously prepared using a series of biotin solutions of known concentration.

3.2.4 GOX immobilization on B/C-PS beads

GOX powder was dissolved in 0.025 M MES buffer (pH 5.9) and stored in a -20 ^{o}C freezer. In 500 µL MES reaction solution, 30 µg GOX was covalently immobilized on the 2.5 mg B/C-PS nanoparticles in the presence of 1 mg EDC. The reaction was carried out at 4^{o} C for 3 h with constant stirring. The unattached GOX and the enzyme-nanoparticle conjugate were separated by micro-centrifugation at 20,000 g for 6 min. The supernatant was removed and the bioconjugates were re-suspended in the PBS buffer. The rinse step was repeated until the GOX was not detectable in the supernatant. The GOX was quantified using a Bradford assay, in which 50 µL of the sample was added into 200 µL of Coomassie Blue dye containing working reagent and the

absorbance at 595 nm was measured using a UV-Vis micro-plate reader (Cary 50 Bio, Varian, Palo Alto, CA). A standard curve was prepared with GOX solutions of known concentrations. The quantity of the attached biotin was determined indirectly by subtracting the amount in the washout from the initial amount.

3.2.5 SHRP immobilization on B/C-PS nanoparticles

To immobilize the SHRP on the B/C-PS nanoparticles, 30 µL of SHRP solution (15 µg) was added to 2.5 mg B/C-PS nanoparticles and the solution was finalized to 500 µL by adding appropriate amount of PBS buffer. The attachment reaction was carried out for 3 h at 4 ^{o}C. The unattached enzyme was separated from the bio-conjugates by micro-centrifugation and this step was repeated until SHRP was not detectable in the supernatant. The washout enzymes were quantified by the Bradford assay and subtracted from the initial amount to determine the amount of attached enzyme.

3.2.6 Simultaneous co-localization of multiple enzymes

500 µL of 4% C-PS nanoparticles were washed by MES buffer and re-suspended in 375 µL MES buffer. Next, 25 µL of GOX in PBS (2 mg/ml), 100 µl of HRP in PBS (2 mg/ml) and 10 mg EDC were added into the solution. The reaction was carried out for 3 h at 4 ^{o}C. The unattached proteins were removed after micro-centrifugation. The adsorbed co-localized sample was prepared in the same way except that there was no EDC in the reaction solution. To characterize the co-localization of the enzymes on the nanoparticles, GOX and HRP were labeled by Alexa Fluor 594 and 488, respectively, according to the procedure provided by the manufacturer. The labeled enzymes were simultaneously co-localized on the C-PS nanoparticles and visualized using an epi-fluorescence microscopy (Lumen 200, Prior Scientific) using a 60X 1.49NA Nikon objective, and the images were collected using a Photometrics HQ^{2} CCD camera. Alexa

Fluor 594 and 488 dyes were excited using 555 nm and 490 nm filters, respectively, and the respective signals were collected with 605 nm and 525 nm filters.

3.2.7 Sequential co-localization of multiple enzymes

SHRP and GOX were sequentially co-localized onto the B/C-PS nanoparticles. To attach SHRP, similar to the immobilization of single SHRP, 15 µg of the SHRP was reacted with 2.5 mg B/C-PS nanoparticles for 3 h at 4 ^{o}C and separated by micro-centrifugation. The collected supernatants were used to determine the loading efficiency. To attach the GOX onto the SHRP-B/C-PS bioconjugates, similar to the immobilization of the single GOX, 10 µg of the GOX was added thereafter and reacted with the SHRP-B/C-PS nanoparticles in the presence of 0.3 mg EDC for 3 h at 4 ^{o}C. Again, the co-localized GOX and SHRP bio-conjugates were separated from the unattached GOX by micro-centrifugation and the GOX was quantified for loading efficiency.

3.2.8 Enzyme activity assays

GOX: A 200 mM glucose storage solution was prepared in PBS buffer (pH 7.2) and equilibrated overnight before use. Various concentrations (1-30 mM) of glucose substrate solution with 50 µM Amplex Red were prepared by adding appropriate amounts of storage glucose solution and Amplex Red into the substrate solution. Then, 10 µL of 10 µg/mL SHRP and 10 µL of 2 µg/mL GOX or immobilized GOX was added into each well of a 96-well plate in sequence, which was previously loaded with 180 µL of substrate solution. Immediately after mixing, the reaction was monitored by a fluorescence plate reader (SynergyMx, Biotek, Winooski, VT) with excitation and emission wavelengths of 560 and 590 nm, respectively. The fluorescence signal was converted into resorufin concentration using a standard curve prepared by resorufin solutions of known concentrations.

SHRP: A 20 mM hydrogen peroxide stock solution was prepared by adding 23 µL of 3% H_2O_2 solution into of 977 µL of PBS buffer. A sub-storage H_2O_2 stock solution was prepared by a 200-fold dilution of the stock solution. A series of hydrogen peroxide concentrations (1-80 µM) were prepared by adding respective appropriate amounts of sub-storage solution into the substrate solution, which contained Amplex Red. 20 µL of 100 ng/mL SHRP or SHRP-B/C-PS was added into 180 µL of substrate solution so that the final reaction solution has 1-80 µM H_2O_2 and 50 µM Amplex Red. The reaction was monitored using a fluorescence plate reader as described previously.

Free GOX and SHRP mixture: To each well of the 96-well plates, 180 µL of substrate solution containing appropriate amount of glucose and Amplex Red was added, and subsequently, 10 µL of SHRP with appropriate concentration and 10 µL of GOX (4µg/mL) were added.

Sequentially co-localized GOX and SHRP: To 195 µL of glucose and Amplex red containing substrate solution, 5 µL of the co-localized sample was added so that the final solution contained 1 mM glucose, 200 µM Amplex Red and appropriate amounts of GOX and SHRP. According to the measured quantity of each enzyme in the co-localized sample, equivalent amounts of each single enzyme bio-conjugate were added to the same substrate solution as a control. Similarly, an equivalent free enzyme mixture was added into the same substrate solution for comparison. The reaction was monitored by a fluorescence plate reader as described previously.

3.3 Results and Discussion

3.3.1 Biotinylation of C-PS nanoparticles

The biotin derivative biotin hydrazide contains one primary amine group, which can be reacted with the carboxylic acid group on the nanoparticle surface. Biotin hydrazide is a small molecule (254 Da, space arm length ≈16 Å) with a significantly smaller dimension compared to the area occupied by the carboxylic acid moieties (approximately 28.8 nmol/mg, where each group occupies ca.154 $Å^2$). It was found that only about 50% of the carboxylic groups were modified due to steric hindrance. The experiments also showed that 40% biotin modification was optimal for co-localization of both GOX and SHRP, because higher biotin coverage limited the accessibility of the carboxylic group for GOX attachment and lower biotin coverage also limited the availability of biotin for SHRP attachment, since both GOX and SHRP can attach onto multiple -COOH and biotin groups, respectively. In the following single enzyme immobilization and sequential co-localization study, the biotinylation percentages on the C-PS beads were all approximately 40%. The ζ-potential of the C-PS nanoparticles was -62.3 ± 2.3 mV, consistent with proton dissociation from the carboxylic acid group in the PBS buffer. After partial biotinylation, that value increased to -32.9 ± 4.8 mV, which is consistent with the fact that more than half of the –COOH groups are still unmodified.

3.3.2 Single enzyme immobilization and kinetic performance

Before the co-localization study, the GOX and SHRP were separately localized on the dual-functionalized nanoparticles to optimize the conditions of the single enzyme attachment process. GOX and SHRP were attached onto the unmodified carboxylic acid and the biotinylated moieties, respectively. These two distinct functional groups were used to selectively immobilize the respective enzymes. Typical loading values for the

GOX and SHRP were found to be 11.0 ± 0.3 μg/mg and 1.6 ± 0.1 μg/mg, respectively, which is consistent with previous work.(El-Zahab et al., 2004; Liu et al., 2009)

Previous work has shown that covalently immobilized GOX on magnetite nanoparticles showed better enzymatic activity compared to free GOX in solution due to favorable conformational change of the enzyme (Rossi et al., 2004). To optimize the attachment process for maximizing the enzyme activity, the performance of the immobilized single enzymes was compared with that of the equivalent amount of free enzymes using a kinetic activity assay. The GOX enzymatic activity assay was carried out by coupling the reaction catalyzed by the SHRP. By adjusting the reaction time, reaction temperature and centrifugation time, the optimized conditions for GOX activity were found to be: 3 h at 4 ^{o}C with 20,000 g micro-centrifugation for 6 min.

To evaluate the enzymatic performance of GOX before and after immobilization, the kinetics of each reaction was studied. The change in the product concentration over time is shown in Figures 3.2 (A) and (B). A second order polynomial was used to model the reaction curve and the derivatives of the polynomial were used to calculate the initial reaction rate. The initial reaction rate as a function of glucose concentrations is shown in Figure 3.2(C).

Using a Michaelis-Menten model, the kinetic parameters K_m and k_{cat} were calculated using the data in Figure 3.2 (C) with a linear least squares method and are shown in Table 3.1. The K_m of the immobilized and free GOX were both 7.9 mM, which indicated that the affinity between the enzyme and the substrate did not change after the immobilization. The k_{cat} of the immobilized GOX decreased slightly (194.3 s^{-1}) in comparison to that of the free GOX (160.1 s^{-1}), indicating that the enzyme turnover number was not quite as efficient. However, the activity of the immobilized GOX is

comparable with that of the free enzyme in solution, indicating nearly no deleterious effects of covalent immobilization on GOX activity.

The kinetics of the reaction catalyzed by SHRP was studied similarly. Figures 3.3 (A) and (B) show the variation of the product concentration with time. Figure 3.3 (C) shows the initial reaction rate as a function of the substrate concentration. As shown in Table 1, the K_m value of the immobilized SHRP (20.9 μM) was slightly lower than that of the free enzyme (23.2 μM) and the k_{cat} of the immobilized SHRP (3.6×10^4 s^{-1}) was slightly higher than that of free SHRP (4.0×10^4 s^{-1}). In general, the immobilized SHRP retained its activity.

3.3.3 Simultaneous co-localization on C-PS nanoparticles

To compare the performance of enzymes simultaneously co-localized by adsorption versus covalent attachment, HRP was co-localized with GOX on the C-PS nanoparticles with and without the presence of EDC. The overall product conversion rates due to adsorption and covalent attachment are shown in Figure 3.4. In contrast to the simultaneous covalent co-localization, the co-localized sample by adsorption did not show a detectable conversion rate, which may be attributed to a combination of lower loading efficiency and partial loss of activity due to conformational changes caused by non-specific adsorption.(Fears et al., 2009; KONDO et al., 1992) This study also showed that any contribution due to adsorption to the optimized covalent attachment condition is negligible.

To further characterize the co-localization of both enzymes, the GOX and HRP were respectively labeled with the spectrally distinct Alexa Fluor 594 and Alexa Fluor 488 dyes by covalent binding. A fraction of the primary amine groups on the enzymes were reacted with the dyes. As shown in Figure 3.7, the yellow color formed by the

overlapping between the green and red channels qualitatively demonstrated the co-localization of the GOX and HRP on the nanoparticles.

In spite of the fact that the covalent attachment outperformed physical adsorption, there are some limitations of the simultaneous co-localization method. One is lack of control over the relative levels of attachment of the two enzymes. Another could be that the amine reactive labeling dye may be a competitor for further attachment of the enzyme-dye onto the particles. Therefore, a more controllable sequential co-localization strategy was developed.

3.3.4 Optimal GOX:SHRP ratio for resorufin production

The enzymatic performance of various free GOX and SHRP enzyme combinations to maximize the production of resorufin was studied by varying the GOX:SHRP ratio as follows: 1:15, 1:7, 1:1 and 3:1. As shown in Figure 3.5, the resorufin production was enhanced with increasing SHRP concentration till a plateau was reached at a GOX:SHRP ratio of 1:7. Beyond this ratio, further increases in SHRP concentration did not improve the overall conversion rate. This experiment indicated that the optimal molar ratio of GOX:SHRP to enhance resorufin production is between 1:1 and 1:7. Based on these results, a GOX to SHRP ratio of 1:3 was selected to perform the sequential co-localization studies.

3.3.5 Sequential co-localization of GOX and SHRP on B/C-PS nanoparticles

The single enzyme immobilization and the combination of free GOX and SHRP studies provided optimal conditions to evaluate sequential co-localization of both enzymes. In previous studies, enhanced catalytic performance was observed in terms of a higher overall conversion rate when two enzymes were simultaneously co-localized on the same layer on a nanoparticle surface.(Keighron and Keating, 2010; Pescador et al.,

2008) In this work, we have designed and developed a sequential co-localization strategy. The SHRP was attached first because it was found that if the GOX was attached first, it lost significant activity mainly due to the high-spin microcentrifugation in the second reaction step. As mentioned previously, in a typical reaction, about 40% carboxylic acid groups were modified by biotin. In the GOX adsorption control experiment where all the experimental conditions are the same except that no EDC was added in the GOX attachment step, the loading efficiency of GOX was very low. Nearly none of the GOX was adsorbed on the remaining areas, probably due to the net negative charged COO^- preventing non-specific adsorption of the negatively charged GOX enzymes in MES buffer.

The performance of the optimized co-localized GOX and SHRP system was compared with that of equivalent amounts of the free enzymes in solution and an immobilized GOX and SHRP mixture. These results are shown in Figure 3.6, which indicate that co-localizing the two enzymes on the same nanoparticles enhanced the overall product conversion two-fold. The performance of the immobilized GOX and SHRP mixture was comparable to that of the free enzyme combination, which is consistent with our previous studies using single enzyme immobilization, indicating that each enzyme retained its activity after immobilization.

These studies demonstrate the clear benefits of sequentially co-localizing multiple enzymes on multifunctional nanoparticles. In many enzymatic systems, it is critical to molecularly localize these enzymes so that the intermediates can rapidly find the next active site for the reaction to proceed. This rigid synthetic C-PS platform provides nano-scale spatial control of multiple active enzymes. By modifying the surface of the C-PS nanoparticles, multiple enzymes were co-localized on these nano-carriers and the relative amounts of the attached enzymes were controllable. In situations where

the intermediate product is particularly reactive, such a strategy may pay even more dividends. In comparison to the adsorption coupling strategy used in previous co-localization studies,(Keighron and Keating, 2010; Pescador et al., 2008; Watanabe and Ishihara, 2005) our sequential covalent binding/streptavidin-biotin approach is more stable and suitable for long term use.(Cui et al., 2001; Drechsler et al., 2004; Su et al., 2007) The step-by-step sequential co-localization strategy was also facile and simple in terms of controlling the loading of each enzyme and quantifying each localized enzyme on the platform. Unlike other co-localization studies(Keighron and Keating, 2010; Pescador et al., 2008), labeling enzymes with dye for quantification is not needed in this approach. This strategy is broadly applicable to other sequentially coupled multiple enzyme reactions by appropriately tailoring the platform and conjugation strategy.

3.4 Conclusions

In this study, a strategy for sequentially co-localizing multiple enzymes on multifunctional nanoparticles was developed by using covalent binding and streptavidin-biotin coupling to immobilize GOX and SHRP on B/C-PS nanoparticles. Optimizing the individual enzyme immobilization led to retention of the activities of both GOX and SHRP. With optimal GOX and SHRP ratios, the GOX and SHRP were sequentially co-localized on B/C-PS nanoparticles. The optimized co-localization of GOX and SHRP enhanced the overall product conversion rate by approximately two-fold compared to the equivalent amount of free enzymes in solution. The performance of the immobilized GOX and SHRP mixture was comparable to that of the free enzyme combination, which is consistent with our previous work using single enzyme immobilization. These studies demonstrate the clear benefits of sequentially co-localizing multiple enzymes on multifunctional nanoparticles, leading to a simple and controllable platform for multi-enzyme co-localization to mimic the efficient multi-enzyme complex structure and function observed in Nature.

Acknowledgements

The authors are grateful to the National Science Foundation (CBET 0932517) for financial support.

References

Albertsson A-C, Varma IK. 2003. Recent developments in ring opening polymerization of lactones for biomedical applications. Biomacromolecules 4:1466–1486.

Aranaz I, Ramos V, De La Escalera S, Heras A. 2003. Co-immobilization of d-hydantoinase and d-carboamylase on Chitin: Application to the Synthesis of p-hydroxyphenylglycine. Biocatalysis Biotransform 21:349–356.

Berron BJ, Johnson LM, Ba X, McCall JD, Alvey NJ, Anseth KS, Bowman CN. 2011. Glucose oxidase-mediated polymerization as a platform for dual-mode signal amplification and biodetection. Biotechnol Bioeng 108:1521–1528.

Carrillo-Conde B, Garza A, Anderegg J, Narasimhan B, 2010. Protein adsorption on biodegradable polyanhydride microparticles. J. of Biomed Mater Res Part A, 95A:40–48.

Caruso F, Schüler C. 2000. Enzyme multilayers on colloid particles: assembly, stability, and enzymatic activity. Langmuir 16:9595–9603.

Christie RJ, Miyata K, Matsumoto Y, Nomoto T, Menasco D, Lai TC, Pennisi M, Osada K, Fukushima S, Nishiyama N, Yamasaki Y, Kataoka K. 2011. Effect of polymer structure on micelles formed between sirna and cationic block copolymer comprising thiols and amidines. Biomacromolecules 12:3174–3185.

Cui Y, Wei Q, Park H, Lieber CM. 2001. Nanowire nanosensors for highly sensitive and selective detection of biological and chemical species. Science 293:1289 –1292.

Determan AS, Wilson JH, Kipper MJ, Wannemuehler MJ, Narasimhan B. 2006. Protein stability in the presence of polymer degradation products: Consequences for controlled release formulations. Biomaterials 27:3312–3320.

Drechsler U, Fischer NO, Frankamp BL, Rotello VM. 2004. Highly efficient biocatalysts via covalent immobilization of candida rugosa lipase on ethylene glycol-modified gold–silica nanocomposites. Adv Mater 16:271–274.

El-Zahab B, Jia H, Wang P. 2004. Enabling multienzyme biocatalysis using nanoporous materials. Biotechnol. Bioeng 87:178–183.

Fazlollahi F, Angelow S, Yacobi NR, Marchelletta R, Yu ASL, Hamm-Alvarez SF, Borok Z, Kim K-J, Crandall ED. 2011. Polystyrene nanoparticle trafficking across MDCK-II. Nanomedicine: NBM 7:588–594.

Fears KP, Sivaraman B, Powell GL, Wu Y, Latour RA. 2009. Probing the conformation and orientation of adsorbed enzymes using side-chain modification. Langmuir 25:9319–9327.

Garcia-Galan C, Berenguer-Murcia Á, Fernandez-Lafuente R, Rodrigues RC.2011. Potential of different enzyme immobilization strategies to improve enzyme performance. Adv Synth Catal 353: 2885–2904.

Hrapovic S, Liu Y, Male KB, Luong JHT. 2003. Electrochemical biosensing platforms using platinum nanoparticles and carbon nanotubes. Anal. Chem. 76:1083–1088.

Jeffrey J G. 2004. The interaction of proteins with solid surfaces. Current Opinion in Structural Biology 14:110–115.

Jia J, Wang B, Wu A, Cheng G, Li Z, Dong S. 2002. A method to construct a third-generation horseradish peroxidase biosensor: self-assembling gold nanoparticles to three-dimensional sol−gel network. Anal. Chem. 74:2217–2223.

Johnson AK, Zawadzka AM, Deobald LA, Crawford RL, Paszczynski AJ. 2007. Novel method for immobilization of enzymes to magnetic nanoparticles. J Nanopart Res 10:1009–1025.

Katz E, Willner I. 2004. Integrated nanoparticle–biomolecule hybrid systems: synthesis, properties, and applications. Angew Chem Int Ed 43:6042–6108.

Keighron JD, Keating CD. 2010. Enzyme: nanoparticle bioconjugates with two sequential enzymes: stoichiometry and activity of malate dehydrogenase and citrate synthase on au nanoparticles. Langmuir 26:18992–19000.

Kondo A, Murakami F, Higashitani K. 1992. Circular-dichroism studies on conformational-changes in protein molecules upon adsorption on ultrafine polystyrene particles. Biotechnol Bioeng 40:889–894.

Lim SH, Wei J, Lin J, Li Q, KuaYou J. 2005. A glucose biosensor based on electrodeposition of palladium nanoparticles and glucose oxidase onto Nafion-solubilized carbon nanotube electrode. Biosens Bioelectron 20:2341–2346.

Liu W, Zhang S, Wang P. 2009. Nanoparticle-supported multi-enzyme biocatalysis with in situ cofactor regeneration. J Biotechnol 139:102–107.

Logan TC, Clark DS, Stachowiak TB, Svec F, Fréchet JMJ. 2007. Photopatterning enzymes on polymer monoliths in microfluidic devices for steady-state kinetic analysis and spatially separated multi-enzyme reactions. Anal. Chem. 79:6592–6598.

Lundqvist M, Stigler J, Elia G, Lynch I, Cedervall T, Dawson KA. 2008. Nanoparticle size and surface properties determine the protein corona with possible implications for biological impacts RID C-6582-2008. Proc. Natl. Acad. Sci. U.S.A. 105:14265–14270.

Lvov Y, Caruso F. 2001. Biocolloids with ordered urease multilayer shells as enzymatic reactors RID A-9587-2011. Anal. Chem. 73:4212–4217.

Matharu Z, Sumana G, Arya SK, Singh SP, Gupta V, Malhotra BD. 2007. Polyaniline Langmuir−Blodgett film based cholesterol biosensor. Langmuir 23:13188–13192.

Matsumoto T, Sawamoto S, Sakamoto T, Tanaka T, Fukuda H, Kondo A. 2011. Site-specific tetrameric streptavidin-protein conjugation using sortase A. J Biotechnol 152:37–42.

Miletić N, Abetz V, Ebert K, Loos K. 2010. Immobilization of Candida antarctica lipase B on Polystyrene Nanoparticles. Macromol Rapid Commun 31:71–74.

Narang U, Prasad PN, Bright FV, Ramanathan K, Kumar ND, Malhotra BD, Kamalasanan MN, Chandra S. 1994. Glucose biosensor based on a sol-gel-derived platform. Anal. Chem. 66:3139–3144.

Niemeyer CM. 2001. Nanoparticles, proteins, and nucleic acids: biotechnology meets materials science. Ange Chem Int Ed 40:4128–4158.

Pandey P, Singh SP, Arya SK, Gupta V, Datta M, Singh S, Malhotra BD. 2007. Application of Thiolated Gold Nanoparticles for the Enhancement of Glucose Oxidase Activity. Langmuir 23:3333–3337.

Pescador P, Katakis I, Toca-Herrera JL, Donath E. 2008. Efficiency of a Bienzyme Sequential Reaction System Immobilized on Polyelectrolyte Multilayer-Coated Colloids. Langmuir 24:14108–14114.

Rossi LM, Quach AD, Rosenzweig Z. 2004. Glucose oxidase-magnetite nanoparticle bioconjugate for glucose sensing. Analytical and Bioanalytical Chemistry 380:606–613.

Rupcich N., Brennan J.D. 2003. Coupled enzyme reaction microarrays based on pin-printing of sol-gel derived biomaterials. Anal Chim Acta 500:3–12.

Su S, Nutiu R, Filipe CDM, Li Y, Pelton R. 2007. Adsorption and covalent coupling of ATP-binding DNA aptamers onto cellulose. Langmuir 23:1300–1302.

Torres MP, Determan AS, Anderson GL, Mallapragada SK, Narasimhan B. 2007. Amphiphilic polyanhydrides for protein stabilization and release. Biomaterials 28:108–116.

Watanabe J, Ishihara K. 2005. Sequential Enzymatic Reactions and Stability of Biomolecules Immobilized onto Phospholipid Polymer Nanoparticles. Biomacromolecules 7:171–175.

Weber P, Ohlendorf D, Wendoloski J, Salemme F. 1989. Structural origins of high-affinity biotin binding to streptavidin. Science 243:85 –88.

West JL, Halas NJ. 2003. ENGINEERED NANOMATERIALS FOR BIOPHOTONICS APPLICATIONS: Improving Sensing, Imaging, and Therapeutics. Annu Rev Biomed Eng 5:285–292.

Williams RA, Blanch HW. 1994. Covalent immobilization of protein monolayers for biosensor applications. Biosens Bioelectron 9:159–167.

Xiao Y, Ju H-X, Chen H-Y. 1999. Hydrogen peroxide sensor based on horseradish peroxidase-labeled Au colloids immobilized on gold electrode surface by cysteamine monolayer. Anal Chim Acta 391:73–82.

Yi X, Huang-Xian J, Hong-Yuan C. 2000. Direct Electrochemistry of Horseradish Peroxidase Immobilized on a Colloid/Cysteamine-Modified Gold Electrode. Anal Biochem 278:22–28.

Table 3-1 Kinetic parameters for free and immobilized enzymes

	GOX	GOX-B-PS	SHRP	SHRP-PS
k_{cat} (s^{-1})	194.3 ± 9.6	160.1 ± 11.0	3.6 ± 0.09 × 10^4	4.0 ± 0.1× 10^4
K_m (μM)	7.9 ± 1.2 × 10^3	7.9 ± 0.9× 10^3	23.2 ± 1.2	20.9 ± 0.8

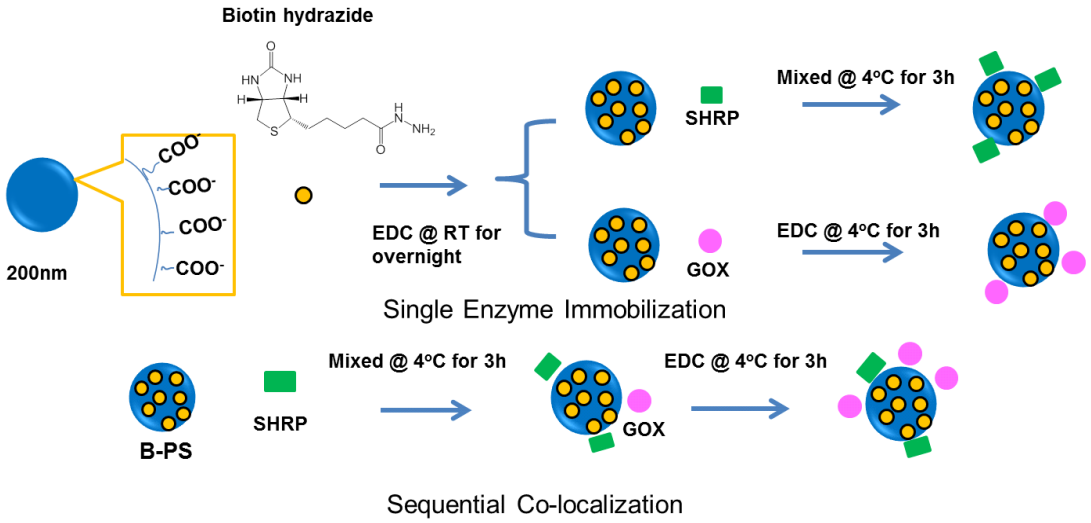

Figure 3.1Schematic of single enzyme immobilization and sequential co-localization strategy.

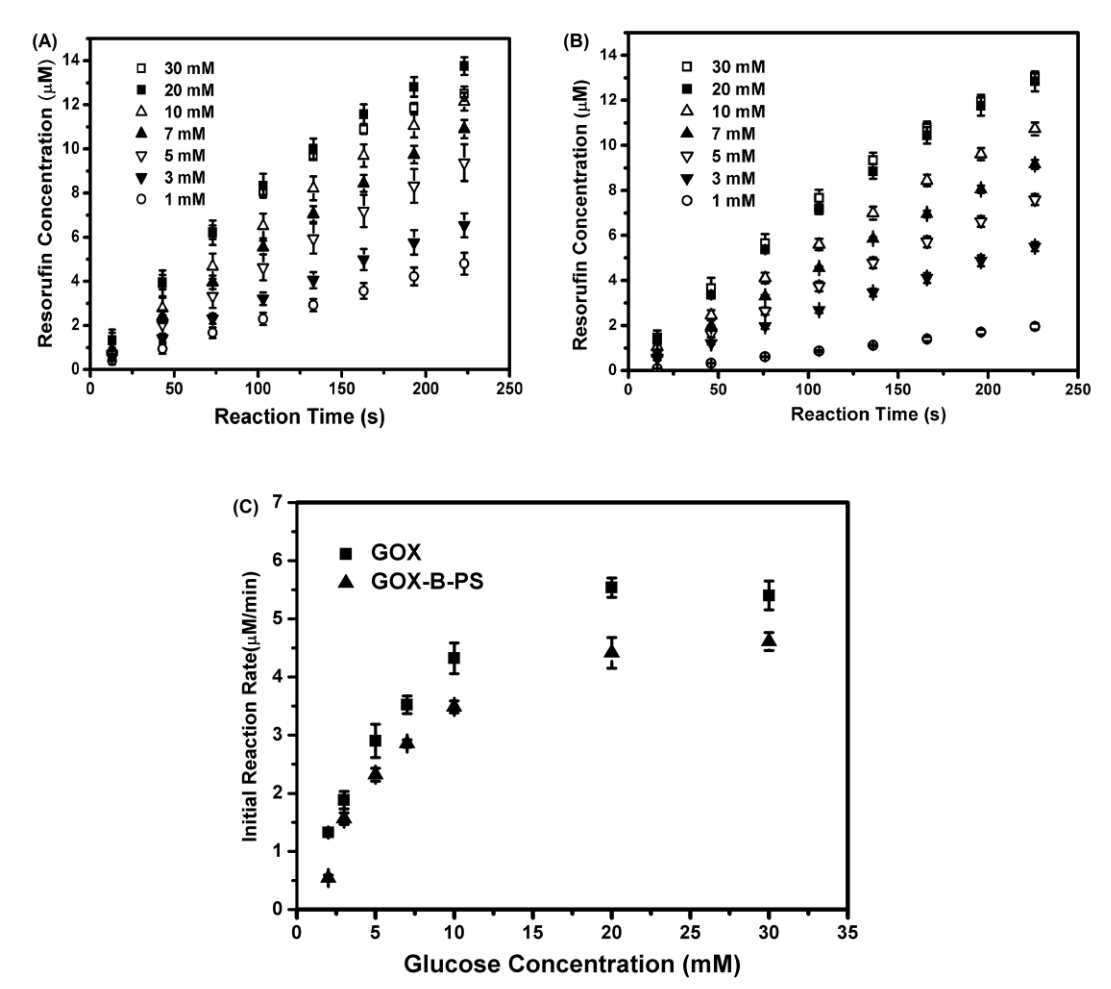

Figure 3.2 Comparison of the reaction kinetics catalyzed by equivalent free and immobilized GOX. (A) Product formation versus time for free GOX. (B) Product formation versus time for GOX-B/C-PS (C) The initial reaction rate as a function of glucose concentration.

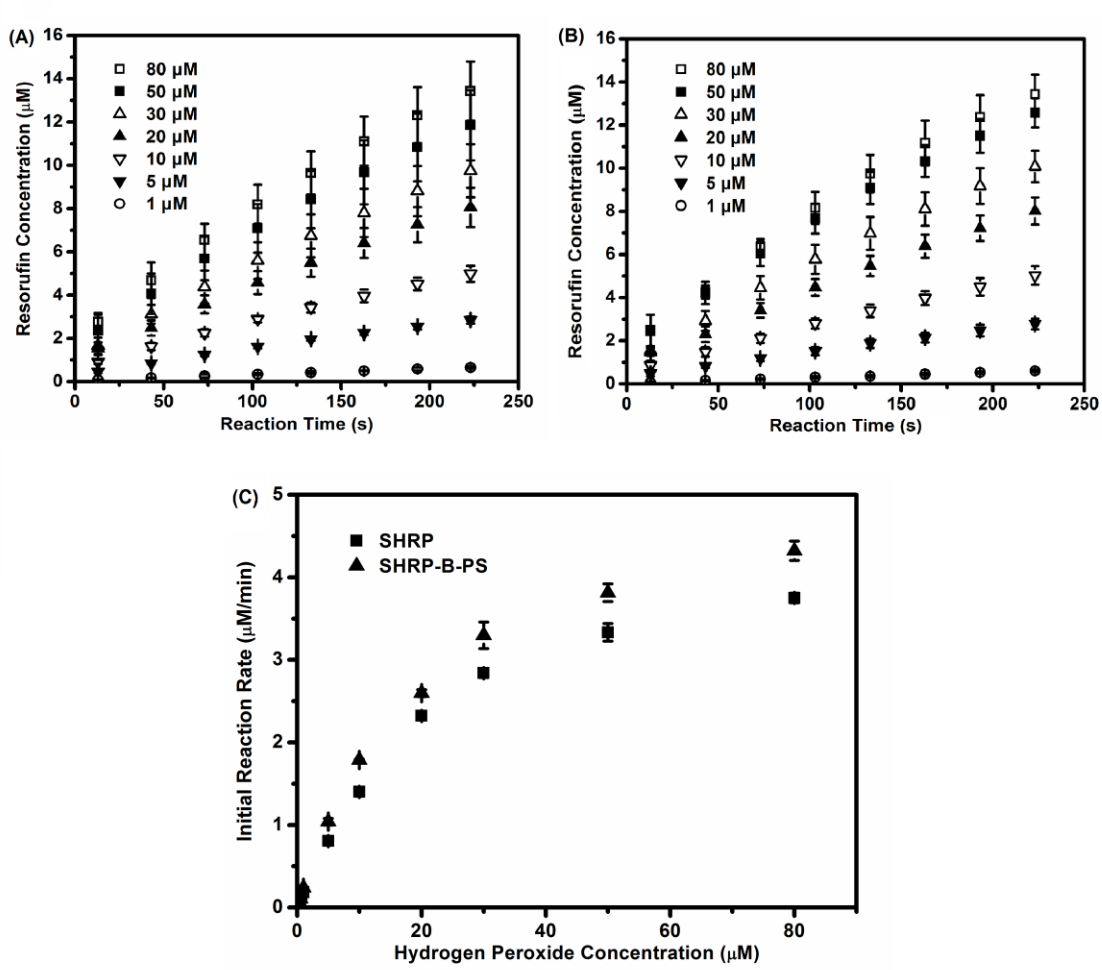

Figure 3.3 Comparison of the reaction kinetics catalyzed by equivalent free and immobilized SHRP. (A) Product formation versus time for free SHRP. (B) Product formation versus time for SHRP-B/C-PS (C) The initial reaction rate as a function of glucose concentration.

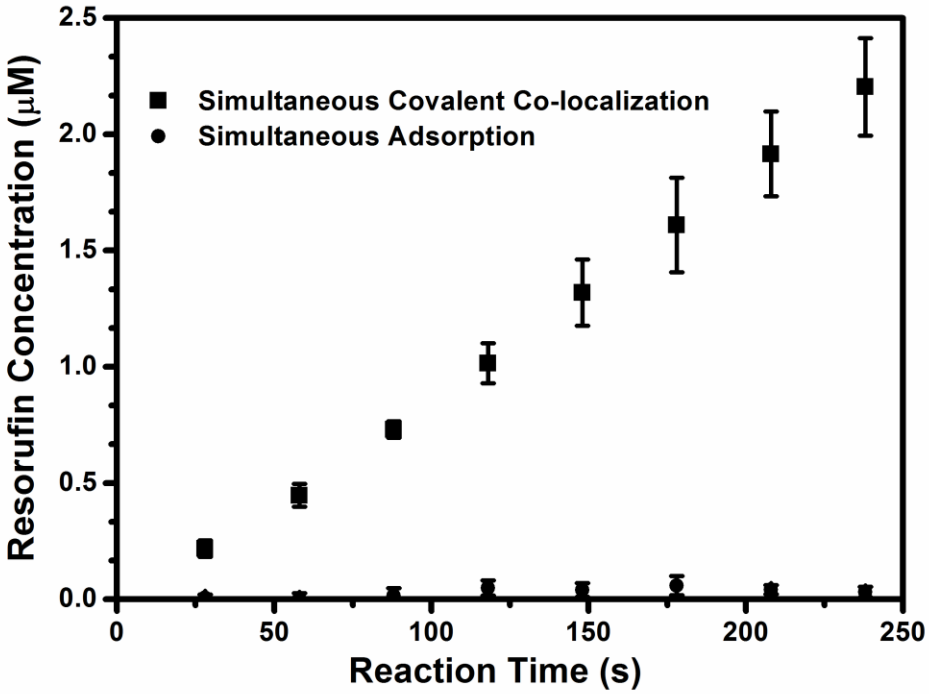

Figure 3.4 Comparison of the overall conversion rate catalyzed by simultaneous covalent co-localization of enzymes with that catalyzed by simultaneous adsorption of enzymes.

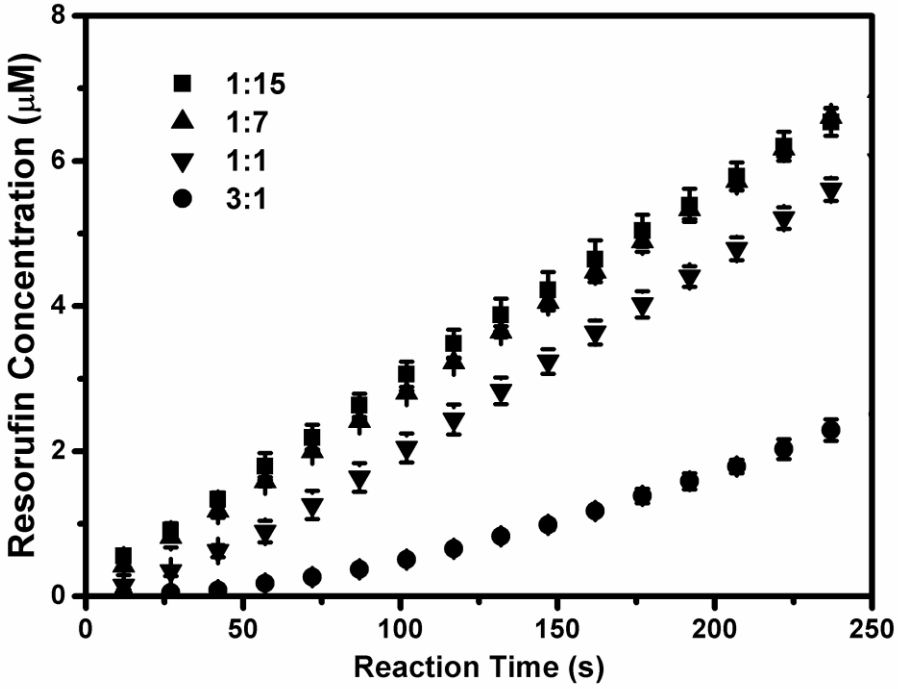

Figure 3.5 The overall conversion rate catalyzed by different molar ratios of free GOX and SHRP. The GOX concentration in all the assays was 0.005 nmol/mL and appropriate amounts of SHRP were added to make the GOX:SHRP molar ratio 1:15, 1:7, 1:1 and 3:1.

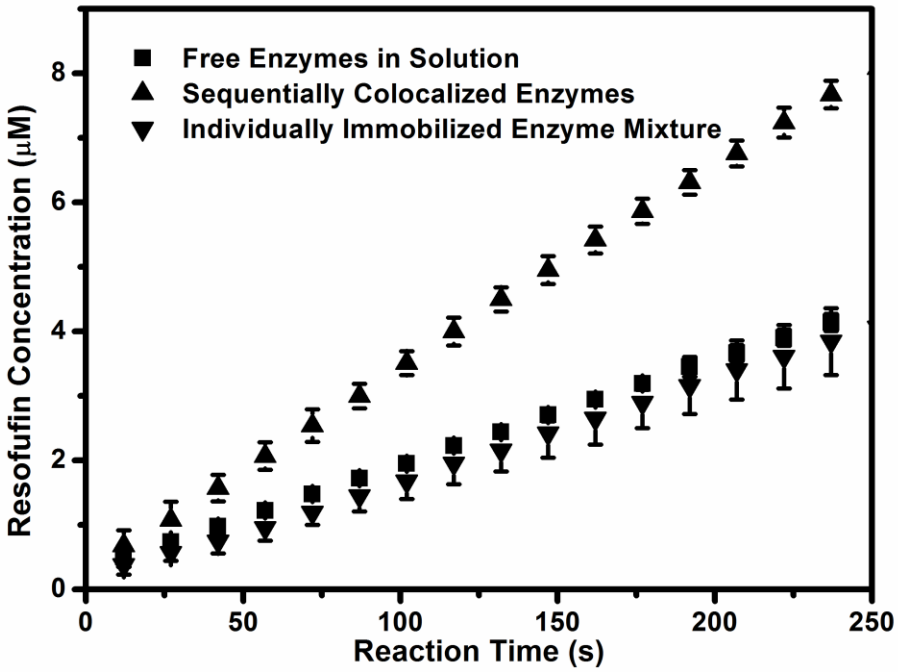

Figure 3.6 Comparison of the performance of sequentially co-localized enzymes with equivalent amount of mixtures of single immobilized enzymes and free enzymes in solution. Each assay contained 0.02 nmol/mL GOX and 0.06 nmol/mL SHRP on the nanoparticles or in solution.

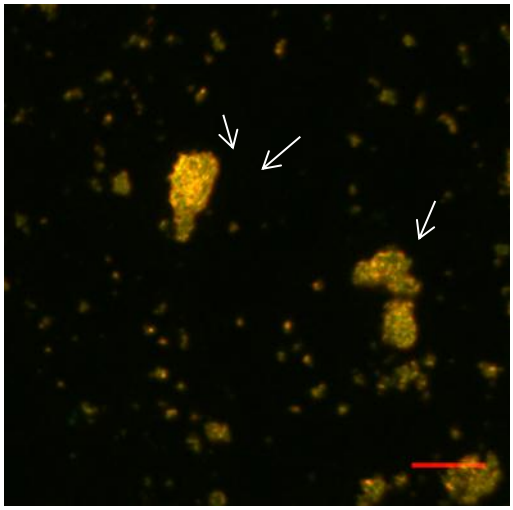

Figure 3.7 Observation of simultaneous co-localization of GOX and SHRP on C-PS nanoparticles using epi-fluorescence microscopy. Representative yellow areas are indicated by the white arrows. Scale bar: 10 µm.

Chapter 4 Block Copolymer-Quantum Dot Micelles for Multi-enzyme Co-localization

(Modified from a paper submitted to *Langmuir*)

Feng Jia, Yanjie Zhang, Balaji Narasimhan, and Surya K. Mallapragada

Department of Chemical and Biological Engineering, Iowa State University, Ames, IA 50011

Abstract

To mimic the structure and functionality of multi-enzyme complexes, which are widely present in Nature, Pluronic®-based micelles were designed to co-localize multiple enzymes. To stabilize the micelles as well as to enable characterization of single enzyme immobilization and multi-enzyme co-localization by Förster Resonance Energy Transfer (FRET), quantum dots (QDs) were encapsulated into the micelles to form Pluronic®-QD micelles using a novel micro-reactor. Model enzymes glucose oxidase and horseradish peroxidase were respectively labeled with fluorescent dyes. The results indicated that FRET quenching occurred between the QDs and dyes that labeled each type of enzyme in single enzyme immobilization studies as well as between the dyes in co-localization studies. These observations were consistent with increases in micelle size after adsorption of dye-enzymes as verified by dynamic light scattering. In addition, the activity of single enzymes was retained after immobilization. An optimized co-localization process improved the overall conversion rate by approximately 100% compared to equivalent concentrations of free enzymes in solution. This study demonstrates a versatile platform for multi-enzyme co-localization and an effective strategy to characterize multi-enzyme immobilization and co-localization, which can be applicable to many other multi-enzyme systems.

4.1 Introduction

The design and development of nanoscale platforms for co-localizing multiple active enzymes has been extensively studied due to its potential for efficient catalytic mechanisms.[1–4] In living cells, multi-enzyme complexes are composed of individual enzymes in a confined space, where each component enzyme works synergistically by transporting reactive intermediates among active sites rapidly to promote the overall cascaded reaction efficiency.[5,6] Such highly concerted mechanisms possess the advantages including maintaining high local concentration of the intermediates and reducing diffusion losses during the long-way transportation, which are especially critical for highly unstable reactive intermediates.[4,7] To mimic this process *in vitro*, researchers have developed various strategies and approaches to spatially co-localize multiple enzymes on carriers to achieve enhancement in reaction kinetics along with the ability to direct the reaction pathway.[8–13]

In one example, multiple enzymes adsorbed on chitin exhibited higher overall catalytic performance and stability at certain ranges of temperature and pH.[8] Another example described immobilization of coupled enzymes in different regions of a porous polymer monolith, which spatially defines small reaction areas to separate multiple enzymes in each portion. In this system, the plug flow direction of the substrate solution corresponding to the order of the cascaded reaction was found to maximize the final product yield.[9] To overcome the drawbacks of internal diffusion resistance in porous materials, researchers have used non-porous nanoparticle platforms based on gold, silica, and polymers to co-localize multiple enzymes, where the surface of rigid support materials were functionalized with soft enzyme layers.[10–13] For example, by mixing separated immobilized single enzymes and co-factors on silica nanoparticles, which was facilitated by Brownian collisions of the nanoparticles, the enzymes and co-factors were

easy to recover.[11] In co-localizing sequential multiple enzymes onto the nanoparticles, the order of each enzyme layer adsorbed on the nanoparticles was found to affect the overall product conversion rate; furthermore, co-localizing the enzymes on the same layer showed the highest catalytic kinetic performance.[12,13] Previous work from our laboratories demonstrated a sequential approach to co-localize enzymes on multi-functionalized polystyrene nanoparticles that resulted in kinetic performance improvements.[14] However, in addition to demonstrating the kinetic benefits of co-localizing multiple enzymes, it is desirable to control and characterize the co-localization of multiple enzymes on the same nanoparticles. In this work, we designed a novel micelle carrier to co-localize multiple enzymes with the ability to characterize enzyme immobilization and control co-localization.

Pluronic® tri-block copolymers and Pluronic®-based amphiphilic pentablock copolymers developed by our laboratory have shown great potential in biomineralization and drug/gene delivery.[15–20] These polymers have demonstrated excellent compatibility with proteins and the corresponding micelle structures are responsive to temperature and pH.[21,22] Recent work has showed that the stability of the micelle structure can be enhanced by encapsulation of hydrophobic semiconductor quantum dots (QDs).[23] QDs have demonstrated great potential for imaging and biosensing due to their unique rapid response, stability, and efficient fluorescence-based features.[24–27] Paired with suitable dyes, QDs can be used to measure nanoscale distances between molecules using principles of Förster resonance energy transfer (FRET).[28,29] In this work, we combined the well-known protein compatibility of Pluronic® micelles and the sensing attributes of QDs to develop a novel multi-enzyme co-localization strategy. Here, hydrophobic organic QDs were encapsulated into self-assembled amphiphilic Pluronic® tri-block micelles in aqueous solution using a flash nano-precipitation process (Figure 4.1). To

demonstrate the feasibility of this nanoscale platform, a model multi-enzyme system based on glucose oxidase (GOX) and horseradish peroxidase (HRP), which is known to exhibit a sequential reaction cascade [7] to produce resorufin was studied. Each enzyme was respectively labeled with appropriate fluorescent dyes to exhibit FRET with the QDs when single enzymes were adsorbed on the micelles and with themselves when the enzymes were co-localized (Figure 4.1). The enzymatic performance of adsorbed enzyme and co-localized multiple enzymes was evaluated by comparing with that of the respective free enzymes.

4.2 Experimental Section

4.2.1 Chemicals

Cadmium selenium (CdSe) quantum dots were synthesized as described previously.[30] Carboxyl reactive Alexa Fluor 594 (AF594) and Alexa Fluor 647 (AF647) fluorescent dyes and Amplex® Red were purchased from Invitrogen (Carlsbad, CA). Pluronic® F127, GOX (~200 U/mg, from *Aspergillus niger*), horseradish peroxidase (HRP) (~250 U/mg, from horseradish), and resorufin were purchased from Sigma-Aldridge (St. Louis, MO). Dimethyl sulfate (DMSO), 3% hydrogen peroxide, sodium chloride, and trisodium phosphate were purchased from Fisher Scientific (Hampton, NH). All the aqueous solutions were prepared using purified water from Thermo Scientific's Barnstead Nanopure Ultrapure Water System.

4.2.2 Fabrication of PLQD micelles

In this procedure, Pluronic® F127 polymers and QDs were pre-dissolved in THF at respective concentrations of 154 mg/mL and 2.3 mg/mL. Next, 2 mL of well-mixed PLQD solution and three equivalent volumes of PBS (0.1 M Na_3PO_4 and 0.15 M NaCl, pH 7.2) were pumped simultaneously into a four-channel micro-reactor using syringe

pumps at a flow rate of 2 mL/min. The organic and aqueous solutions were mixed in the central mixing compartment, where nucleation and growth of the micelles occurred in the presence of the QDs. The solutions exited the reactor and flowed into a beaker containing 2 mL of PBS buffer for quenching. The final product contained 20% THF, 31 mg/mL Pluronic® F127 and 0.5 mg/mL QDs, which was stored at 4 ^{o}C. The size of the PLQD and the enzyme-PLQD micelles was measured using a Malvern Zetasizer Nano-ZS90 dynamic light scattering system using Malvern disposable cuvettes (Malvern Instruments, Southborough, MA).

4.2.3 Enzyme labeling

Both GOX and HRP were labeled with fluorescent dyes that exhibit FRET with the QDs encapsulated in the micelles. First, 1 mg of carboxyl-reactive fluorescent dyes (AF594) were separated into 8 aliquot portions into 1.7 mL centrifuge tubes. All the aliquots were dried with nitrogen and stored at -80 ^{o}C. The attachment procedure was modified from the manufacturer's manual. Briefly, for individual enzyme labeling, in each aliquot dye-containing tube, 5 mg of GOX or HRP and 0.5 mL PBS buffer were added. The pH was adjusted using 0.5 M Na_3CO_3 solution to 8.3, which promoted the attachment reaction. The reaction mixture was incubated rotationally at room temperature for 1 h and continued at 4 ^{o}C overnight. The unattached dyes were separated using a dialysis membrane centrifuge tube at 10,000 X g for 10 min. The conjugated enzyme-dye solution retained in the dialysis tube was collected and diluted to a protein concentration of 1 mg/mL. The enzyme concentration was determined using UV-Vis spectroscopy (Cary 50 MPR microplate reader, Varian, USA) following the manufacturer's procedure. The resultant product was stored at 4^{o}C.

4.2.4 Adsorption of single enzymes onto PLQD micelles

Initially, centrifuge tubes were pretreated with 1 mg/mL BSA buffer to prevent non-specific protein adsorption onto the wall of the tubes. In each reaction tube, appropriate volumes of AF594 labeled GOX or HRP were mixed with 250 µL of stock PLQD micelle solution. PBS buffer was used to bring up the total volume to 500 µL. The reaction was carried out overnight with rotation at 4^{o}C. The experiments were performed at various enzyme concentrations. In the final solution, the concentrations of GOX-AF594 were 0.1 µM, 0.25 µM and 0.625 µM respectively, and the corresponding values for AF594-HRP were 0.91 µM and 2.27 µM, respectively.

4.2.5 Multi-enzyme co-localization on PLQD micelles

To co-localize both GOX-AF594 and HRP-AF647 on PLQD micelles, appropriate volumes of dye-enzyme conjugates were added to a 250 µL PLQD stock solution with PBS buffer to obtain a final solution volume of 500 µL. The reaction solution containing 0.1 nM GOX and 1.1 nM HRP was incubated overnight with rotation at 4 ^{o}C.

4.2.6 Single enzyme adsorption and multi-enzyme co-localization using FRET

A FRET study of GOX-AF594- or HRP-AF594-PLQD solution was carried out using a dual monochromator spectrofluorimeter (Fluoromax-4, Horiba Jobin Yvon, USA) with excitation at 440 nm and slit widths of 4 nm (excitation and emission) with 5 fold-dilution. For the GOX-AF594 and HRP-AF647 co-localization on the PLQDs, a wavelength of 594 nm was used to excite the samples.

4.2.7 Enzyme assays

The individual enzyme and multi-enzyme assays were performed as described previously[14]. For HRP, the kinetic reactions were carried out by adding 20 µL of 100

ng/mL HRP-AF594 or HRP-AF594-PLQD into 180 µL of substrate solution in a 96-well plate and monitored using a fluorescent plate reader. For GOX, 10 µL of 5 µg/mL HRP was added into the 180 µL substrate solution and the reaction was subsequently initiated by adding 10 µL of 2 µg/mLGOX-AF594 or GOX-AF594-PLQD. For the co-localized enzymes, 10 µL of the prepared co-localized sample was added to 190 µL of substrate solution containing glucose and Amplex red and the reaction was monitored using a fluorescent plate reader as described above. To compare with the free enzyme mixture, equivalent concentrations of each individual enzyme was added into the same substrate solution and used as a control.

4.2.8 Statistical Analysis

The mean and standard deviation data presented herein were the results of independent experiments that were performed in triplicate. Significant differences between groups were evaluated by a Student's t-test with $p \leq 0.05$.

4.3 Results and Discussion

4.3.1 Adsorption of single enzymes on PLQDs

The PLQD micelles were produced in a multi-inlet vortex mixer based on flash nano-precipitation, in which the hydrophobic organic QDs were encapsulated into self-assembled amphiphilic Pluronic® tri-block micelles. In general, smaller particles exhibit higher enzyme loading capacity because of their large surface area per unit volume. However, nanoparticles that are too small may significantly reduce the probability of co-localization of multiple enzymes on the same nanoparticles. The size of the individual QD nanoparticles and that of the Pluronic® micelles ranged from 2 to 10 nm.[31] It has been reported that on average, the loading capacity of one QD particle is up to 3 molecules of HRP.[32] The average size of the PLQD micelles fabricated was approximately 145 nm, which resulted in larger loading capacity for enzymes when compared to QD particles or Pluronic® micelles. In the subsequent enzyme adsorption studies, the inner core of the PLQDs, which consists of the QDs and the hydrophobic segment of the polymer primarily attract the enzyme molecules and retain them on the micelles. The outer brushes, formed by the hydrophilic blocks of the polymer, also interact with the protein to prevent unfavorable conformational changes, leading to preservation of the enzymatic activity. The size of the micelles before and after adsorption of dye-conjugated enzymes was measured using DLS. As shown in Figure 2, the size distribution of the micelles prior to adsorption was narrow. While the adsorption of the dye-conjugated enzymes did not significantly affect the micelle size distribution, it increased the mean size of the micelles (Table 4.1). Overall, the micelle size increased with increasing enzyme concentration. The larger micelle size at high enzyme concentration may be attributed to a combination of compact loading and adsorption of multiple layers of enzymes onto the micelles. When the enzyme concentrations were

further increased (i.e., to twice the highest concentrations used), the size of the PLQD-enzyme micelles decreased to approximately 40-50nm (data not shown). This apparent decrease may be attributed to oversaturation of the enzyme, and the smaller size is a result of a bi-modal distribution of free dye-conjugated enzyme molecules and the PLQD-enzyme micelles. The subsequent single enzyme kinetics studies were carried out at or below the higher enzyme concentration(s) to minimize the presence of free enzymes in solution.

4.3.2 FRET study between QDs and dye-conjugated enzymes

To further characterize single enzyme adsorption onto the micelles, each enzyme was labeled with a fluorescent dye that can be paired with the QDs and exhibit FRET. Typically, FRET occurs when the distance between the donor and the accepter is within 10 nm.[33] An excitation wavelength of 440 nm was used to maximize the excitation of QDs and minimize the direct excitation of the dye. Figure 3 shows energy transfer from the QDs to the dyes as indicated from the quenching of the primary QD peak at 570 nm by adsorption of the dye-conjugated enzymes. In control experiments, the QD peak was not quenched by adsorption of enzymes without dye labeling (blue curve in Figure 4.3). From these experiments, it is reasonable to surmise that the presence of the dye caused significant quenching of the QD peak, which suggests that the distance between the dye and QD is 10 nm or less. The peak of the dye at 620 nm was not obvious, which may be because the energy used was not high enough to excite the dye. In the PLQD micelles, the QDs on the outer shell were quenched by the dyes on the enzyme close to the micelle surface. Hence, the dyes on the enzymes that are far away from the QDs cannot be excited. The energy transferred from the QDs was not high enough to excite all the dyes, which may also explain the lack of a linear correlation between quenching and enzyme concentration.

4.3.3 Catalytic performance of single enzymes adsorbed on PLQDs

Before performing co-localization studies, the catalytic performance of single enzymes adsorbed onto PLQDs was evaluated to ensure that enzyme activity was not affected by adsorption. Previous studies have shown that covalently immobilized GOX on magnetite nanoparticles has similar activity as free enzyme in solution, likely because conformational changes did not block access to the active site.[34] To maximize the loading as well as enzymatic activity, the reaction was carried out overnight at 4 ^{o}C. In these experiments, the single enzymes were labeled with AF594 dye for consistency.

The kinetics of the reaction catalyzed by each enzyme was evaluated to compare enzymatic performance of adsorbed enzyme vs. free enzyme in solution. The amount of final product concentration in solution as a function of time was measured at each glucose substrate concentration using UV-Vis spectroscopy. All the initial reaction rates were estimated from the derivatives of a polynomial equation, which modeled the change in the resorufin concentration with reaction time. The data in Figure 4.4(a) were obtained by plotting initial reaction rates vs. substrate concentration and indicate that the adsorbed and free enzymes displayed similar kinetic behavior. To determine the kinetic parameters, a Michaelis-Menten model was used and the K_m and v_{max} values of free and adsorbed GOX were estimated using a linear least squares method. These values are shown in Table 4.2. The K_m values for both adsorbed and free GOX were 8.9 mM, which indicated that the affinity of the enzyme active site to the substrate did not change after adsorption. Likewise, the v_{max} values of both adsorbed and free enzyme were 11.1 μM/min. Overall, the GOX activity was retained after adsorption. Similar analyses were performed to obtain the kinetic parameters of free and adsorbed HRP (Figure 4.4(b)). As shown in Table 4.2, the K_m and v_{max} values for both free and adsorbed HRP were statistically indistinguishable, indicating that the adsorbed HRP also retained its activity.

4.3.4 Co-localization of GOX-AF594 and AF-647-HRP on PLQD micelles

To maximize the production of resorufin, the ratio of the concentrations of free GOX and HRP was varied from a GOX:HRP molar ratio of 1:4 to 1:40. The results indicated that resorufin production increased with increasing HRP concentration and a plateau was reached at a GOX:HRP ratio of 1:10 (data not shown). Based on these results, a GOX to HRP molar ratio of 1:10 was selected to perform the co-localization studies.

In these studies, an excitation wavelength of 594 nm was chosen to maximize the emission of QDs and to minimize the direct excitation of the dye(s). When both HRP-AF647 and GOX-AF594 were mixed with the PLQD micelles, the primary AF594 peak at 620 nm was quenched (Figure 4.5) in contrast to the situation when an equivalent concentration of GOX-AF594 was adsorbed onto the PLQD micelles. The quenching demonstrates energy transfer between the AF594 and AF647 dyes. The quenching also indicated that the dyes were within a few nm of each other, providing indirect evidence of co-localization on the same PLQD micelles.

The enzymatic performance of the optimized co-localized GOX and HRP system was evaluated by measuring the kinetics of the coupled reaction catalyzed by this “artificial” multi-enzyme complex. Equivalent concentrations of free enzymes in solution were studied under the same experimental conditions as a control. The results shown in Figure 4.6 indicate that co-localizing the two enzymes on the same PLQD micelles enhanced the overall product conversion by 100%.

These results demonstrate the clear benefits of sequentially co-localizing multiple enzymes on nanoscale platforms. In many real-world systems, it is critical to co-localize enzymes so that reaction intermediates can rapidly find the next active site for the

reaction to proceed. In situations where the intermediate product has a short lifetime, such a strategy may pay even more dividends. It is important to co-localize the enzymes within a few nm of each other (as demonstrated by FRET in this study) to enable production of the desired product. The biomimetic strategy outlined herein shows the value of using nanoscale platforms to accomplish this goal. This strategy is broadly applicable to other sequentially coupled multi-enzyme reactions by appropriately tailoring the nanoscale platform and co-localization methodology.

4.4 Conclusions

In this study, novel QD-embedded Pluronic®-based micelles were designed to co-localize multiple enzymes. It was shown that adsorption of single enzymes led to quenching of the fluorescence due to the QDs, indicative of FRET between the enzyme and the QDs. The catalytic activity of single enzymes was retained after immobilization. The occurrence of FRET between the two enzymes, when conjugated to the micelles, demonstrated that the enzymes were within a few nm of each other, which is indirectly indicative of co-localization on the same PLQD micelle. The co-localization of both enzymes on PLQD micelles enhanced the overall conversion rate by approximately 100% compared to the equivalent concentration of free enzymes in solution. This study describes the design of a nanoscale biomimetic materials platform for multi-enzyme co-localization and an effective strategy to characterize multi-enzyme immobilization and co-localization.

Acknowledgments

The authors are grateful to the National Science Foundation (CBET 0932517) for financial support. BN acknowledges the Vlasta Klima Balloun Professorship in Chemical

and Biological Engineering and SKM acknowledges the Stanley Chair of Interdisciplinary Engineering.

References

(1) Fernandez-Lafuente, R. Stabilization of multimeric enzymes: Strategies to prevent subunit dissociation. *Enzyme. Microb. Technol.* **2009**, *45*, 405–418.
(2) Garcia-Galan, C.; Berenguer-Murcia, A.; Fernandez-Lafuente, R.; Rodrigues, R. C. Potential of different enzyme immobilization strategies to improve enzyme performance. *Adv. Synth. Catal.* **2011**, *353*, 2885–2904.
(3) Tran, D. N.; Balkus, K. J. Perspective of recent progress in immobilization of enzymes. *ACS Catal.* **2011**, *1*, 956–968.
(4) Schoffelen, S.; van Hest, J. C. M. Multi-enzyme systems: bringing enzymes together in vitro. *Soft Matter* **2012**, *8*, 1736–1746.
(5) Domingo, G. J.; Chauhan, H. J.; Lessard, I. A. D.; Fuller, C.; Perham, R. N. Self-assembly and catalytic activity of the pyruvate dehydrogenase multienzyme complex from Bacillus stearothermophilus. *Eur. J. Biochem.* **2001**, *266*, 1136–1146.
(6) Ermakov, G. L.; Goldstein, B. N. Kinetic manifestations of structural self-organization for the components of the pyruvate dehydrogenase complex. A mathematical model. *Biochem.-Moscow* **1997**, *62*, 583–595.
(7) Conrado, R. J.; Varner, J. D.; DeLisa, M. P. Engineering the spatial organization of metabolic enzymes: mimicking nature's synergy. *Curr. Opin. Biotechnol* **2008**, *19*, 492–499.
(8) Aranaz, I.; Ramos, V.; Escalera, S. D. L.; Heras, A. Co-immobilization of d-hydantoinase and d-carboamylase on chitin: application to the synthesis of p-hydroxyphenylglycine. *Biocatal. Biotransform* **2003**, *21*, 349–356.
(9) Logan, T. C.; Clark, D. S.; Stachowiak, T. B.; Svec, F.; Fréchet, J. M. J. Photopatterning enzymes on polymer monoliths in microfluidic devices for steady-state kinetic analysis and spatially separated multi-enzyme reactions. *Anal. Chem.* **2007**, *79*, 6592–6598.
(10) Watanabe, J.; Ishihara, K. Sequential enzymatic reactions and stability of biomolecules immobilized onto phospholipid polymer nanoparticles. *Biomacromolecules* **2005**, *7*, 171–175.
(11) Liu, W.; Zhang, S.; Wang, P. Nanoparticle-supported multi-enzyme biocatalysis with in situ cofactor regeneration. *J.of Biotechnol.* **2009**, *139*, 102–107.
(12) Keighron, J. D.; Keating, C. D. Enzyme:nanoparticle bioconjugates with two sequential enzymes: stoichiometry and activity of malate dehydrogenase and citrate synthase on au nanoparticles. *Langmuir* **2010**, *26*, 18992–19000.
(13) Pescador, P.; Katakis, I.; Toca-Herrera, J. L.; Donath, E. Efficiency of a bienzyme sequential reaction system immobilized on polyelectrolyte multilayer-coated colloids. *Langmuir* **2008**, *24*, 14108–14114.
(14) Jia, F.; Mallapragada, S.; Narasimhan, B. Biomimetic multi-enzyme complexes based on nanoscale platforms. *AIChE Lett.*
(15) Yusufoglu, Y.; Hu, Y.; Kanapathipillai, M.; Kramer, M.; Kalay, Y. E.; Thiyagarajan, P.; Akinc, M.; Schmidt-Rohr, K.; Mallapragada, S. Bioinspired synthesis of self-assembled calcium phosphate nanocomposites using block copolymer-peptide conjugates. *J. of Mater. Res.* **2008**, *23*, 3196–3212.
(16) Zhang, B.; Jia, F.; Fleming, M. Q.; Mallapragada, S. K. Injectable self-assembled block copolymers for sustained gene and drug co-delivery: An in vitro study. *Int. J. Pharm.* **2012**, *427*, 88–96.
(17) Prozorov, T.; Mallapragada, S. K.; Narasimhan, B.; Wang, L.; Palo, P.; Nilsen-Hamilton, M.; Williams, T. J.; Bazylinski, D. A.; Prozorov, R.; Canfield, P. C. Protein-

Mediated Synthesis of Uniform Superparamagnetic Magnetite Nanocrystals. *Adv. Funct. Mater.* **2007**, *17*, 951–957.
(18) Hu, Y.-Y.; Liu, X. P.; Ma, X.; Rawal, A.; Prozorov, T.; Akinc, M.; Mallapragada, S. K.; Schmidt-Rohr, K. Biomimetic Self-Assembling Copolymer−Hydroxyapatite Nanocomposites with the Nanocrystal Size Controlled by Citrate. *Chem. Mater.* **2011**, *23*, 2481–2490.
(19) Prozorov, T.; Palo, P.; Wang, L.; Nilsen-Hamilton, M.; Jones, D.; Orr, D.; Mallapragada, S. K.; Narasimhan, B.; Canfield, P. C.; Prozorov, R. Cobalt Ferrite Nanocrystals: Out-Performing Magnetotactic Bacteria. *ACS Nano* **2007**, *1*, 228–233.
(20) Anderson, B. C.; Cox, S. M.; Bloom, P. D.; Sheares, V. V.; Mallapragada, S. K. Synthesis and Characterization of Diblock and Gel-Forming Pentablock Copolymers of Tertiary Amine Methacrylates, Poly(ethylene glycol), and Poly(propylene glycol). *Macromolecules* **2003**, *36*, 1670–1676.
(21) Determan, M. D.; Cox, J. P.; Seifert, S.; Thiyagarajan, P.; Mallapragada, S. K. Synthesis and characterization of temperature and pH-responsive pentablock copolymers. *Polymer* **2005**, *46*, 6933–6946.
(22) Sharma, P. K.; Bhatia, S. R. Effect of anti-inflammatories on Pluronic® F127: micellar assembly, gelation and partitioning. *Int. J. Pharm.* **2004**, *278*, 361–377.
(23) Zhang, Y.; Clapp, A. Overview of Stabilizing Ligands for Biocompatible Quantum Dot Nanocrystals. *Sens.* **2011**, *11*, 11036–11055.
(24) Resch-Genger, U.; Grabolle, M.; Cavaliere-Jaricot, S.; Nitschke, R.; Nann, T. Quantum dots versus organic dyes as fluorescent labels. *Nat. Methods.* **2008**, *5*, 763–775.
(25) Miyawaki, A. Visualization of the Spatial and Temporal Dynamics of Intracellular Signaling. *Dev. Cell* **2003**, *4*, 295–305.
(26) Mattoussi, H.; Mauro, J. M.; Goldman, E. R.; Anderson, G. P.; Sundar, V. C.; Mikulec, F. V.; Bawendi, M. G. Self-Assembly of CdSe−ZnS Quantum Dot Bioconjugates Using an Engineered Recombinant Protein. *J. Am. Chem. Soc.* **2000**, *122*, 12142–12150.
(27) Wang, J.; Xin, X.; Lin, Z. Cu_2ZnSnS_4 nanocrystals and graphene quantum dots for photovoltaics. *Nanoscale* **2011**, *3*, 3040.
(28) Schuler, B.; Eaton, W. A. Protein folding studied by single-molecule FRET. *Curr. Opin. Struct. Biol.* **2008**, *18*, 16–26.
(29) Zhang, C.-Y.; Yeh, H.-C.; Kuroki, M. T.; Wang, T.-H. Single-quantum-dot-based DNA nanosensor. *Nat. Mater.* **2005**, *4*, 826–831.
(30) Zhang, Y.; Schnoes, A. M.; Clapp, A. R. Dithiocarbamates as Capping Ligands for Water-Soluble Quantum Dots. *ACS Appl. Mater. Interfaces* **2010**, *2*, 3384–3395.
(31) Ipe, B. I.; Lehnig, M.; Niemeyer, C. M. On the Generation of Free Radical Species from Quantum Dots. *Small* **2005**, *1*, 706–709.
(32) Fruk, L.; Rajendran, V.; Spengler, M.; Niemeyer, C. M. Light-Induced Triggering of Peroxidase Activity Using Quantum Dots. *ChemBioChem* **2007**, *8*, 2195–2198.
(33) Yun, C. S.; Javier, A.; Jennings, T.; Fisher, M.; Hira, S.; Peterson, S.; Hopkins, B.; Reich, N. O.; Strouse, G. F. Nanometal Surface Energy Transfer in Optical Rulers, Breaking the FRET Barrier. *J. Am. Chem. Soc.* **2005**, *127*, 3115–3119.
(34) Rossi, L. M.; Quach, A. D.; Rosenzweig, Z. Glucose oxidase-magnetite nanoparticle bioconjugate for glucose sensing. *Anal. Bioanal. Chem.* **2004**, *380*, 606–613.

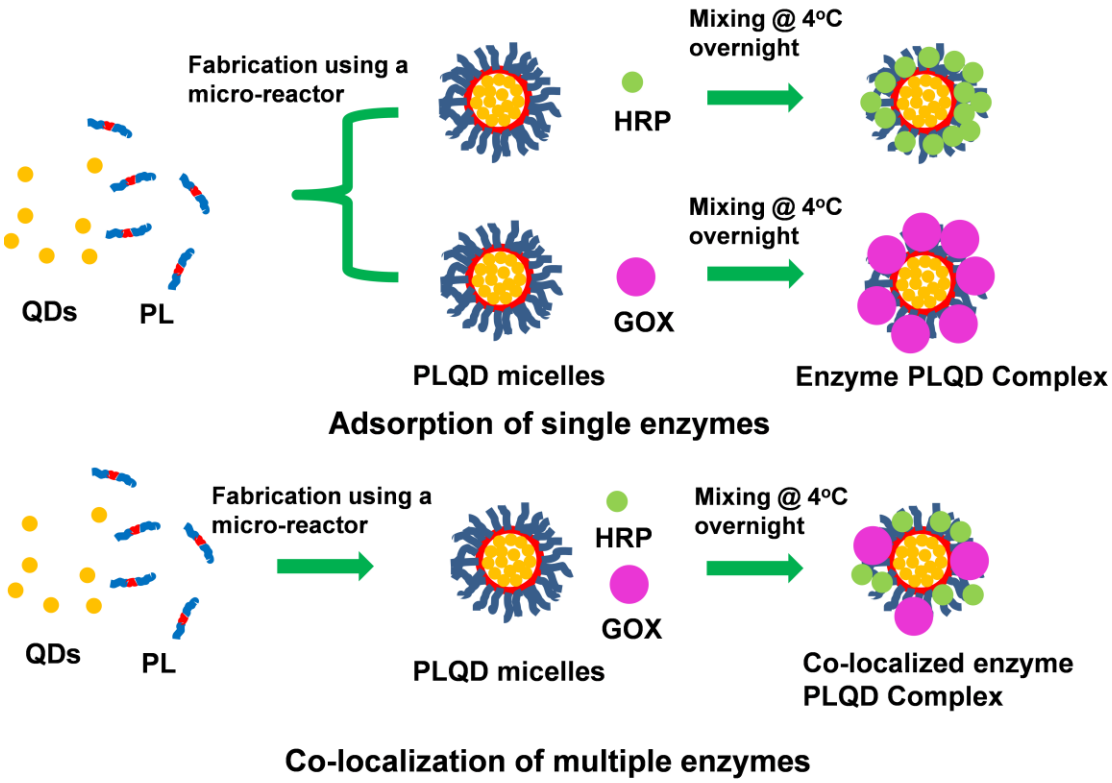

Figure 4.1 Schematic representation of the strategies for adsorption of single enzymes (top) and co-localization of multiple enzymes (bottom) on Pluronic®-QD (PLQD) micelles. Note that the polymers, QDs and enzymes are approximately drawn to scale.

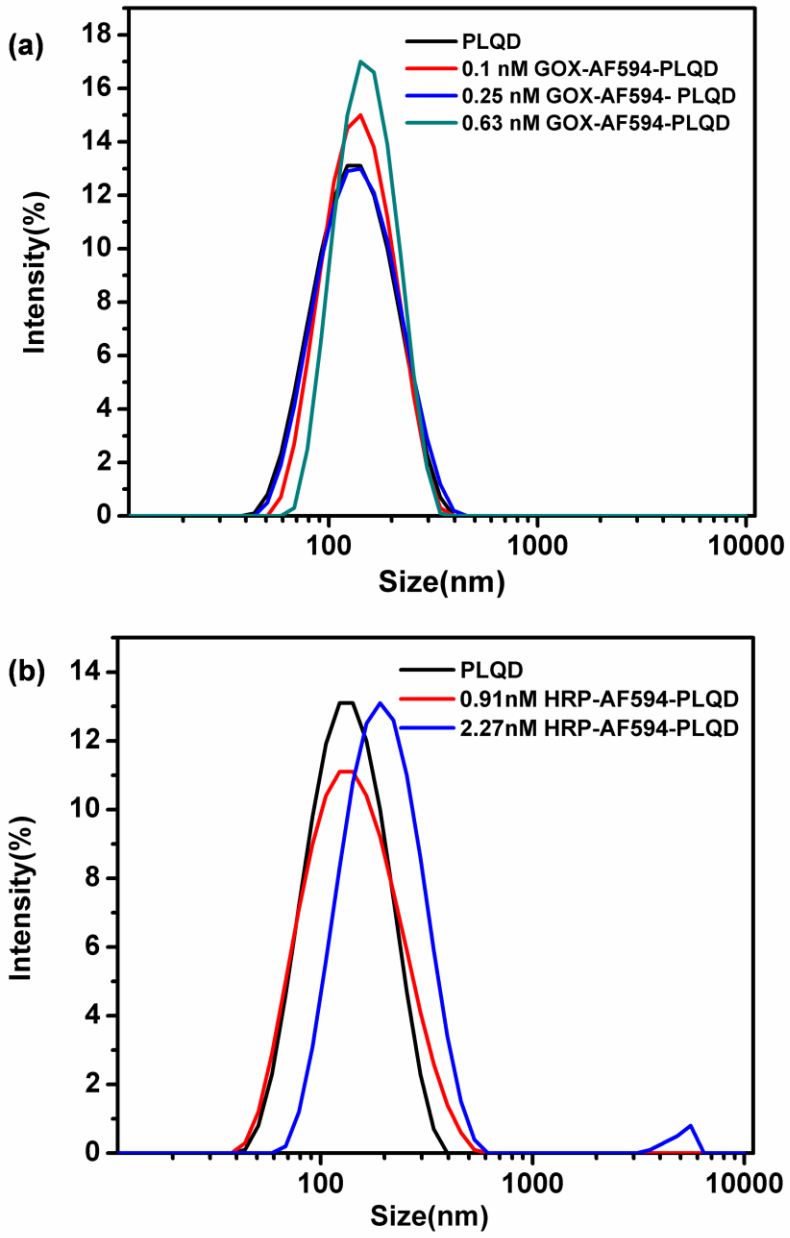

Figure 4.2 Size distribution of PLQD micelles characterized by DLS: (a) after adsorption of GOX-AF594 at three different concentrations; and (b) after adsorption of HRP-AF594 at two different concentrations.

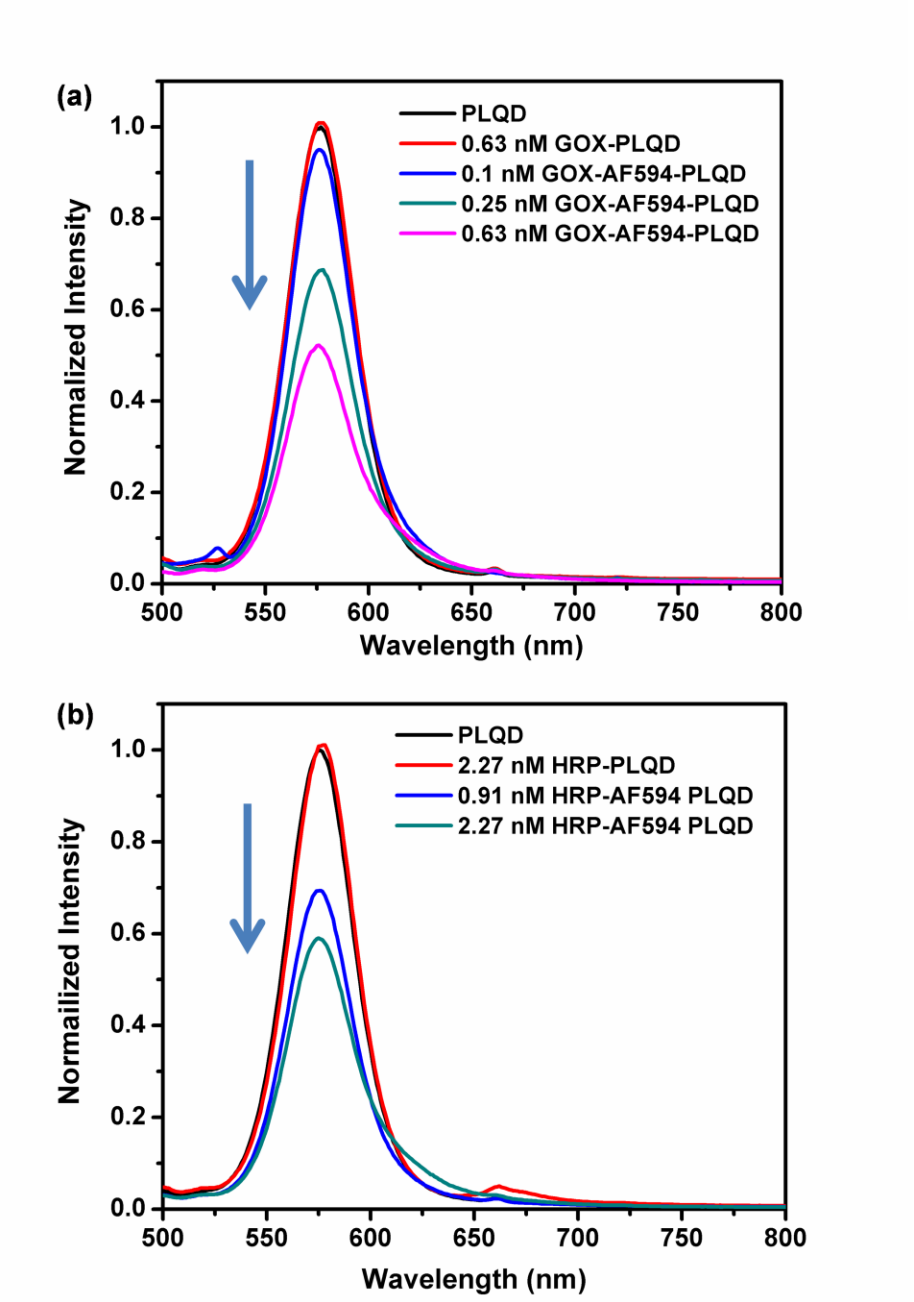

Figure 4.3 Demonstration of FRET between the QDs and AF594 dye-conjugated enzyme: (a) GOX-AF594 and (b) HRP-AF594. The arrow indicates quenching of the primary peak at 570 nm. In each figure, the fluorescence intensities of samples with enzymes or dye-enzymes were normalized to that of PLQD micelles.

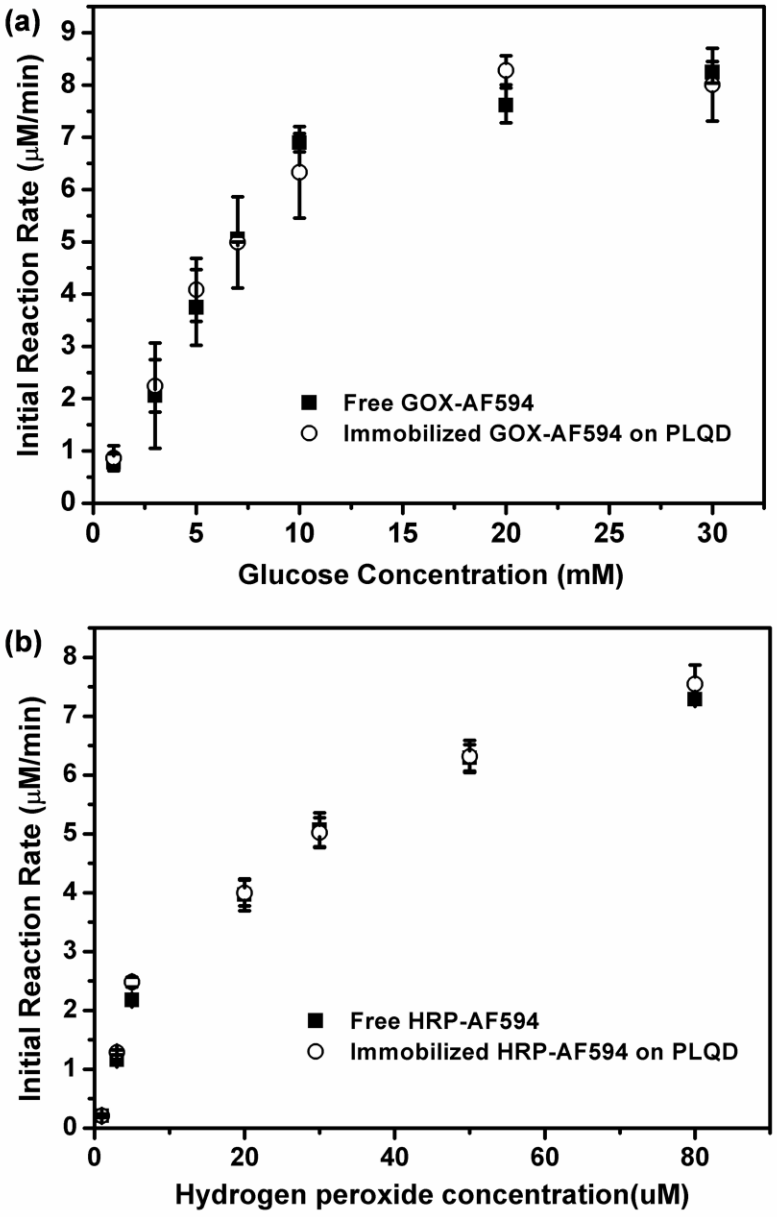

Figure 4.4 Initial reaction rate as a function of substrate concentration for: (a) free and adsorbed GOX-AF594 and (b) free and adsorbed HRP-AF594.

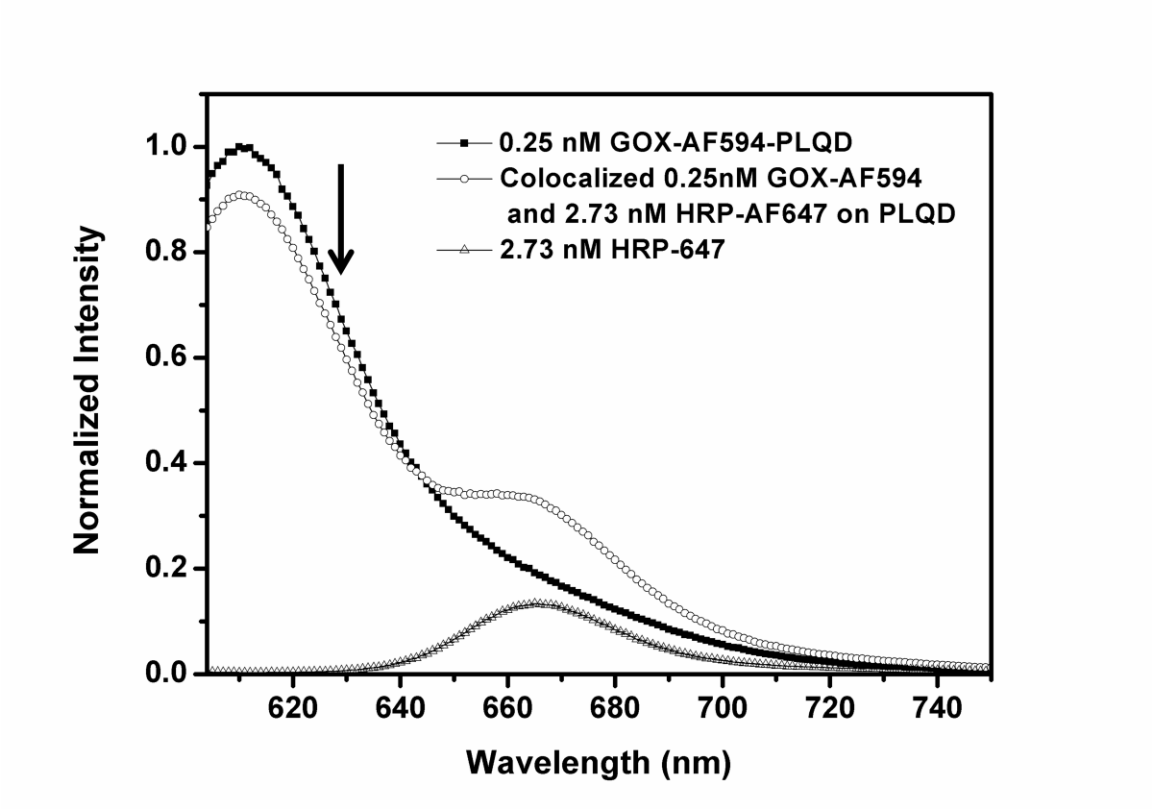

Figure 4.5 Demonstration of FRET between GOX-AF594 and HRP-AF647 co-localized on PLQD micelles. The arrow indicates quenching of the AF594 dye in the presence of the AF647 dye.

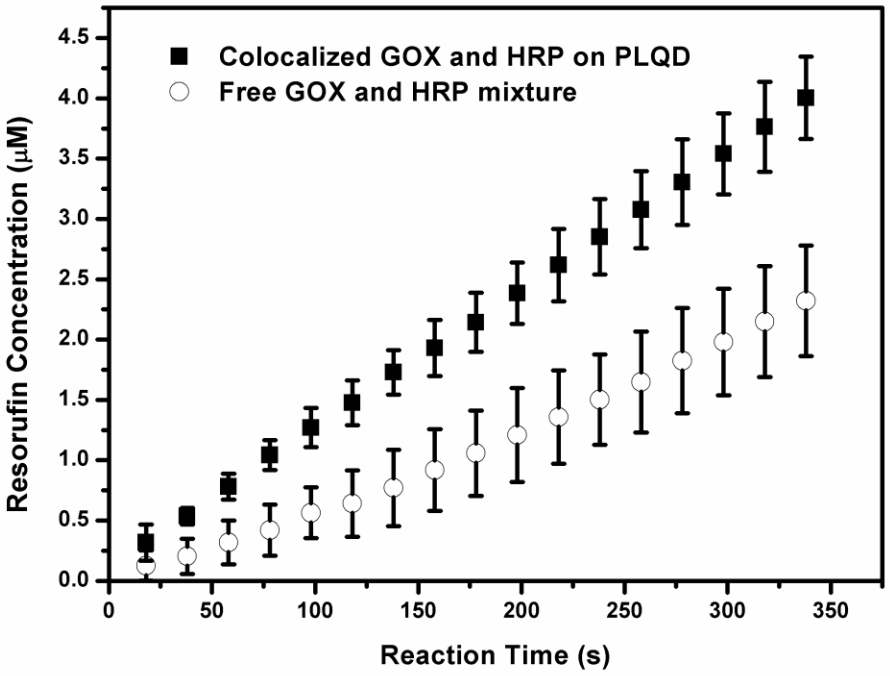

Figure 4.6 Resorufin conversion catalyzed by co-localized GOX-AF594 and HRP-AF647 on PLQD micelles compared to that catalyzed with equivalent concentrations of free GOX-AF594 and HRP-AF647 in solution.

Table 4-1Size and size distribution of PLQDs and enzyme-PLQDs

	PLQD	0.1 μM GOX-AF594-PLQD	0.25 μM GOX-AF594-PLQD	0.625 μM GOX-AF594-PLQD	0.91 μM HRP-AF594 PLQD	2.27 μM HRP-AF 594-PLQD
Size (nm)	143.0	144.0	147.2	156.1*	148.6	209.0*
Standard deviation	2.8	2.6	1.4	0.7	6.7	3.2

n = 3, * represents a statistically significant difference when compared with PLQD micelles ($p \leq 0.05$)

Table 4-2 Comparison of kinetic parameters of free enzymes and enzymes adsorbed onto PLQD micelles. No statistically significant differences were observed between the parameters of the free enzymes and that of the adsorbed enzymes.

	GOX-AF594	GOX-AF594 PLQD	HRP-AF594	HRP-AF594 PLQD
v_{max} (μM/min)	11.1 ± 1.1	11.1 ± 0.8	9.0 ± 0.6	8.9 ± 1.1
K_m (mM for GOX, μM for HRP)	8.9 ± 2.6	8.9 ± 1.1	21.8 ± 5.6	19.8 ± 5.6

Chapter 5 Multi-enzyme immobilization and co-localization on nanoparticles assisted by DNA hybridization

Manuscript to be submitted to *ACS Nano*

Abstract

Multi-enzyme complexes (MECs) in Nature exhibit highly efficient catalytic mechanisms in reaction cascades. Researchers have developed distinctive strategies to co-localize enzymes on nano-carriers to improve multi-enzyme catalytic efficiency by mimicking the MEC's structure and function. Numerous studies have indicated that the spatial arrangement and orientation of multiple enzymes in confined spaces are very critical in facilitating cooperative enzymatic activity in multi-enzyme co-localization. Biomolecule scaffolds based on DNA hybridization have attracted great attention because of their unique effective control of the relative positions of different enzymes in multi-enzyme co-localization. To demonstrate this concept, glucose oxidase (GOX) and horseradish peroxidase (HRP) were co-localized onto polystyrene nanoparticles via specific DNA hybridization. The particle geometry was selected, because it is hypothesized that, compared to planar surfaces, nanoparticle geometry is more suitable for co-localization of multi-layers of enzymes due to lesser steric hindrance. Free DNA hybridization and co-localization efficiency were studied using FRET techniques. The immobilization of single enzymes was studied to investigate the steric hindrance. The co-localization of the GOX and HRP was evidenced by FRET studies of the dyes labeling the two tag DNAs. Finally, it was found that co-localizing GOX and HRP via DNA hybridization significantly improved the overall reaction efficiency as compared to single enzyme immobilization mixture, which is not responsive to the carrier DNA density and showed great stability over time. In summary, the DNA directed co-localization of

the enzymes on nanoparticles is an effective way to control the relative positioning of the enzymes to mimic MECs.

5.1 Introduction

Enzymes, which are nature's catalysts that are involved in many reactions that take place in living organisms, have evolved to catalyze various chemical reactions including multi-step reactions.[1] Multi-enzyme complexes (MECs) are composed of multiple enzyme subunits or large polypeptides with defined tertiary and quaternary structure containing compact multiple catalytic centers that are in close proximity to each other. By bringing the enzymatic catalytic active sites together, reaction intermediates can be transported rapidly among the active sites via a "substrate channeling" effect, which can reduce the diffusion loss as occurred in free enzyme catalytic process and maintain high local concentration of intermediates, which is especially critical for unstable intermediates. In addition, MECs significantly increase the overall reaction turnover efficiency. The benefits of MECs have inspired researchers to design artificial MECs to mimic the structure and functionalities of MECs. A number of ways have been designed as summarized in our review paper.[2] Enzyme immobilization-oriented strategies exhibits great potential because of their economical reusability, enhanced kinetic performance, and higher stability under harsh operating conditions (e.g., extreme pH and temperature). [3,4]

Nanoparticles have attracted much attention because of large surface areas for immobilization and no internal diffusion, as opposed to porous materials. Polymeric nanoparticles are relatively inexpensive and provide large flexibility in terms of selecting materials and designing architectures compared to inorganic materials. The unique solution behavior of nanoparticles provides enhanced mobility of biocatalysts in solution, which potentially could promote the catalytic performance. [5] It has been widely recognized that the spatial orientation of multiple enzymes plays a significant role in mimicking the MECs in Nature.[6] For example, it has been demonstrated that enzymes

co-localized in the same layers on nanoparticles have higher kinetic performance than those in separate layers. Our group has designed two distinct strategies of fabricating biomimetic artificial MECs demonstrated by co-localizing GOX and HRP on multifunctional nanoparticles[7] and Pluronic-QD micelles[8], respectively. In both cases, the activity of each individual enzyme was retained in single component immobilization and the co-localized enzymes exhibited superior kinetic performance compared to free enzymes in catalyzing cascade reactions.[7,8] In addition, the Pluronic-QD platform enabled the characterization of enzyme attachment onto the micelles by FRET.[8]

Most recently, researchers have used biomolecule scaffolds such as DNA to direct the co-localization of multiple enzymes to in cascaded reaction systems. [9–13] The unique and precise hybridization by complementary DNA provides powerful control over the spatial arrangement of the enzymes, compared to other co-localization strategies. The relative positions of multiple enzymes can be controlled by hybridization of the tag DNA with the complementary capture DNA as well as the various DNA sequence length. DNA hybridization, which is the key to self-assembly of artificial MECs, is the process of combining two complementary single-stranded DNA (ssDNA) molecules in helical structure using the four basic nucleotides to achieve pairing in a mild reaction environment. Thus, DNA-directed co-localization provides exceptionally high stability for DNA-enzyme conjugates by preserving the enzymatic activity. [14] Niemeyer et al. reported co-localization of NAD(P)H: FMN oxidoreductase (NFOR) and luciferase (Luc) that catalyze cascaded reactions via DNA hybridization and demonstrated the application of this approach for co-localization on planar surfaces.[9] That resulted in a significant improvement in overall enzymatic activity. They also showed that the steric hindrance significantly impacted the formation of the DNA-enzyme complex.[9] Likewise, Müller and Niemeyer used protein engineering combined with DNA hybridization

directed evolution to develop supra-molecular complexes using DNA as a scaffold for enzyme assembly. They attached glucose oxidase (GOX) and horseradish peroxidase (HRP) by covalent binding to short single-stranded biotinylated and thiolated DNA oligonucleotides (ssDNA) and brought them together using DNA-directed hybridization of short DNA with long complementary capture DNA to form a scaffold. The activity of the multi-enzyme complex was significantly enhanced compared to enzymes immobilized on separated strands and it was demonstrated that the efficiency of the self-assembly significantly depended on position and steric factor between the DNA-enzyme conjugates.[10]

It is hypothesized that the DNA hybridization efficiency can be higher for nanoparticle geometry compared to other geometries such as planar surfaces because of less steric hindrance,[9,10] which might be further impacted by particle size. In this work, our goal is to develop a biomimetic strategy based on DNA hybridization to co-localize multiple enzymes on nanoparticles via DNA-directed hybridization (Figure.5.1). Specifically, the co-localization of two tag DNAs as well as tag DNA enzyme conjugates was verified using FRET by conjugating the DNAs with respective fluorescent dyes. Singe enzyme immobilization by DNA hybridization was studied and optimized. The enzyme co-localization was studied with various configurations and significant enhancement of kinetics was found. HRP and GOX were used in a cascade reaction to form the highly red-fluorescent oxidation product, resorufin. The use of this approach will lead to DNA-conjugates that form a double-stranded DNA scaffold with spatial control that can be applied for other applications. Here, we present our work on DNA-directed co-localization of two enzymes on nanoparticles.

5.2 Materials and Methods

5.2.1 Chemicals

Streptavidin-conjugated polystyrene (SPS) beads (0.3-0.39 μm) were purchased from Spherotech. Streptavidin-HRP (SHRP) and Avidin-GOX(AGOX) were purchased from BioLegend and Vector Lab, respectively. Amplex® Red was purchased from Invitrogen. Hydrogen peroxide, sodium chloride, and trisodium phosphate were purchased from Fisher Scientific. Oligonucleotides sequences [10] were synthesized by Integrated DNA Technologies, and the corresponding sequences are listed in Table 5.1. All aqueous solutions were prepared using purified water from Thermo Scientific's Barnstead Nanopure Ultrapure Water System.

5.2.2 Biotinylated DNA attachment onto SHRP, AGOX and S-PS nanopartilces

To attach tag DNA A or B to SHRP or AGOX, 27 μL of 0.1 nmol/mL of DNA solution was mixed with 500 μL of 0.5 mg/mL SHRP or 120 μL of 5 mg/mL AGOX solution and incubated for 1 h (1:1 molar ratio of biotin and streptavidin) at room temperature. To attach carrier DNA onto S-PS nanoparticles, 150 μL of 1% of SPS nanoparticle suspension was mixed with an appropriate amount of 0.1 nmol/mL carrier DNA solution with a range of molar ratio (biotin binding capability in terms of nmol per mg nanoparticles was provided by the manufacturer based on biotin-FITC binding efficiency). Specifically, the S-PS particles were mixed with the carrier DNA solution and incubated for 1 h or 3h using constant speed ~4 in a Roto-shaker at room temperature. Alexa Fluor 594 dye labeled carrier DNA was used to investigate the reaction time study. After reaction, the mixture was micro-centrifuged at 16,000 X g for 6 min to separate the nanoparticles from the original supernatants and the particles at the bottom were re-suspended in Tris buffer. The sample was dispersed using sonication for 10 seconds

(pulse - 20% Amp) and separated again by micro-centrifugation for 6 min at 16,000 X g. The supernants was collected and this wash step was repeated until no significant intensity was observed. The DNA in the supernatants was quantified according to fluorescent intensity.

5.2.3 Co-localization of DNA by hybridization studied by FRET

To evaluate how the two short tag DNA strands co-localize by hybridization with the corresponding segments on the long carrier DNA strand, two fluorescent dyes were conjugated with tag DNA: Alexa Fluor 594 conjugated B(B-AF594) and Alexa Fluor 647 conjugated A (A-AF647) were used to hybridize with c(AB) conjugated PS-STV nanoparticles. The dye-DNA conjugated was synthesized by Integrated DNA Technologies. Specifically, in a reaction tube, 6 µL 0.1 nmol/µL AF594-B was mixed with 100 µL of 1.4 nmol/mg carrier DNA -SPS first, and 6 µL of 0.1 nmol/µL AF647-A was added. The emission fluorescence from 604 to 750 nm was monitored under excitation of 594 nm with time. For initial control sample, instead of adding 6 µL of AF647-A, equivalent volume of Tris buffer was added.

5.2.4 Co-localization of DNA-enzymes characterized by FRET

To investigate the co-localization of the DNA-enzyme conjugates on the long carrier DNA chain, the tag DNAs were conjugated with fluorescent dyes that can be paired to have FRET occur. The dye conjugated DNAs, AF594-B and AF647-A were further used for attaching to the AGOX and SHRP, respectively as described above, to obtain AF594-B-AGOX and AF647-A-SHRP. Capture DNA-PS was conjugated with the S-PS as mentioned above. Specifically, 40 µL AF594-B-AGOX was mixed with 50 µL of 1.4 nmol/mg carrier DNA conjugated with PS-STV first, and 160 µL of AF647-A-SHRP was added. The emission fluorescence from 604 to 750 nm was monitored under

excitation of 594 nm with time. For initial control sample, instead of adding 160 µL of AF647-A, an equivalent volume of Tris buffer was added.

5.2.5 SHRP and AGOX immobilization on S-PS via DNA hybridization

SHRP was immobilized onto the SPS beads via hybridization of the short tag DNA and long carrier DNA strands. Each sample containing 50 µL of 10 mg/mL nanoparticles with 1.4 nmol carrier DNA per mg SPS in Tris were mixed with appropriate volume of A-SHRP, B-SHRP or both to make the reaction ratio of tag DNA and carrier DNA about 1:1. The samples were incubated for 3h at room temperature. After the reaction, each sample was separated by micro-centrifugation for 6 min at 16,000 X g. The supernatants were removed and this step was repeated until no protein was detectable in the supernatant. Similarly, AGOX were immobilized by hybridization of short tag DNA and long carrier DNA strands.

5.2.6 SHRP and AGOX co-localization on S-PS via DNA hybridization

Prior to co-localizing SHRP and AGOX on the S-PS nanoparticles, SHRP-tag DNA, AGOX-DNA and carrier DNA-S-PS were prepared as described above. With the product obtained, the two enzymes were co-localized on the nanoparticles by mixing the enzyme-DNA conjugate and the DNA-S-PS simultaneously. In one single sample, 50 µL of c(AB) or c(BA) conjugated S-PS were mixed with appropriate volume of A or B conjugated SHRP and AGOX and incubated for 3 h. The unconjugated enzyme-DNA mixtures were removed by microcentrifugation and the process was repeated until enzyme-DNA was not detectable in the supernatants. To prepare the control, either AGOX or SHRP conjugates were mixed with the c(AA) or c(BB) to have single type enzyme immobilized on the S-PS nanoparticles.

5.2.7 Enzyme kinetics assay

For all the samples and controls, 90 µL of substrate solution containing hydrogen peroxide and Amplex Red was loaded into 96-well plates. For co-localized samples, 10 µL of enzyme-particle solution was added in the substrate solution; For the mixture control sample, 5 µL of each immobilized enzyme was added into the corresponding substrate solution. In the final 100 µL solution, the concentrations of H_2O_2, Amplex Red, and PS-STV were 10 µM, 55 µM and 5 µg/mL, respectively. The reaction was monitored using a fluorescent microplate reader.

5.3 Results and Discussion

5.3.1 Carrier DNA attachment study

The streptavidin and biotin have high affinity for each other, which is comparable to covalent binding, to conjugate the carrier DNA to the PS nanoparticle surface and tag DNA to the enzymes. Biotinylated DNA and streptavidin coated nanoparticles were used, along with streptavidin conjugated HRP, and avidin conjugated GOX, in the study. The reaction was carried out for two time periods- 1 h and 3 h, by attaching fluorescent dye conjugated carrier DNA to study the reaction time. It was found that the longer times did not significantly increase the reaction efficiency as opposed to shorter times. For the following experiment of attaching tag DNA to the enzymes and carrier DNA to the PS nanoparticles, a 1 hour reaction time was used

5.3.2 DNA hybridization study by FRET

DNA hybridization was monitored by using dye conjugated tag DNA and carrier DNA, as shown in figure 5.2, and the successful hybridization was confirmed by FRET between the dye conjugated tag DNA as well as respective segments on the carrier DNA.

The hybridization was completed within 1 h, and both hybridizations were found for the free DNA chains and on the PS nanoparticles.

5.3.3 Co-localization two tag DNAs characterized by FRET

FRET was used to characterize the co-localization of the two tag DNA chains via hybridization with the corresponding segments on the carrier DNA on SPS. Two fluorescent dyes that can be paired to have FRET occur were respectively conjugated on the two tag DNAs. As shown in Figure 5.3, it was found that based upon addition of A-AF647 DNA-dye conjugates, the peak corresponding to the donor dye AF594 conjugated with B was significantly quenched, and that of the acceptor dye AF647 was excited in the far range. As the DNA hybridization reaction proceeded, more quenching and exciting occurred between the two dyes that labeled the tag DNAs. This can only occur when the donor and acceptor dyes are within 10 nm or less of each other, which provided strong evidence that the two DNA units were co-localized on the long DNA chains. In addition, the FRET did not change significantly after 1 h. At 2 h, the DNA hybridization reaction was completed. To maximize the reaction efficiency, the hybridization reaction was carried out for 3h to ensure complete reaction.

5.3.4 Co-localization of SHRP and AGOX by FRET study

Similar to the DNA co-localization study, the co-localization of AGOX and SHRP were characterized using FRET. Bi-functional tag DNAs were used in this study. The fluorescent dyes AF594 and AF647 were respectively conjugated to the 3’ end of B and A tag DNAs, respectively. Both tag DNAs have biotin functional groups on the 5’ end, which were respectively used to conjugate with the AGOX and SHRP. As shown in Figure 5.3(b), the donor dye AF594 conjugated with B was significantly quenched after addition of SHRP-A-AF647 conjugates, and the acceptor dye AF647 was excited at the far range. This occurred because the donor and acceptor dyes are within 10 nm or less,

which just provided evidence that the two enzyme dye conjugates were co-localized on the long DNA chains.

5.3.5 SHRP immobilization on SPS nanoparticles via DNA hybridization

Single enzyme DNA conjugate A-SHRP was immobilized on the PS nanoparticle surface in three different configurations as shown in Figure 5.4. For immobilization on carrier DNA c(AB), SHRP was located at the inside segment that is closer to the PS surface as compared to c(BA) carrier. There was more steric hindrance for that type of configuration, leading to lesser enzymatic activity observed in catalyzing the reaction. In c(AA) carrier, both inner and outer segments on long DNA chains were hybridized with the tag DNA to have A-SHRP immobilized. It was found that the activity was close to the sum of those of c(AB) and c(BA), and the increase of the activity is from the greater number of enzyme-DNA conjugates immobilized on the PS surface. The capability of taking more enzymes on c(AA) as opposed to either c(AB) or c(BA) meant that the two enzyme DNA conjugate molecules can be actually co-localized on the same long DNA chain, which provide evidence for feasibility of co-localizing two components on carrier DNA by hybridization. A control sample which has no carrier DNA was used, and the enzymatic activity was observed, but significantly less than on the samples with carrier DNAs.

5.3.6 AGOX immobilization on SPS nanoparticles via DNA hybridization

A similar immobilization study was conducted using single enzyme DNA conjugate A-AGOX and carrier DNA c(AB), c(BA) and c(AA). As shown in Figure 5.5, the sample of A-GOX immobilized on c(AB), located at the inside segment that is closer to the PS surface as compared to c(BA) carrier, exhibited less enzymatic activity. Steric hindrance for that type of configuration was responsible for less enzymatic activity observed in catalyzing the reaction. As predicted, the sample of c(AA) carrier, where

both inner and outer segments on long DNA chains were hybridized with the tag DNA to have A-AGOX immobilized, has shown higher enzymatic activity, which was closer to the sum of those of c(AB) and c(BA). The adsorption control sample with no carrier DNA showed high enzymatic activity. This might be caused by the “unwanted” and uncontrolled co-localization of AGOX and SHRP, resulting from non-specific adsorption of SHRP enzyme on PS nanoparticle that used in the activity assay process.

5.3.7 Kinetic enhancement by co-localizing the enzymes

To co-localize the enzymes, both AGOX and SHRP were conjugated with short tag DNAs. In the first set of experiments, AGOX and SHRP were conjugated with B and A tag DNA, respectively, and the enzyme –DNA conjugates were co-localized on c(AB) and c(BA) separately. Equivalent quantities of carrier DNA c(AA) and c(BB) were used to immobilize the same feed quantities of A-SHRP and B-AGOX separately. Then the mixture of immobilized AGOX and SHRP were used as controls. The coupled reactions catalyzed by co-localized enzymes and the mixture are compared in Figure 5.6. The overall product conversion rates were significantly higher for the co-localized B-AGOX and A-SHRP compared to the mixture control. The efficiency of c(BA) sample was slightly lower than that of c(AB), which might be caused by less co-localization efficiency of the two enzymes because of steric hindrance. In the second set of experiments, AGOX and SHRP were conjugated with A and B tag DNAs, respectively as shown in Figure 5.7. The co-localized enzymes showed more improvement in the kinetics efficiency on c(BA) than c(AB), which is the opposite of relations as observed in the first set of experiments as expected. However, the kinetics of the coupled reaction efficiency was not high for c(AB) as compared to the controls, and it is believed that the steric effect is somehow higher in that configuration. Modifying the carrier DNA by inserting a short spacer might solve the issue, which is currently being investigated. The

manufacturer provided the information of biotin binding capacity on the streptavidin coated polystyrene nanoparticles, which is based on the biotin-FITC. Due to the different sizes of the FITC and DNA, the real capacity might be different. In Muller's study, it was found that the lower concentration of DNA led to greater co-localization efficiency because of less steric effects involved.[10]

The impact of DNA density on co-localization on nanoparticles was studied in this work, and a series of concentrations of biotin-DNA chains were used to attach to the streptavidin on the PS surface at a constant PS concentration 0.75 mg/mL. As listed in table 2, once the DNA concentration was increased to 1.5 nmol, only about 70% of the initial input was conjugated on the particle surface, which means that the saturated concentration is around 1.4 nmol/mg. The average density of the "saturated" DNA concentration (3.6 nm) was actually lower than the lowest average DNA density used in Muller's work (1.3 nm) between carrier DNA chains as illustrated in Figure 5.8 To further investigate the DNA density impact, 1.2 nmol/mL and 0.7nmol/mL was used; however, the enzymatic activity was not further improved in that case, as shown in Figure 5.9.

5.3.8 Stability of co-localizedSHRP and AGOX

The co-localized enzymes were further studied to gauge the effect of storage on enzyme stability. The samples were stored under 4 ^{o}C environment and their activity tested periodically. It was found that both the co-localized and immobilized enzymes did not lose activity over a period of one week. To the best of our knowledge, this is the first study based on the shelf life of co-localized enzyme, which shows great promise for long term storage potential in the future application. Longer term stability studies are ongoing right now.

5.4 Conclusions

In this study, multi-enzyme co-localization on nanoparticles with precise spatial control using DNA hybridization was investigated. DNA direct co-localization has attracted great attention because of its unique effective control of the relative positions of different enzymes in multi-enzyme co-localization. Glucose oxidase (GOX) and horseradish peroxidase (HRP) were used to evaluate the performance of co-localized enzymes by DNA hybridization. Free DNA hybridization and co-localization efficiency were studied using FRET techniques. Various capture DNA concentrations were compared and optimized. The immobilization of single enzyme was studied to investigate the steric hindrance effect. The co-localization of the GOX and HRP were evidenced by FRET studies of the dyes labeling the two tag DNAs. Finally, it was found that the co-localized GOX and HRP via DNA hybridization significantly improved the overall reaction efficiency as compared to single enzyme immobilization mixture. The kinetics enhancement was observed in the both sets of comparison with different DNA-enzyme conjugates. As opposed to non-specific spatial control method in co-localization, DNA-based co-localization techniques provide strong control over spatial arrangement and organization in multi-enzyme co-localization study, which can also been seen from the FRET characterization and greater kinetics enhancement The nanoparticles provide significant larger capacity for immobilizing multiple enzymes comparing to the flat surface platform. The less dense carrier DNA density as well as less steric effect in particle geometry might contribute the higher overall kinetics enhancement. The long term stable co-localized enzymes provide more promise in long term applications. Overall, the DNA directed co-localization of the enzymes is superior in controlling the relative positioning of the enzymes to mimic MECs.

Acknowledgements

The authors are grateful to the National Science Foundation (CBET 0932517) for financial support. B.N. acknowledges the Vlasta Klima Balloun Professorship in Chemical and Biological Engineering and SKM acknowledges the Stanley Chair in Interdisciplinary Engineering.

References

(1) Costas, M.; Mehn, M. P.; Jensen, M. P.; Que, L. Dioxygen Activation at Mononuclear Nonheme Iron Active Sites: Enzymes, Models, and Intermediates. *Chem. Rev.* **2004**, *104*, 939–986.

(2) Jia,Feng; Narasimhan, Balaji; Mallapragada, Surya Strategies for multi-enzyme immobilization and co-localization: a review. *Biotechnol. Bioeng.*

(3) Pescador, P.; Katakis, I.; Toca-Herrera, J. L.; Donath, E. Efficiency of a Bienzyme Sequential Reaction System Immobilized on Polyelectrolyte Multilayer-Coated Colloids. *Langmuir* **2008**, *24*, 14108–14114.

(4) Keighron, J. D.; Keating, C. D. Enzyme:Nanoparticle Bioconjugates with Two Sequential Enzymes: Stoichiometry and Activity of Malate Dehydrogenase and Citrate Synthase on Au Nanoparticles. *Langmuir* **2010**, *26*, 18992–19000.

(5) Jia, H.; Zhu, G.; Wang, P. Catalytic behaviors of enzymes attached to nanoparticles: the effect of particle mobility. *Biotechnol. Bioeng.* **2003**, *84*, 406–414.

(6) Schoffelen, S.; van Hest, J. C. M. Multi-enzyme systems: bringing enzymes together in vitro. *Soft Matter* **2012**, *8*, 1736–1746.

(7) Jia, F.; Mallapragada, S.; Narasimhan, B. Biomimetic multi-enzyme complexes based on nanoscale platforms. *Aiche J.* **2013**, *59*, 355–360.

(8) Jia, F.; Narasimhan, B.; Mallapragada, S. Novel sequential co-localization of multiple enzymes on multifunctional nanoparticles. *Langmuir*.

(9) Niemeyer, C. M.; Koehler, J.; Wuerdemann, C. DNA-Directed Assembly of Bienzymic Complexes from In Vivo Biotinylated NAD(P)H:FMN Oxidoreductase and Luciferase. *ChemBioChem* **2002**, *3*, 242–245.

(10) Müller, J.; Niemeyer, C. M. DNA-directed assembly of artificial multienzyme complexes. *Biochem. Biophys. Res. Commun.* **2008**, *377*, 62–67.

(11) Fruk, L.; Müller, J.; Niemeyer, C. M. Kinetic Analysis of Semisynthetic Peroxidase Enzymes Containing a Covalent DNA–Heme Adduct as the Cofactor. *Chem. – Eur. J.* **2006**, *12*, 7448–7457.

(12) Freeman, R.; Sharon, E.; Tel-Vered, R.; Willner, I. Supramolecular Cocaine−Aptamer Complexes Activate Biocatalytic Cascades. *J Am Chem Soc* **2009**, *131*, 5028–5029.

(13) Wilner, O. I.; Weizmann, Y.; Gill, R.; Lioubashevski, O.; Freeman, R.; Willner, I. Enzyme cascades activated on topologically programmed DNA scaffolds. *Nat. Nanotechnol.* **2009**, *4*, 249–254.

(14) Jonkheijm, P.; Weinrich, D.; Schroeder, H.; Niemeyer, C. M.; Waldmann, H. Chemical Strategies for Generating Protein Biochips. *Angew. Chem.-Int. Ed.* **2008**, *47*, 9618–9647.

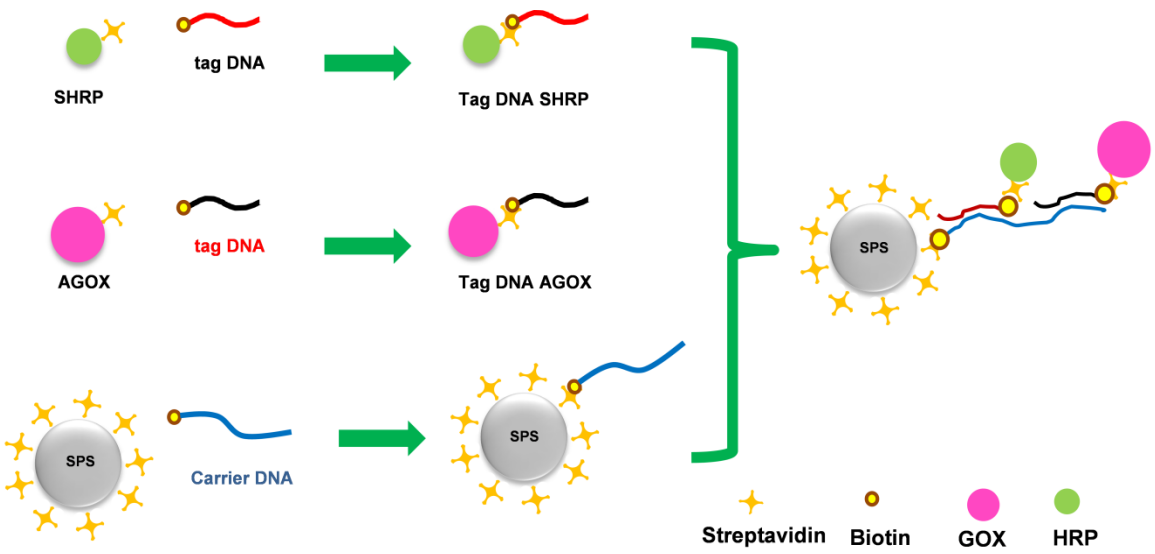

Figure 5.1Schematic approach for co-localizing SHRP and AGOX on PS nanoparticles by hybridization of short tag DNA and respective segments on long carrier DNA chain. The figure is drawn approximately to scale.

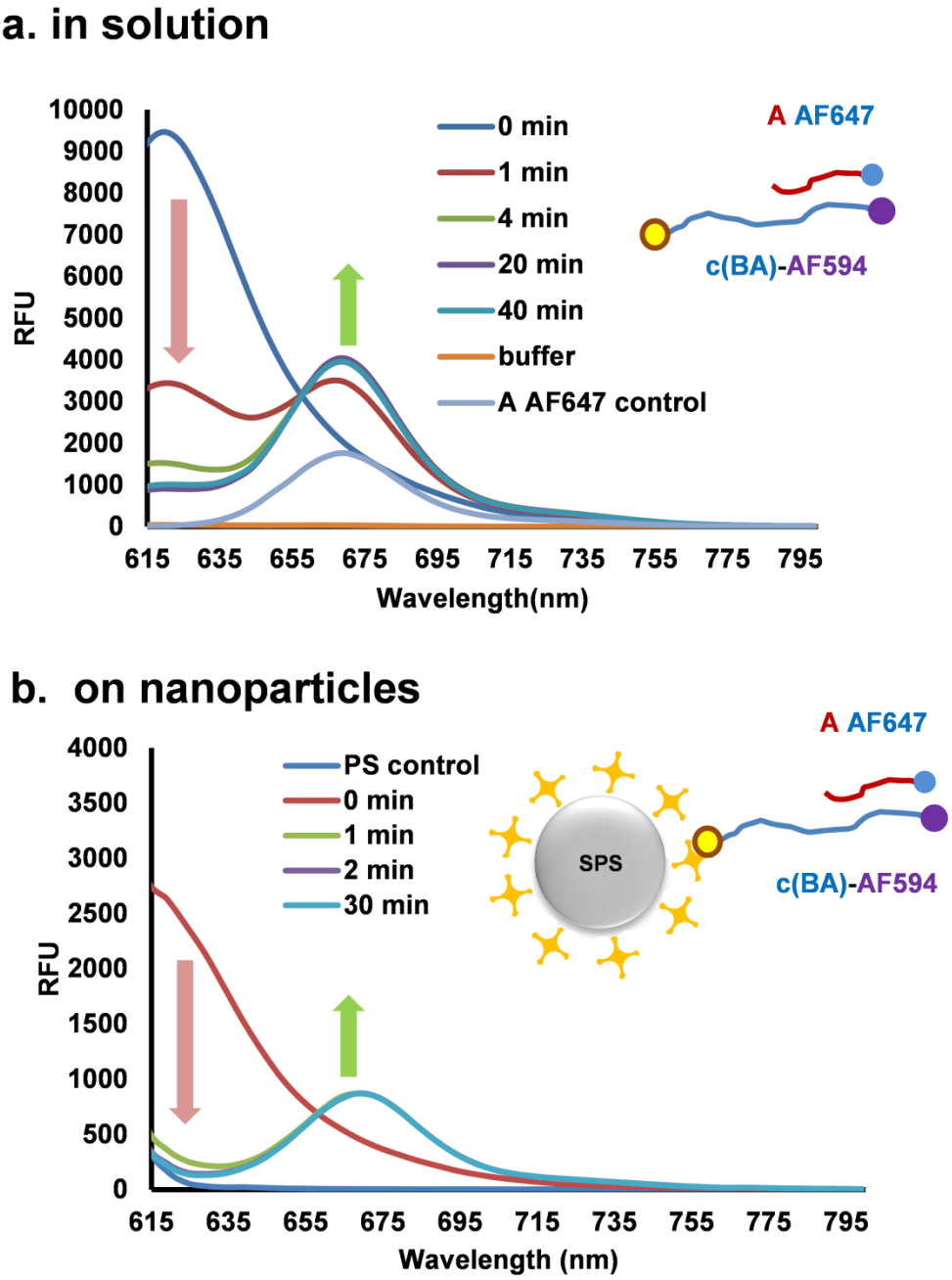

Figure 5.2Hybridization of tag DNA and corresponding complementary segment on long DNA chain. (a) free DNA chains in solution (b) carrier DNA on SPS.

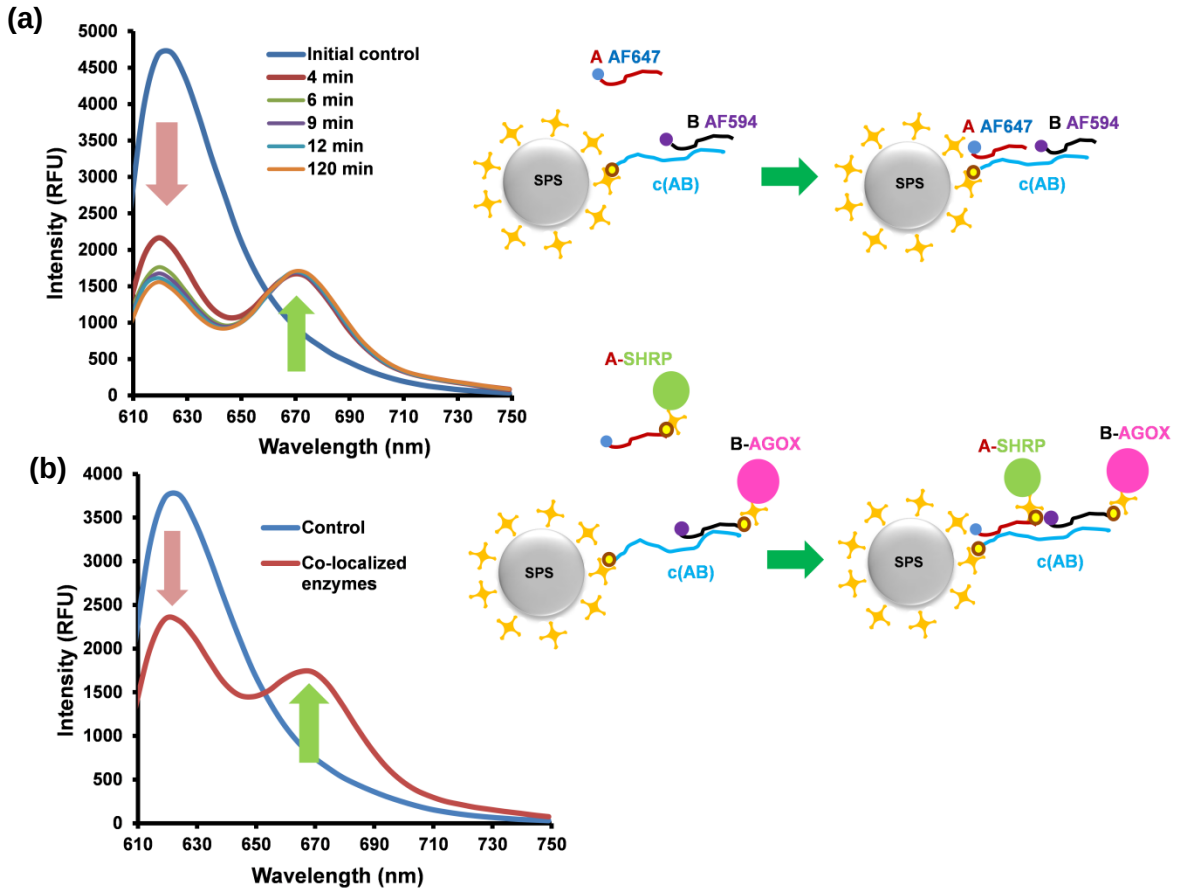

Figure 5.3 Co-localization of (a) two tag DNAs chains on carrier DNA chains and (b) two enzyme-DNA conjugates characterized by FRET between the two fluorescent dyes

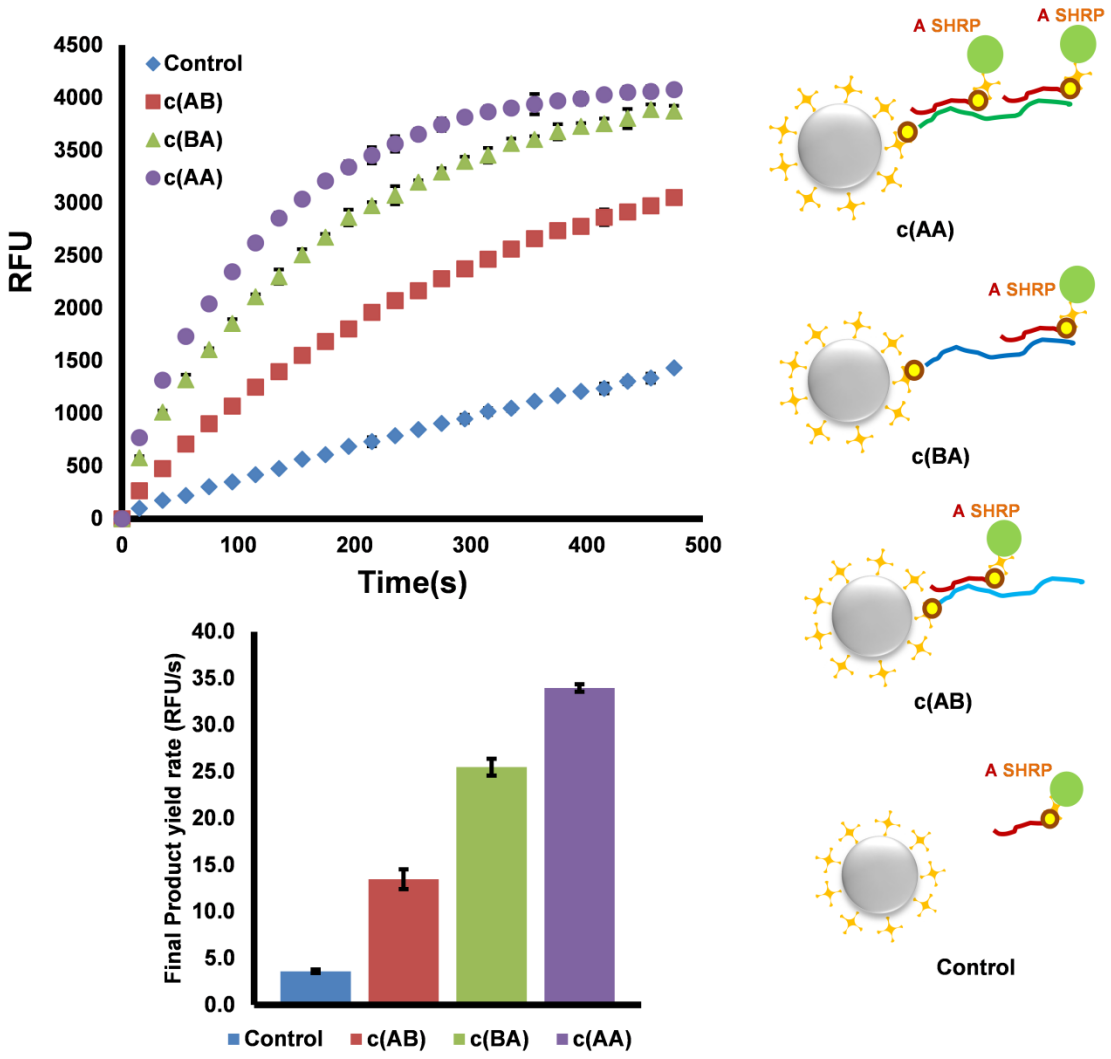

Figure 5.4SHRP immobilization on SPS via hybridization of tag DNAs with three different types of carrier DNA, c(AB), c(BA) and c(AA).

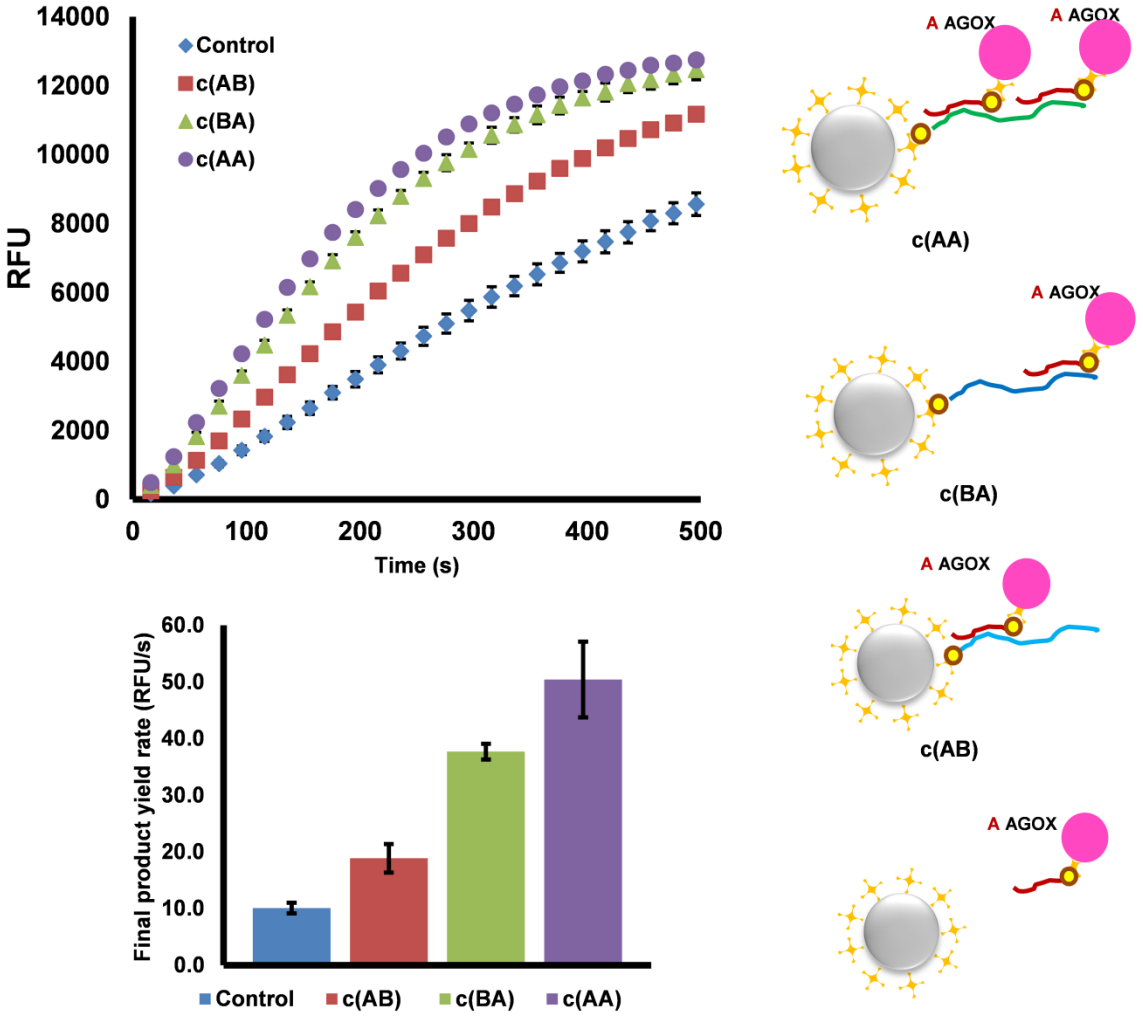

Figure 5.5 GOX immobilization on SPS via hybridization of tag DNAs with three different types of carrier DNA, c(AB), c(BA) and c(AA).

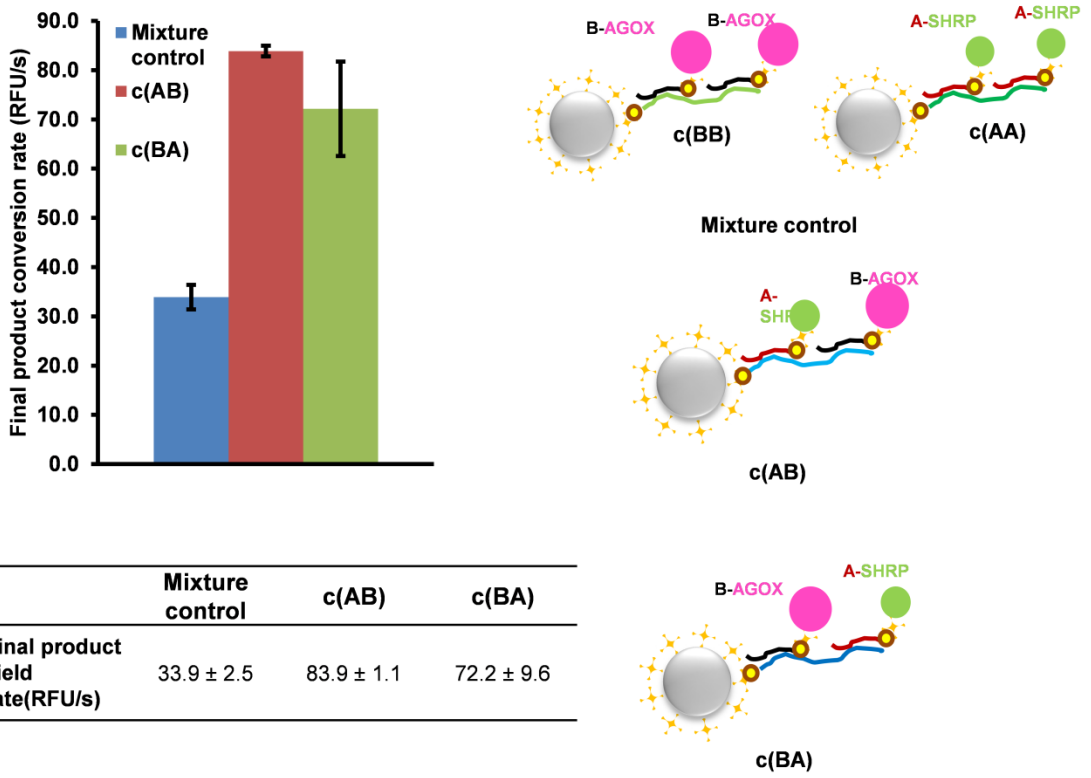

	Mixture control	c(AB)	c(BA)
Final product yield rate(RFU/s)	33.9 ± 2.5	83.9 ± 1.1	72.2 ± 9.6

Figure 5.6 Kinetic enhancement by co-localizing A-SHRP and B-AGOX.

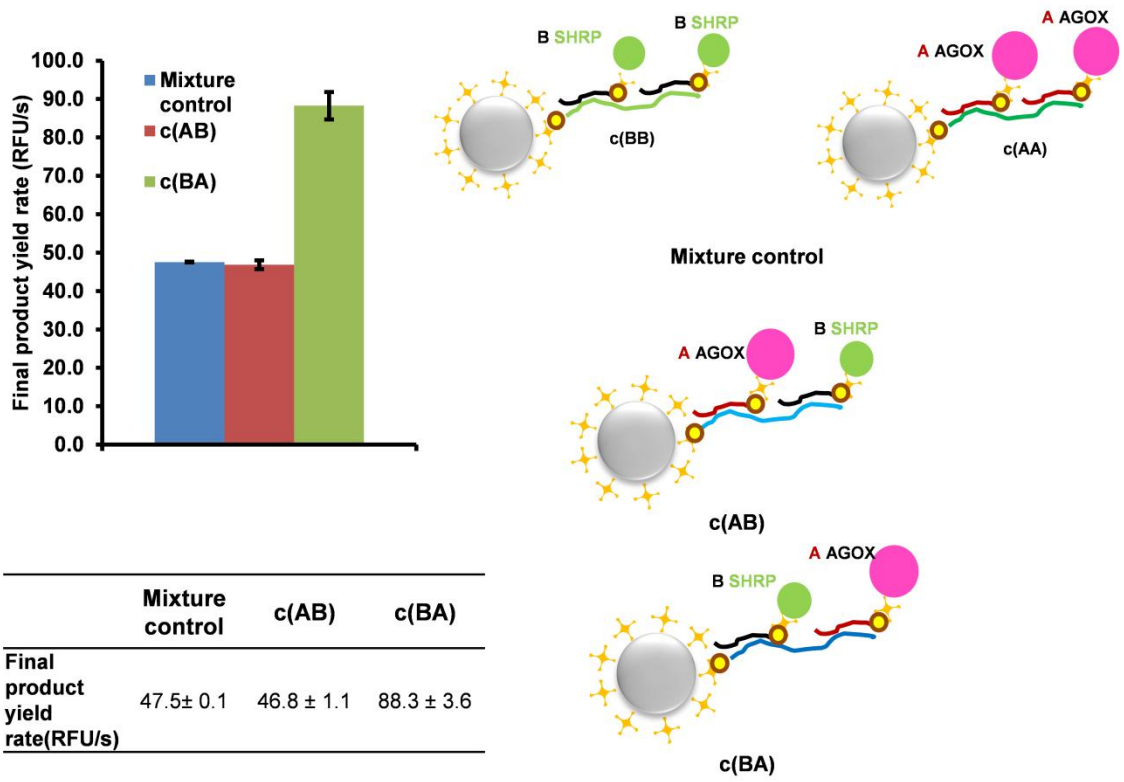

	Mixture control	c(AB)	c(BA)
Final product yield rate(RFU/s)	47.5± 0.1	46.8 ± 1.1	88.3 ± 3.6

Figure 5.7 Kinetic enhancement by co-localizing B-SHRP and A-AGOX.

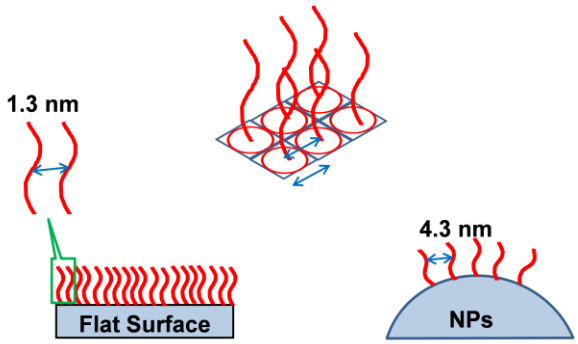

Figure 5.8 Illustration of lowest DNA densities on flat surface and highest on NPs surface

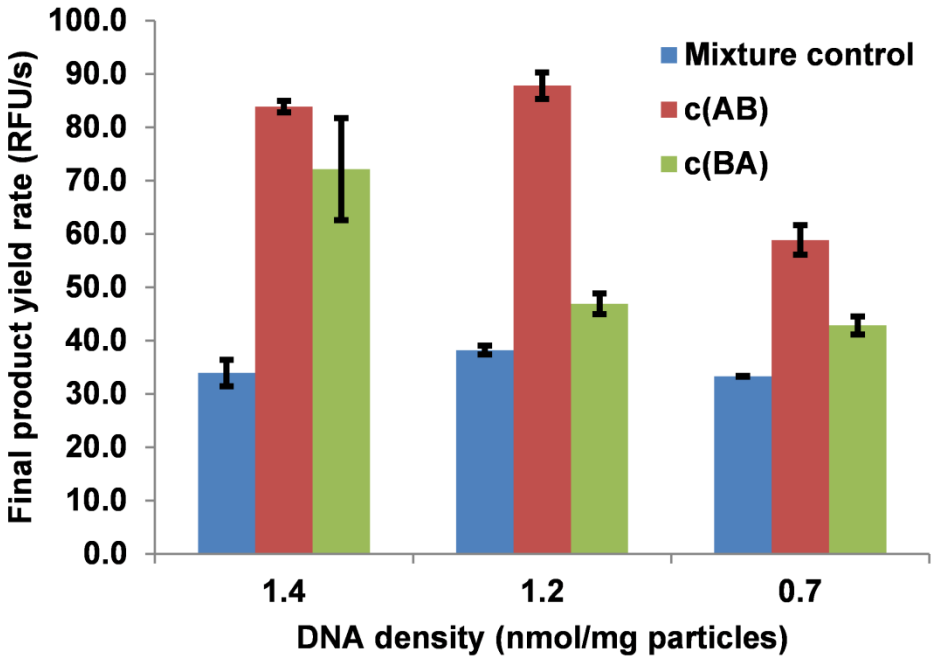

Figure 5.9 Effect of DNA density on enzyme co-localization

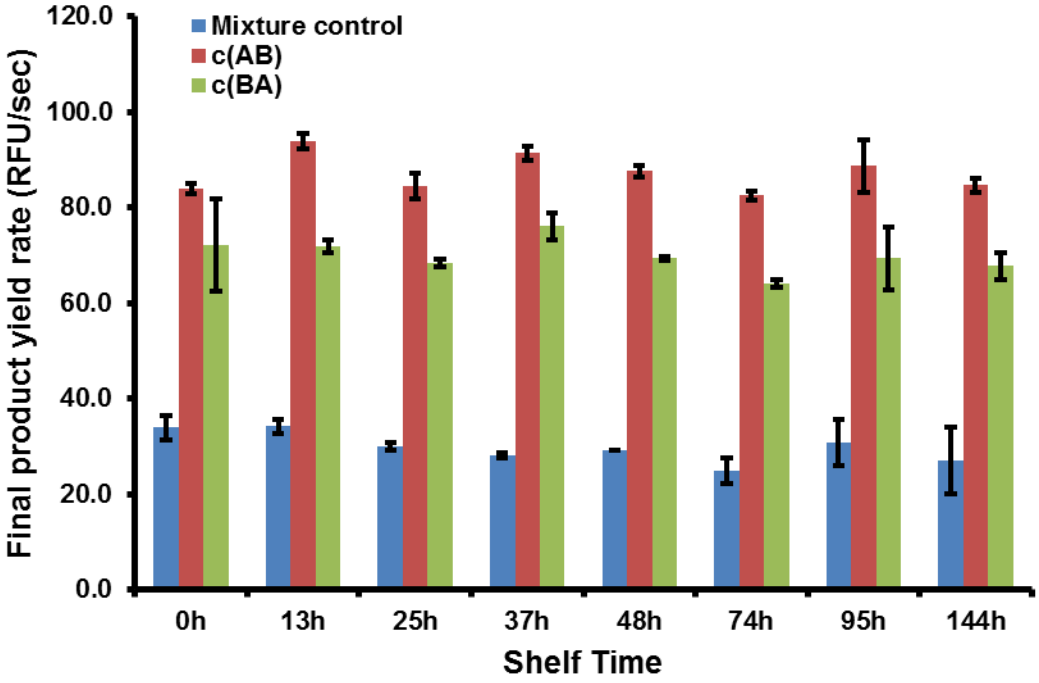

Figure 5.10Stability of co-localized and immobilized enzymes over time

Table 5-1DNA sequences used in this work

Abbreviation	Function	Sequences
A	Tag DNA	5’-biotin-GGT CCG GTC ATA AAG CGA TAA G - 3’
B	Tag DNA	5'- biotin-GT GGA AAG TGG CAA TCG TGA AG -3'
c(AB)	Carrier DNA	5'-biotin-CT TAT CGC TTT ATG ACC GGA CCCT TCA CGA TTG CCA CTT TCC AC -3'
c(BA)	Carrier DNA	5'-biotin-CT TCA CGA TTG CCA CTT TCC ACCT TAT CGC TTT ATG ACC GGA CC -3'
c(AA)	Carrier DNA	5'-biotin-CT TAT CGC TTT ATG ACC GGA CCCT TAT CGC TTT ATG ACC GGA CC -3'
c(BB)	Carrier DNA	5'-biotin-CT TCA CGA TTG CCA CTT TCC ACCT TCA CGA TTG CCA CTT TCC AC -3'

Table 5-2 DNA density data used in the enzyme co-localization studies

Feed DNA quantity (nmol)	PS-STV (mg)	Efficiency	DNA density (nmol/mg)
0.25	0.75	0.98±0.01	0.3
0.5	0.75	0.97±0.01	0.7
1	0.75	0.87±0.01	1.2
1.5	0.75	0.68±0.004	1.4

Chapter 6 Conclusions

Biocatalysts have been broadly studied and applied in both scientific and industrial settings due to their highly energy efficient catalytic mechanisms, unique selectivity for substrates, and enhanced stability under harsh reaction environments. MECs existing in Nature have inspired researchers to design synthetic analogs to promote the overall catalytic efficiency *in vitro* by co-localizing multiple enzymes to mimic the MECs' unique functionalities. A number of efforts have been devoted to designing synthetic MECs in the past couples of decades, which exhibit great potential in enhancing the overall enzymatic performance. Immobilization derived material based multiple enzyme co-localization approach has attracted much attention because of potential great promise for reliable industrial application. Multi-enzyme co-localization on platforms shares many common features with single enzyme immobilization. The different attachment techniques used in single enzyme immobilization and multiple enzyme co-localization have a direct impact on the overall enzyme orientation and activity. The various types of platforms developed for single enzyme immobilization enriched the starting choices for co-localizing multiple enzymes. Non-porous nanoparticle platforms provide advantageous characteristics for enzyme immobilization and co-localization due to their inherently large surface area for attaching enzymes and their solution properties in catalytic processes.

In multi-enzyme co-localization, the involvement of multiple components brings unique challenges. The various properties of the different enzymes (e.g., size, conformational stability) makes the co-localization process more complicated and a careful and rational selection of appropriate attachment techniques and platforms is necessary to retain enzymatic activity and improve performance. The relative positions of the multiple enzymes in a confined space play another significant role in affecting the

interaction between different enzymes. This thesis work has been focused on developing novel strategies to design nano-carriers for multi-enzyme co-localization to realize kinetics enhancement and strong control of spatial arrangement of the enzymes. Three distinct approaches have been designed using different methods and platforms as compared in table 6.1, which will be summarized in below.

In the first study discussed in Chapter 3, multifunctional polystyrene nanoparticles were designed for immobilization and sequential co-localization of multiple enzymes GOX and SHRP using covalent binding and streptavidin-biotin coupling attachment techniques. Individual single enzyme immobilization was optimized to retain both GOX and SHRP activities. Then the GOX and SHRP were sequentially co-localized on B/C-PS nanoparticles, which enhanced the overall product conversion rate by approximately two-fold compared to the equivalent amount of free enzymes in solution. Those initial studies demonstrated the concept of mimicking structure and functions by co-localizing multiple enzymes to have clear kinetics benefits. The sequential co-localization strategy was designed to control each individual type of enzyme attachment.

The polystyrene nanoparticles are a relatively robust and stable organic platform in aqueous solution. Facile separation methods such as micro-centrifugation can be used, indicating broad application potentials. However, the non-specific adsorption induced by the highly hydrophobic surface might cause unfavorable configuration changes of some vulnerable amphiphilic enzymes, which potentially results in “unwanted” enzymatic activity loss.

In this second study discussed in Chapter 4, more biocompatible amphiphilic Pluronic-QD micelles were designed to co-localize multiple enzymes. This was designed to investigate the effect of a more flexible substrate, compared to the rigid polystyrene particles, and provide an effective way to characterize the co-localization of multiple

enzymes. The hydrophobic QDs accumulated in the center core serve as primary attracting force to retain the enzymes on the micelles, which also can be used to characterize the adsorption of enzymes by FRET. It was shown that adsorption of single enzymes led to quenching of the QDs and excitation of acceptor fluorescent dyes, indicative of FRET occur and adsorption of the enzymes on the micelles. The catalytic activity of single enzymes was retained after adsorption. Similarly, the FRET between the dyes on the two respective enzymes was also used to characterize the co-localization of the two enzymes on the same micelle. Finally, the two co-localized enzymes enhanced the overall conversion rate by approximately 100% compared to the equivalent concentration of free enzymes in solution, which is very comparable to the findings in the first study.

Pluronic block polymers used in this work have shown great compatibility with vulnerable enzymes. However, the feature of “soft” micelles made separation challenging as compared to the polystyrene platform. Appropriate enzyme feed concentrations needed to be optimized to minimize the presence of free enzymes in solution. The similar improvement for kinetics might come from the random co-localization strategy used in both studies. To further increase the kinetics enhancement, more precisely control on the relative position of co-localized enzymes needs to be designed to bring the active sites on the enzymes closer. Precise DNA hybridization was used in this context and less hydrophobic streptavidin coated polystyrene nanoparticles were chosen as carriers.

In the third study discussed in Chapter 5, DNA directed multi-enzyme co-localization on streptavidin coated polystyrene nanoparticles was investigated. The precise hybridization of complementary DNA chains has attracted great attention because of its unique effective control of the relative positions of different components.

Two short DNAs can hybridize with the corresponding complementary segments on the long DNA to realize co-localization, which can be further controlled by the length of DNA sequence. In that study, free DNA hybridization and co-localization efficiency were firstly studied using FRET techniques. Various capture DNA concentrations were compared and optimized. The immobilization of single enzyme was studied to investigate the steric hindrance effect. The co-localization of the GOX and HRP were evidenced by FRET studies of the dyes labeling the two tag DNAs. Finally, it was found that the co-localized GOX and HRP via DNA hybridization significantly improved the overall reaction efficiency as compared to single enzyme immobilization mixture. The kinetics enhancement was observed in the both sets of comparison with different DNA-enzyme conjugates.

As opposed to non-specific spatial control method in co-localization, DNA-based methods provide strong control over spatial arrangement and organization in multi-enzyme co-localization study, which can also been seen from the FRET characterization and greater kinetics enhancement. Streptavidin coated surfaces are more compatible with enzymes, and can improve the long term stability of co-localized enzymes. Overall, the DNA directed co-localization on SPS combines the advantages of the previous two studies and shows great promise for potential scientific and industrial applications.

In summary, three different approaches were designed and they have their own advantages and disadvantages so far in this dissertation. In order to achieve optimized multi-enzyme co-localization, appropriate strategy needs to be designed according to specific applications. Based on the studies in this thesis, it is important to consider the following perspectives: (1) The structure and function of each enzyme component needs to be carefully considered for multi-enzyme co-localization; (2) Appropriate attachment techniques and carrier platforms need to be rationally selected for all the enzymes; (3)

Insights gained from single enzyme immobilization studies need to be used to optimize the reaction conditions for retaining the activity of the attached enzymes during co-localization; and (4) Using the above considerations, novel strategies need to be developed for single enzyme immobilization and co-localization. Overall, current research has amply demonstrated the superior potential of co-localized multiple enzymes in terms of kinetically-driven benefits. Future studies will need to focus on the stability of the co-localized enzymes for sustainable activity with multiple uses. Looking forward, the design of sustainable and re-usable multi-enzyme biocatalysts would lead to both scientifically exciting research as well as economically viable designs for next generation catalysts and biosensors.

Table 6-1comparison of co-localization approaches developed in this dissertation

	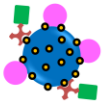 PS nanoparticles	 PLQD micelles	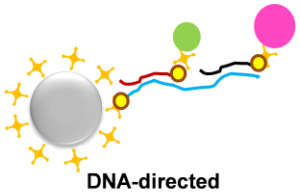 DNA-directed colocalization on PS
Attachment	Biotin-streptavidin coupling; covalent binding	Adsorption	DNA hybridization
Platform	Rigid	Flexible	Rigid
Co-localization	Sequential	Simultaneous	Simultaneous
Characterization	Kinetic comparison	DLS and FRET	FRET
Enhancement in kinetic performance	100%	100%	>150%

Chapter 7 Ongoing work and future directions

The enzyme co-localization strategies developed in this work have been demonstrated using the GOX-HRP system, but can potentially be applied to a wide range of enzyme systems. Therefore, work is ongoing to extend the validity of this approach to multiple enzyme co-localization systems, as described below. Progress to date on these fronts is provided below.

7.1 Multi-enzyme co-localization for flavan-3-ol biosynthesis

7.1.1 Introduction and background

Flavon-3-ols are natural products that are members of the flavonoid family, which are powerful antioxidants that have been implicated as major contributors to cardio-protective and anti-cancer properties.[1] They are rich in foods such as green tea, blueberry, grape and dark chocolate.[2,3] Previous research has shown that the biosynthesis of flavon-3-ols involves two key enzymes that work sequentially: anthocyanidin synthetase (ANS) and anthocyanidin reductase (ANR). Specifically, these reactive oxy-cation containing substances are derived from other flavonoid metabolism pathways via anthocyanidin intermediates, formed from leucoanthocyanidins by the 2-oxoglutarate- and iron-dependent dioxygenase ANS, and reduced to form flavan-3-ols by the NADPH-dependent ANR.[4,5] However, in the presence of ANS alone, products rich in oxidized flavonols are produced, with only a small fraction of cyanidin, which is the substrate for ANR.[6,7] The leucocyanidin, the substrates for ANS enzyme, which are produced in the upstream reaction catalyzed by DFR, are very unstable. Meanwhile, considerable insights have recently been obtained by cloning studies and mechanistic investigations of the individual DFR, ANS and ANR enzymatic genes[4,5,8] leading to the likelihood that DFR and ANS are complexed with ANR *in vivo*. Such a metabolic enzyme complex (or metabolome) would then be expected to allow specific transfer of the

anthocyanidin oxy-cation intermediate directly from ANS to the subsequently acting enzyme. Therefore, it is believed that the rapid transport of anthocyanidin oxy-cation intermediate from ANS to the subsequent enzyme ANR could prevent further oxidation by ANS, which can be realized when ANS is complexed with ANR. However, no biological evidence has been reported to demonstrate the complex between DFR, ANS and ANR. Here, we propose to use confinement within a nano-carrier to achieve an equivalent “complexation” effect. Specifically, by confining DFR, ANS and ANR within a nano-carrier, transfer of the reactive oxy-cation anthocyanidin intermediate will be optimized (Figure 7.1).

7.1.2 Materials and Methods

Chemicals

Cyanidin chloride, epicatechin NADPH were purchased from Sigma-Aldridge (St. Louis, MO). Methanol (MeOH), acetonitrile N-Hydroxysuccinimide (NHS) and 1-ethyl-3-[3-dimethylaminopropyl] carbodiimide hydrochloride (EDC) were from Fisher Scientific (Hampton, NH). 200 nm 4% (w/v) C-PS nanoparticles were purchased from Invitrogen (Carlsbad, CA). ANR enzyme was supplied by our collaborator, Prof. Reuben Peters, at Iowa State University. All aqueous solutions were prepared using purified water from Thermo Scientific’s Barnstead Nanopure Ultrapure Water System.

HPLC analysis and data integration

HPLC analysis used an Agilent1200 series machine and a C18 reverse phase column with UV detection at 260 nm and 280 nm for detecting epicatechin and cyanidin chloride. Twenty µL samples were injected at a flow rate of 0.5 mL /min. The product peaks were identified by retention time using standard solution as reference. The products were quantified by comparing the areas under the peak with that of standards.

ANR activity assay

In 1 mL ANR solution, 200 µL of 10 mM NADPH, appropriate cyanidiin chloride stock solution, and reaction buffer were mixed and preheated to 30^{o}C using a water bath prior to addition of enzyme solution. To initiate the reaction, 20 µL of 4 mg/mL ANR was added and the reaction solution was incubated for 30 min. The reaction was stopped by adding 2 mL ethyl acetate and separated by brief centrifugation, which was repeated three times. Nitrogen gas was used to dry the ethyl acetate, and the remained extracted products were re-dissovled into 100 µL MeOH for HPLC analysis.

ANR attachment on PS nanoparticles

The PS nanoparticles were activated by 40 mg/mL NHS in the presence of 20 mg/mL EDC. The free carboxylic acid end groups on the particle surface formed a sub-stable NHS ester. Then, approximately 1.5 mg of ANR was added and incubated for 2 h at 4 ^{o}C. The unattached proteins were separated by centrifugation and repeated until no free enzyme were found in the supernatants by using UV-Vis spectrophotometry. The resulting samples were further lyophilized overnight for characterization by X-ray photoelectron spectroscopy (XPS).

XPS analysis

XPS analysis was used to determine the amount of ANR attached on the surface of the nanoparticles. The original data was acquired using a PHI 5500 Multi-technique system (Physical Electronics, Chanhassen, MN). Standard aluminum source was used with carbon as reference for charge correction. Blank nanoparticles were used as controls. High-resolution C1s peaks were collected and fitted used CasaXPS software (RBD Instruments, Bend, OR). Binding energies were referenced to the aliphatic hydrocarbon peak at 285.0 eV.

7.1.3 Preliminary Results

Optimization of mobile phase for HPLC analysis

By comparing two different solvents used for cyanidin and epicatechin standards in HPLC analysis, it was found that the original solvent (MeOH)[5] produced split peaks during analysis by HPLC, making quantitation questionable. This problem was solved by using the HPLC mobile phase as the solvent (Figure 7.2).

Epicatechin calibration

To enable quantification of the epicatechin, which is produced in the ANR assay, the mobile phase was used as solvent in preparing standards. Detectors at 254 nm and 280 nm were compared and it was found that the quantitation was more sensitive at 280 nm. The detection limit was found to be ~0.125 µg. Epicatechin was kept frozen at -80 ^{o}C between analyses and was found to be stable. Reproducible calibration curves were obtained with standards stored for at least a week under these conditions. Figure 7.3 shows the epicatechin calibration curve constructed with two different detectors.

ANR kinetics studies

ANR activity was measured at cyanidin concentrations ranging from 6-300 µM to determine kinetic parameters. A double reciprocal plot of 1/V against 1/S was constructed as shown in Figure 7.4 to obtain the K_m and v_{max} values using Michaelis-Menten kinetics. The precision between the K_m and v_{max} values obtained in replicate assays (Table 7.1) was poor, which is likely due to losses during the process of separating, purifying and concentrating the products. However, the values are in the same molar range as values reported in the literature.[5] It is also possible that substrate inhibition of the enzyme at high cyanidin concentrations may have occurred, as reported elsewhere.[5]

XPS characterization of ANR attachment onto PS nanoparticles

XPS spectra provided elemental atomic concentrations on the PS nanoparticle surface as indicated in Table 7.2. The free enzyme and blank PS particles showed a C/O number ratio of 3.17 and 6.18, respectively. After attachment, the C/O ratio on the particle surface decreased to 3.49, which is in between the respective values for the free enzyme and the blank nanoparticles. The nitrogen concentration on the ANR-PS particle surface was 10.74, which is also in between that of the free enzyme and blank PS nanoparticles. These data provide indirect evidence of ANR attachment to PS nanoparticles.

To further investigate the carbon composition of each sample, the C1s spectra were fitted with four main components based on aliphatic hydrocarbons at 285.0 eV (C1), ether and amine groups at 286.5 eV (C2), carbonyl and amide groups at 288.2 eV (C3), and ester and carboxylic acid groups at 289.1 eV (C4). As shown in Table 7.3, the C3 (amide peak) of the PS-ANR sample falls in between that of the blank PS nanoparticles and ANR, which suggests that the PS nanoparticle surface is covered by a protein, resulting in an increase in the amide bond peak. Correspondingly, in these samples, the carboxylic acid groups on the surface (i.e., C4) decreased because they are consumed during protein attachment. Finally, the blank PS nanoparticles showed the largest fraction of aliphatic hydrocarbon bonds (C1) at 285.0 eV as expected and the pure ANR contained the largest fraction of ether and amine groups (C2) at 288.2 eV.

7.1.4 Future work

The immobilization of individual DFR, ANS and ANR will be investigated using PS nanoparticles as a starting point. The attachment will be optimized to maintain the activity of the immobilized enzymes. DNA directed co-localization will also be used to co-localize DFR, ANS and ANR on nanoparticles. It is expected by co-localizing DFR, ANS

and ANR, the highly reactive oxy-cation containing substances can be mediated to maximize the yield of flavon-3-ols.

7.2 AgAS enzyme system

7.2.1 Introduction

As an alternative to the ANS-ANR MEC, Abeitadiene Synthase from *Abies grandis* (AgAS) is also being investigated. Abietadiene synthase is known to catalyze a two-step (i.e., class II (protonation-initiated) and class I (ionization initiated)) cyclization reaction at separate active sites in resin acid biosynthesis, resulting in a mixture of abietadiene double-bond isomers.[9] In the class II protonation-initiated cyclization, the stable bicyclic intermediate copalyl diphosphate is synthesized from the universal diterpene precursor geranylgeranyl diphosphate. In the class I magnesium ion-dependent reaction, the tricyclic perhydrophenanthrene-type backbone is generated via a diphosphate ester ionization-initiated cyclization, which is coupled, to a 1,2-methyl migration that generates the C13 isopropyl group characteristic of the abietane structure by intermolecular proton transfer within a transient pimarenyl intermediate. The co-localization enzymes are the mutants that carry the two reactions. The product profile produced by the native enzyme varies as a function of pH, which is expected to be different upon co-localization. The final product is tunable and controlled as with other coupled multi-enzyme systems.[9–12]

7.2.2 Materials and Methods

Chemicals

NHS and EDC were purchased from Fisher Scientific (Hampton, NH). AgAS enzymes were supplied by our collaborator, Prof. Reuben Peters, at Iowa State

University. All aqueous solutions were prepared using purified water from Thermo Scientific's Barnstead Nanopure Ultrapure Water System.

AgAS attachment on nanoparticles

The poly(1,6-bis-(*p*-carboxyphenoxy)hexane) (CPH) or poly(CPH) nanoparticles were fabricated using an anti-solvent precipitation method as described previously.[13,14] The AgAS enzyme was attached to the free carboxylic acid group on the poly(CPH) nanoparticle surface via covalent binding. In 1mL AgAS storage buffer (50mM disodium phosphate, 300 mM NaCl, 10% $MgCl_2$, 10% glycerol and 1 mM DTT),10 mg of nanoparticles were suspended and activated by 40 mg/mL NHS in the presence of 20 mg/mL EDC. Approximately 1.5 mg of AgAS was added and incubated for 2 h At 4 ^{o}C. The unattached proteins were separated by centrifugation and repeated until no free enzyme were found in the supernatants by using UV-Vis spectrophotometry. The resulting samples were further lyophilized overnight for characterization by X-ray photoelectron spectroscopy (XPS).

XPS analysis

XPS analysis was used to determine the amount of ANR attached on the surface of the nanoparticles. The original data was acquired using a PHI 5500 Multi-technique system (Physical Electronics, Chanhassen, MN). Standard aluminum source was used with carbon as reference for charge correction. Blank nanoparticles were used as controls. High-resolution C1s peaks were collected and fitted used CasaXPS software (RBD Instruments, Bend, OR). Binding energies were referenced to the aliphatic hydrocarbon peak at 285.0 eV.

7.2.3 Preliminary Results

Nanoparticle fabrication and characterization

Initial studies conducted by Prof. Peters' laboratory indicated that the anhydride monomer CPH is suitable in terms of maintaining a high product yield. Thus, poly(CPH) nanoparticles were used as a preliminary candidate for immobilizing AgAS. The nanoparticles before and after enzyme immobilization were characterized by SEM as shown in Figure 7.5. The morphologies and size of the particles did not change after enzyme attachment. The nanoparticle sizes were in the range of 200 to 900 nm. These observations will be corroborated with dynamic light scattering. XPS analysis provided elemental atomic concentration on the particle surface (Table 7.4). The free enzyme and blank poly(CPH) particles exhibited a C/O number ratio of 2.33 and 3.24, respectively. No nitrogen was found on the blank particles as expected. After attachment, the C/O ratio on the particle surface decreased to 2.79, which is in between the value of the free enzyme and that of the blank particles. The nitrogen concentration was 9.98, which is also in between that of the free enzyme and the blank particles. These data provide indirect evidence of AgAS attachment. To further quantitatively evaluate the carbon bond composition of each sample, the C1s spectra were obtained as described before. As shown in Table 7.5, the value of the C3 (amide peak) of the poly(CPH)-AgAS sample falls in the range between that of poly(CPH) and AgAS, which suggests the presence of protein on the nanoparticle surface, accounting for the increase in amide bond formation. As expected, the carboxylic acid groups (C4) decreased because they are used for attaching the proteins.

7.2.4 Future Work

The AgAS enzyme co-localization will be investigated along with the individual mutant immobilization. These enzymes are known to not assemble into an enzymatic

complex, and the intervening intermediate is not reactive. Nevertheless, these provide a reasonable alternative for incorporation of enzymatic biocatalysts into the proposed nano-carrier platforms. The activity of the co-localized enzymes will be compared with that of the native enzymes.

7.3 Sclareol biosynthesis

In Nature, multi-enzyme co-localization concepts can be also used to control biosynthetic pathways and enhance the desired reaction efficiency. Sclareol, as starting material in synthetic approach, is a type of chemical compound that has great commercial value for synthesizing Ambergis, which can be used as fragrance product in cosmetics, perfume and even flavoring in food industry. Sclaerol, typically exists in the plant *Salvia sclarea*, where two types of enzymes catalyze two types of reaction- class II and class I reactions, are very critical in mediating the sequential pathway as illustrated in figure 7.6.[15] Previous research results have indicated that the two distinct class enzymes were indeed single enzyme scarrying two functions.[16] We are investigating our biosynthetic approach to co-localize the two enzymes on nanocarriers to mimic this naturally occurring MEC, which can potentially improve the product yield significantly and lead to industrial applications. The broad goal of this work is to design bioinspired MECs in vitro using materials-based approaches to co-localize enzymes on nanocarriers.

References

(1) Aron, P. M.; Kennedy, J. A. Flavan-3-ols: Nature, occurrence and biological activity. *Mol. Nutr. Food Res.* **2008**, *52*, 79–104.

(2) Crespy, V.; Williamson, G. A Review of the Health Effects of Green Tea Catechins in In Vivo Animal Models. *J Nutr* **2004**, *134*, 3431S–3440S.

(3) Serafini, M.; Bugianesi, R.; Maiani, G.; Valtuena, S.; Santis, S. D.; Crozier, A. Plasma antioxidants from chocolate. *Nature* **2003**, *424*, 1013.

(4) Xie, D.-Y.; Shashi B, S.; Paiva, N. L.; Ferreira, D.; Dixon, R. A. Role of Anthocyanidin Reductase, Encoded by BANYULS in Plant Favonid Biosynthesis. *Science* **2003**, *299*, 396–399.

(5) Xie, D.-Y.; Shashi B, S.; Dixon, R. A. Anthocyanidin reductase from Medicago Truncatula and Arabidopsis Thaliana. *Arch. Biochem. Biophys.* **2003**, *422*, 91–102.

(6) Turnbull, J. J.; Sobey, W. J.; Aplin, R. T.; Hassan, A.; Schofield, C. J.; Firmin, J. L.; Prescott, A. G. Are anthocyanidins the immediate products of anthocyanidin synthase? *Chem. Commun.* **2000**, 2473–2474.

(7) Turnbull, J. J.; Nagle, M. J.; Seibel, J. F.; Welford, R. W. D.; Grant, G. H.; Schofield, C. J. The C-4 stereochemistry of leucocyanidin substrates for anthocyanidin synthase affects product selectivity. *Bioorg. Med. Chem. Lett.* **2003**, *13*, 3853–3857.

(8) Turnbull, J. J.; Nakajima, J.; Welford, R. W. D.; Yamazaki, M.; Saito, K.; Schofield, C. J. Mechanistic Studies on Three 2-Oxoglutarate-dependent Oxygenases of Flavonoid Biosynthesis ANTHOCYANIDIN SYNTHASE, FLAVONOL SYNTHASE, AND FLAVANONE 3β-HYDROXYLASE. *J. Biol. Chem.* **2004**, *279*, 1206–1216.

(9) Peters, R. J.; Croteau, R. B. Abietadiene synthase catalysis: Mutational analysis of a prenyl diphosphate ionization-initiated cyclization and rearrangement. *Proc. Natl. Acad. Sci.* **2002**, *99*, 580–584.

(10) Zhou, K.; Peters, R. J. Investigating the conservation pattern of a putative second terpene synthase divalent metal binding motif in plants. *Phytochemistry* **2009**, *70*, 366–369.

(11) Peters, R. J.; Flory, J. E.; Jetter, R.; Ravn, M. M.; Lee, H.-J.; Coates, R. M.; Croteau, R. B. Abietadiene Synthase from Grand Fir (Abies grandis): Characterization and Mechanism of Action of the “Pseudomature” Recombinant Enzyme†. *Biochemistry (Mosc.)* **2000**, *39*, 15592–15602.

(12) Peters, R. J.; Ravn, M. M.; Coates, R. M.; Croteau, R. B. Bifunctional Abietadiene Synthase: Free Diffusive Transfer of the (+)-Copalyl Diphosphate Intermediate between Two Distinct Active Sites. *J. Am. Chem. Soc.* **2001**, *123*, 8974–8978.

(13) Torres, M. P.; Vogel, B. M.; Narasimhan, B.; Mallapragada, S. K. Synthesis and characterization of novel polyanhydrides with tailored erosion mechanisms. *J. Biomed. Mater. Res. A* **2006**, *76*, 102–110.

(14) Torres, M. P.; Determan, A. S.; Anderson, G. L.; Mallapragada, S. K.; Narasimhan, B. Amphiphilic polyanhydrides for protein stabilization and release. *Biomaterials* **2007**, *28*, 108–116.

(15) Caniard, A.; Zerbe, P.; Legrand, S.; Cohade, A.; Valot, N.; Magnard, J.-L.; Bohlmann, J.; Legendre, L. Discovery and functional characterization of two diterpene synthases for sclareol biosynthesis in Salvia sclarea (L.) and their relevance for perfume manufacture. *Bmc Plant Biol.* **2012**, *12*.

(16) Schalk, M.; Pastore, L.; Mirata, M. A.; Khim, S.; Schouwey, M.; Deguerry, F.; Pineda, V.; Rocci, L.; Daviet, L. Toward a Biosynthetic Route to Sclareol and Amber Odorants. *J. Am. Chem. Soc.* **2012**, *134*, 18900–18903.

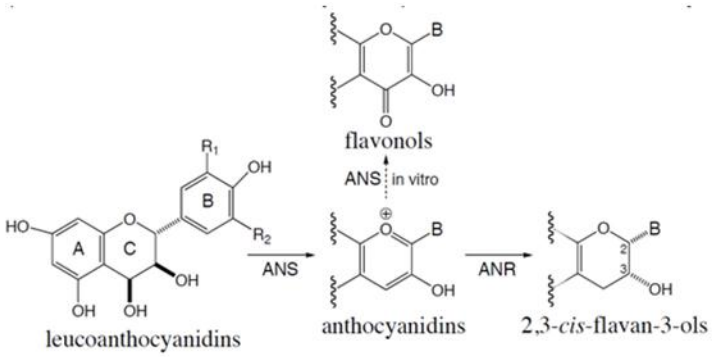

Figure 7.1Scheme of cascade reactions catalyzed by DFR, ANS and ANR

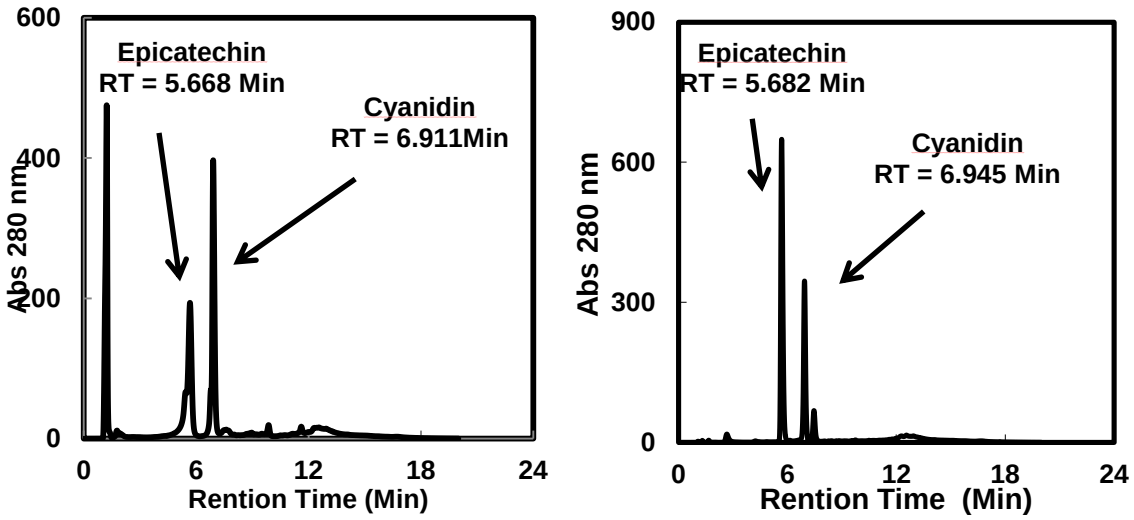

Figure 7.2 HPLC profile of epicatechin and cyanidin-Cl in MeOH (left) and mobile phase (Right). Note split peaks due to use of MeOH as the solvent for the standards. HPLC profile of epicatechin and cyanidin-Cl. Replacing MeOH with mobile phase as the solvent for the standards eliminates formation of split peaks. Mobile Phase: Mixture of 10 parts 1% HCOOH in acetonitrile + 90 parts 1% HCOOH in water.

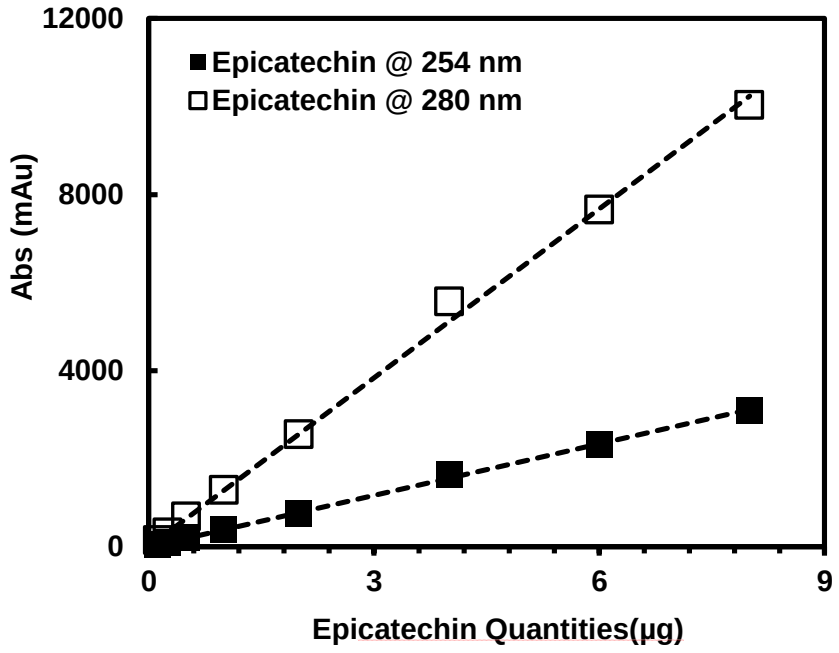

Figure 7.3 HPLC calibration profile for epicatechin. Elimination of split peaks improves quantitation. As little as ~0.125 µg of epicatechin was reliably and reproducibly detected.

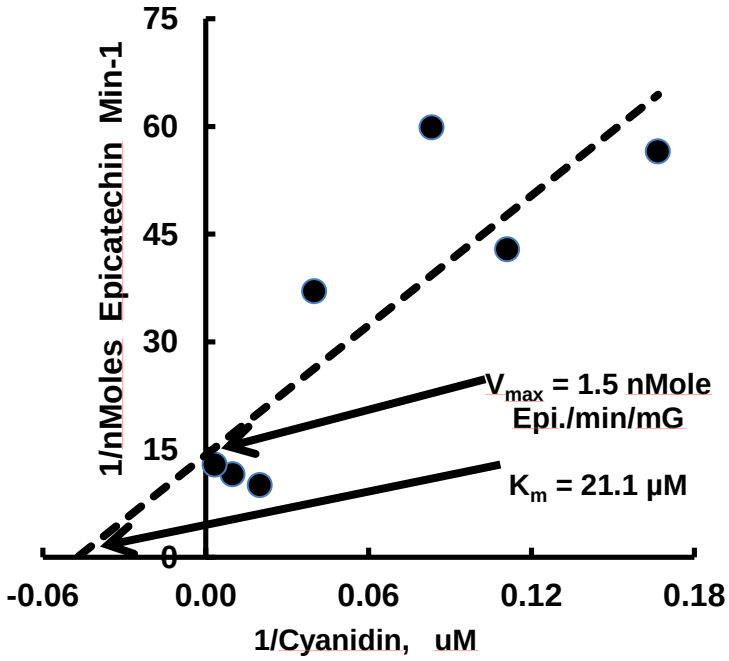

Figure 7.4 Determination of K_m and V_{max} for *A. thaliana* ANR using cyanidin-Cl as a substrate. Concentration range for cyanidin-Cl was from 6-300 µM. Epicatechin was detected by HPLC.

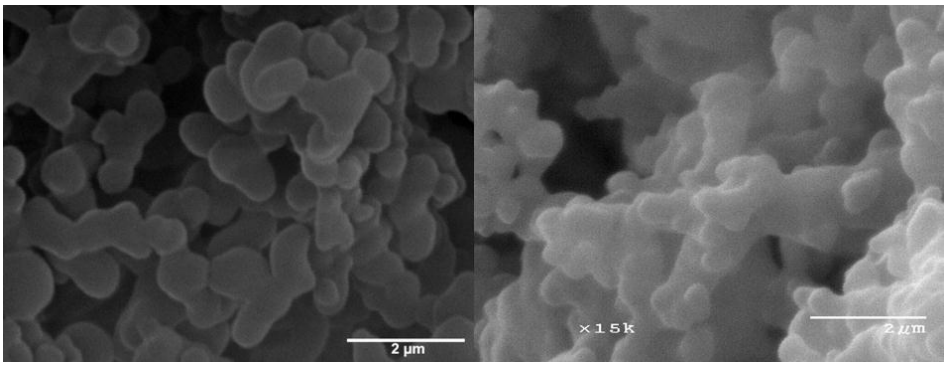

Figure 7.5 SEM images of polyCPH (left) and polyCPH-AgAS (right).

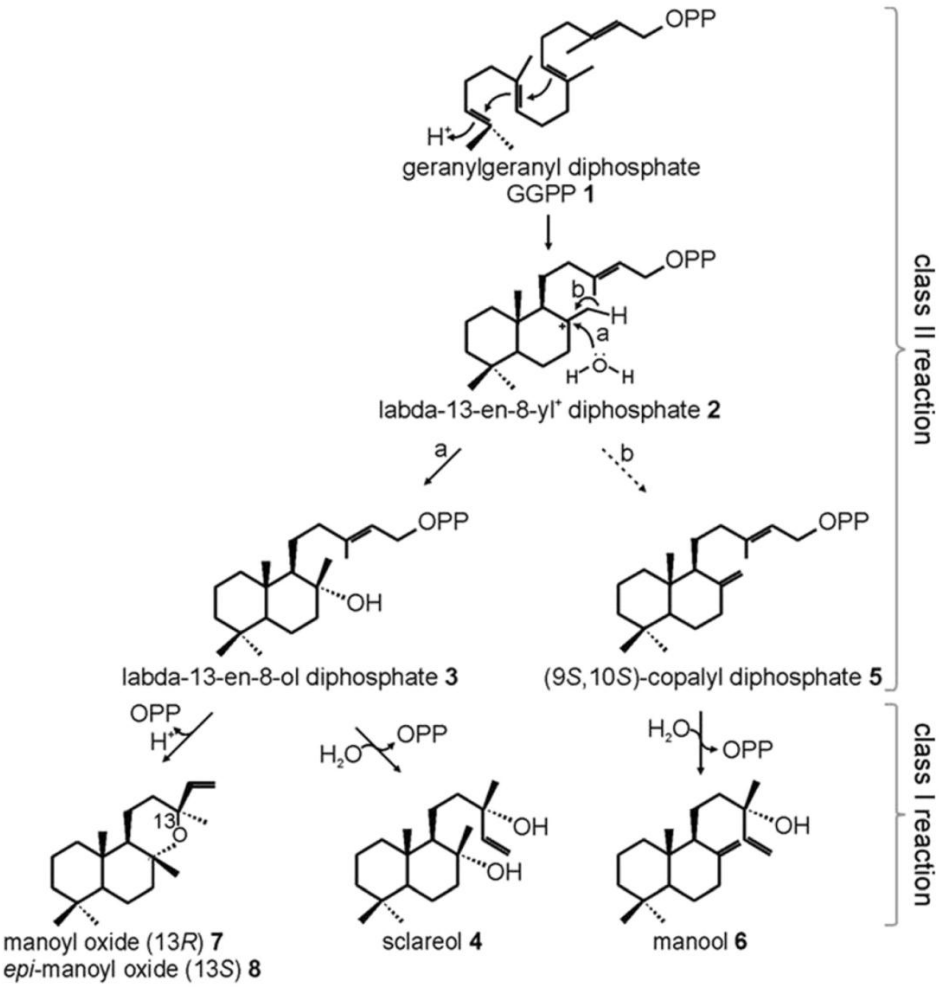

Figure 7.6 Biosynthesis pathway of sclareol with involvement of NgCPS and sSsSS enzymes. [23]

Table 7-1Km and Vmax values for cyanidin-Cl and epicatechin, respectively.

Trial #	K_m for Cyanidin-Cl (μM)	V_{max} for Epicatechin (nM/min/mg ANR)
2	**21.1**	**1.46**

Literature values: K_m: 74 μM; V_{max}: 10 nMole/min/mg ANR protein (Xie et al, Arch. Biochem. Biophys. **422**:91 (2004)).

Table 7-2 Elemental analysis of ANR-conjugated nanoparticles using XPS

Sample	C%	N%	O%	C/O
ANR	66.55	12.46	20.99	3.17
PS	85.5	0.31	13.84	6.18
PS-NHS	78.07	4.53	17.4	4.49
PS-ANR	69.36	10.74	19.9	3.49

Table 7-3 Quantification of components fitted to of C1s spectra

	ANR	PS	PS-NHS	PS-ANR
C1	64.46	94.76	88.56	71.83
C2	19.4	0	4.53	13.95
C3	15.37	0	5.6	14.05
C4	0.76	2.01	1.31	0.17
C5		3.23		

C1:	Aliphatic hydrocarbon	285.0 eV
C2:	Ether and amine groups	286.5 eV
C3:	Carbonyl and amide groups	288.2 eV
C4:	Ester and carboxylic acid groups	289.1 eV
C5:	Aromatic shake-up due to π-π transition on the aromatic rings	291.7 eV

Table 7-4 Elemental analysis of AgAS-conjugated nanoparticles using XPS

Sample	C%	N%	O%	C/O
AgAS	60.62	13.28	25.98	2.33
poly(CPH)	76.42	0.00	23.58	3.24
poly(CPH)-NHS	76.42	1.08	22.42	3.41
poly(CPH)-AgAS	65.88	9.98	23.58	2.79

Table 7-5Quantification of components fitted to C1s spectra

Component*	poly(CPH)	AgAS	poly(CPH)-NHS	poly(CPH)-AgAS
C1	72.64	62.46	75.79	66.66
C2	23.45	22.79	17.48	19.71
C3	0	14.13	3.36	10.86
C4	3.91	0.61	3.38	2.77